

1N-02

76084

NASA TM-88534

R/05

NASA TECHNICAL MEMORANDUM

THE AERODYNAMIC OPTIMIZATION OF WINGS AT SUBSONIC SPEEDS
AND THE INFLUENCE OF WINGTIP DESIGN

H. Zimmer

Translation of "Die aerodynamische Optimierung von Tragflügeln im
Unterschallgeschwindigkeitsbereich und der Einfluß der Gestaltung
der Flügelenden," Stuttgart, Universität, Fakultät für Luft- und
Raumfahrttechnik, Dr.-Ing. Dissertation, 1983, 122 pages,
84A36992.

(NASA-TM-88534) THE AERODYNAMIC
OPTIMIZATION OF WINGS AT SUBSONIC SPEEDS AND
THE INFLUENCE OF WINGTIP DESIGN Thesis
(NASA) 105 p Avail: NTIS HC A06/MF A01 GS

N87-22627

CSCL 01A 02/02 Unclas
0076084

NATIONAL AERONAUTICS AND SPACE ADMINISTRATION
WASHINGTON, DC 20546 MAY 1987

1. Report No. NASA TM-88534	2. Government Accession No. 84A36992	3. Recipient's Catalog No.	
4. Title and Subtitle THE AERODYNAMIC OPTIMIZATION OF WINGS AT SUBSONIC SPEEDS AND THE INFLUENCE OF WINGTIP DESIGN		5. Report Date May 1987	6. Performing Organization Code
		8. Performing Organization Report No.	
7. Author(s) H. Zimmer		10. Work Unit No.	
		11. Contract or Grant No. NASW-4006	
9. Performing Organization Name and Address The Corporate Word, inc. 3 Gateway Ctr., 18 S. Pittsburgh, PA 15222		13. Type of Report and Period Covered Translation	
12. Sponsoring Agency Name and Address National Aeronautics and Space Administration Washington, DC 20546		14. Sponsoring Agency Code	
15. Supplementary Notes Translation of "Die aerodynamische Optimierung von Tragflügeln im Unterschallgeschwindigkeitsbereich und der Einfluss der Gestaltung der Flugelenden," Stuttgart, Universität, Fakultät für Luft- und Raumfahrttechnik, Dr.-Ing. Dissertation, 1983, 122 pages, 84A36992.			
16. Abstract Some of the objectives of modern aircraft development are related to an achievement of a lower fuel consumption and the reduction of aircraft noise. The present investigation is mainly concerned with the aerodynamic aspects of the objectives of aircraft development. The principal aim is related to a critical discussion of the possibilities for the reduction of the induced drag. New studies regarding the design of the wing, and in particular, the wing tips are considered. The induced drag is important, because in cruising flight it accounts generally for approximately one-third of the entire drag for the aircraft, while in climbing one-half of the entire drag is provided by the induced drag. A survey is presented of the wing geometries and wing tip designs studied, and theoretical investigations of different planar wings with systematically varied wing tip forms are conducted. Attention is also given to a theoretical study of some planar and nonplanar wings and a comparison with experimental data. ORIGINAL PAGE IS OF POOR QUALITY			
17. Key Words (Selected by Author(s))		18. Distribution Statement Unlimited	
19. Security Classif. (of this report) Unclassified	20. Security Classif. (of this page) Unclassified	21. No. of Pages 105	22. Price

SUMMARY

The theme of this study is the importance of optimizing the induced drag of wings as an element of the entire drag of the aircraft. Principles of aerodynamics are primary, although questions regarding weight and structure load are also explored. Conclusions are based on phenomenological observations and theoretical deductions which have been confirmed by experimental results. Familiar relationships are critically reexamined, and various wing designs are also systematically studied to determine the possibilities and limits of induced drag reduction. As an important point of departure, the studies include data on so-called natural wing designs, that is, those of land and sea-based soaring birds.

It is already known that a nonplanar wing system (double decker, tip plates, fanned wing tips) has less induced drag than a planar elliptical wing of equal span. Thus, designs of this type were commonly suggested in the past, their authors having arrived at various nonplanar optimal designs with very different limits of drag reduction which have not, however, been proven in tests.

Wings with systematically varied tip designs have been studied theoretically with the help of a vortex net procedure involving the flow of nonplanar wakes, and observations of wing wake energy, as well as experimental evidence and research on natural planar and fanned wing designs. These studies have shown that natural designs determine the limits of possible drag reduction. This is true not only from a theoretical viewpoint, but also in technical applications. Wings that have fanned tips represent a group distinct from planar and simple non-planar wings. Earlier very optimistic expectations regarding this wing type have been proven unrealistic, and based on undependable simplifications. The planar backswept triangular wing tip has proven to be the optimal design under practical conditions.

FOREWORD

The following study arose at the suggestion of Professor F.X. WORTMANN, Ph.D., Eng., Institute for Aerodynamics and Gasdynamics of the University of Stuttgart, in connection with work being done by DORNIER, GmbH, Friedrichshafen, in the area of flight physics and research .

I am grateful to Dr. F.X. WORTMANN for suggesting the following work and for the specific encouragement he offered through his numerous and helpful suggestions, advice and explanations, as well as for serving as principle jurist.

My special thanks also go to Professor J.R. HEYNATZ, Ph.D., Eng., from the Department of Air and Space Technology of the University of Stuttgart and the firm of DORNIER GmbH, Friedrichshafen, for his untiring willingness to engage in helpful discussions and offer encouraging suggestions, as well as for serving as co-jurist.

I am grateful to DORNIER GmbH, and in particular to Dr. H. MAX, Ph.D., Eng., head of the department of flight physics and research, for the generous support offered in supplying exhibits and making available technical support materials, as well as providing assistance in the technical production of this work.

OVERVIEW

In recent years, modern aircraft development has had to pay greater attention to considerations of economy and environmental stresses. Thus, for example, an aircraft has the greatest commercial value if it has the smallest possible drag and weight for its given purpose, the parameters for which can be fairly wide. The steep climbing angle which this also makes possible can minimize the stress on the environment.

Although, of course, several possibilities exist for improving aircraft design, induced drag is examined in the following work. This drag element is particularly important because it makes up a third to a half of the total drag of the aircraft. Although significant efforts toward understanding this drag element have been made since the beginnings of research on air travel, the most recent research and development have shown that there still exists a wide field of possibilities for improvement and optimization. Familiar mathematic-physical model designs are critically reexamined to highlight the possibilities and limits of reducing induced drag.

For example, it has been known since the beginnings of air travel research (one need only be reminded of names such as PRANDTL, LANCHESTER, MUNK and BETZ) that nonplanar wing systems (e.g., double decker, wingtips) can significantly lower the induced drag below that of smooth elliptical wings of equal span. An introductory phenomenological section considers the many previous studies made in this area. The notable result is that practically all authors arrived at various nonplanar optimal designs, although basically the same mathematical model was used, i.e., fixed wake. Then the very different limits of drag reduction of such wing designs are presented, some that are even substantially "subelliptical". Comparison with the experiment shows, however, that a "subelliptical" induced drag has never been measured on multi-sectioned, fanlike wing tips (the design previously most expected to reduce drag), not even on a soaring land bird measured in flight, which represents the ideal design of this type of wing.

These discrepancies have not previously been mathematically and physically explained. An in-depth examination has been undertaken in the following work, however, because eliminating these discrepancies has been considered important to the understanding of the mechanism of induced drag in the context of wing optimization. In addition, it is also an effort generally to specify even simpler wing tip designs which optimize drag.

Theoretical and experimental studies on systematically varying planar and nonplanar wing designs (where wing weight and construction cost are indirectly considered over the relevant aerodynamic parameters) show that various typical wing designs will have to vary. Namely,

- a) Planar "straight" wings whose carrying vortices essentially run in a straight line.
- b) Sweptback planar wings with pointed tips, which are effectively nonplanar.
- c) Simple nonplanar wings, e.g., wings with wing tips or turned down tips.
- d) Nonplanar wings with slotted edges, consisting of two partial wings which exert strong interference on each other as a result of their close proximity.
- e) Nonplanar wings with expanded, fanlike edges on two or more partial wings.

The following examinations, which were initially undertaken with the help of a relatively complex vortex net procedure, show that wing groups a) to d) can be adequately described, but wing group e) provides unusable data. Therefore, specified observations regarding wing wake energy were made for this group. These observations also reconfirm results obtained for wing groups a) to d).

Of great interest for wing optimization is knowing the limit of induced drag reduction under realistic physical tip conditions such as, for example, for the simultaneously lowest friction drag, weight, and construction cost. This makes it obvious that the elliptical wing certainly represents a limit to drag reduction, but only for group a) of straight, planar wings. By contrast, group b) proves to be the limit of drag resistance, or the optimal design, of the four wing groups a) through d), i.e., wing designs like those of, for example, ocean soaring birds. These wing designs deliver roughly 90% to 95% of the induced drag of the elliptical wing with fixed wake.

Although a nonlinear wake model, similar to MUNK's model for a fixed wake, helps to determine the limit of drag resistance for wing groups a) to d), the fanlike wings of group e) must be examined separately, as mentioned. This work not only determines whether the drag resistance that is expected in accordance with previously published theoretical research, is significantly stronger than the given percentages, proves to be correct; but also explains the discrepancies between the theoretical and experimental results. The optimal design and limits of drag resistance for this wing design are also provided through observations of the energy in the wing wake and with the help of a new combination of the wing wake models of BETZ and of SPREITER and SACKS. This both eliminates the previous discrepancies in measurement and also significantly dampens the expectations for a technological application of this type of wing.

Applying an analysis of the knowledge gained to practical wing design shows that a wing that is designed in accordance with the principles of group b) cannot be surpassed by any other planar or nonplanar wing design, if, in addition to the lowest induced drag, it is simultaneously also to have the lowest friction drag and the lowest weight.

TABLE OF CONTENTS

	<u>Page</u>
SUMMARY	3
FOREWORD	4
OVERVIEW	5
ABBREVIATIONS	9
1. INTRODUCTION	11
2. OVERVIEW OF PREVIOUSLY STUDIED WING DESIGNS AND PARTICULARLY WING TIP DESIGNS	16
2.1 In General	16
2.2 Planar designs	16
2.3 Nonplanar designs, simple	18
2.4 Nonplanar designs, multiple sectioned	20
2.5 The elliptical wing	23
2.6 Natural wing designs	24
2.7 Conclusions from previous studies	24
3. THEORETICAL EXAMINATION OF VARIOUS PLANAR WINGS WITH SYSTEMATICALLY VARIED WING DESIGNS	25
3.1 Fundamentals	25
3.2 The lift of wings being considered	28
3.3 The drag of wings being considered	29
4. THEORETICAL EXAMINATION OF A FEW SELECTED PLANAR AND NONPLANAR WINGS, COMPARISON WITH THE EXPERIMENT	32
4.1 The wing with planar and nonplanar triangular edge	32
4.2 The wing with wing tips	33
4.3 Comparison of the wing designs "wing tips" and triangular tip	34
4.3.1 Aerodynamic characteristics	34
4.3.2 Wing weight	36
4.4 Wing selection for practical application	38
4.4.1 General observations	38
4.4.2 Wing tips developed for practical use	39
4.5 The wing with slotted edge and forked points	41
5. DETERMINING THE LIMITS OF INDUCED DRAG REDUCTION FROM OBSERVATIONS OF THE ENERGY IN WING WAKE	44
5.1 Preparatory remarks	44
5.2 Discussion of various wing wake models	44
5.2.1 The impulse model	44
5.2.2 The wake vortex model of SPREITER and SACKS	46
5.2.3 The wake vortex model of BETZ	50
5.2.4 Observations on the combined application of the wake vortex models	54

5.3	The induced drag of soaring birds and the limits of possible drag optimization	56
5.3.1	General comments	56
5.3.2	Induced drag of soaring land birds	56
5.3.3	Induced drag of soaring ocean birds	58
5.3.4	Summary of the knowledge gained about soaring birds	61
5.4	Discussion and critique of the application of the principle of displacement	61
5.5	Discussion and critique of the interpretation and use of optimal condition	62
6.	CONCLUDING DISCUSSION OF POSSIBLE DRAG REDUCTION FOR NONPLANAR AND PLANAR WING DESIGNS	63
6.1	General data	63
6.2	The wing with multiple sectioned edges	64
6.2.1	Results of the model test	64
6.2.2	Results of the flight test	65
6.3	Wings with forked points and with slotted edges	66
6.4	Wing with tips	66
6.5	Planar wing designs	66
	REFERENCES	68
	ILLUSTRATIONS	77
	RESUME	105

...
 ...
 ...

ABBREVIATIONS

A	Lift
a	Distance
b	Span
b^1	Distance of wake vortex
b^-	Span of a smooth wing equivalent to a nonplanar wing
C_A	Total lift correction value
c_a	Local lift correction value
C_{MB}	Correction value of root flex moment
C_{M25}	Correction value of the pitch moment around the 1/4 point
C_p	Pressure correction value
Δc_p	Local load dispersion
C_s	Thrust correction value
C_w	Drag correction value
C_{w0}	Zero drag correction value
C_{wi}	Correction value of induced drag (local c_{wi})
Δc_{wi}	Local dispersion of induced drag
D	Diameter (rotary wing)
d_e	Span extension of wingtip
d_b	Half span of base wing
E	Kinetic energy
\dot{E}	Energy per unit of time
E^*	Energy per unit of length
F, F_B	Reference plane (Rotation plane)
F_{tot}	Total wing surface
f_w	Camber height
G	Relative wing weight per applied weight function
h	Height of wing system
K	Factor
l	Wing depth
\dot{m}	Air mass displaced by wing in unit of time
M_B	Wing root flex moment
P	Power output, rotor output
p	Output point
Q	Average plane of displaced air mass
q	Dynamic pressure
QR	Airelon
R	Radius of wake vortex
r	Running radius
Re	REYNOLDS number (in reference to wing depth)
r_k	Radius of wake vortex center
s	Path
TNT	Airfoil of new technology
t	Profile thickness
U_∞	Flow velocity
v	Tangential velocity of wake vortex
w	Velocity of downward current directly on wing
W	Turning point
W_i	Induced drag
X, Y, Z	Cartesian coordinate system
\bar{y}	Distance between centers of wake circulation outside the observed station

a Angle of incidence
 α_v Angle of the wing chord
 β Angle of the partial wing to the wing chord
 r Circulation on the wing
 r_0 Circulation in the wing center
 r' Circulation in the wake
 σ Angle at which output point appears according to BIOT-SAVART law
 ϵ Flow angle on the first bearing vortex
 ϵ_H Angle of the horizontal tail unit
 n Non-dimensional position on span axis
 n_K Position of break point in the circulation dispersion
 n_R Span of the right-angle wing
 n_{RB} Non-dimensional condition in the area of the wing tip
 n_W Position of the turning point in the circulation dispersion
 n^* Integration variable
 α V-angle of the individual wings
 K_{ell} Ratio of induced drag to that of the planar elliptical wing with rigid wake
 Λ Extension ($= b^2/F$)
 π Circle ratio value ($= 3.14159\dots$)
 p Air thickness, non-dimensional radius
 p^* Integration variable
 ϕ Velocity potential
 ψ Sweep angle

Indices

B Flex
 b Basis
 D Wing with triangular edge
 e Wing tip
 ell Elliptical, elliptical wing
 H Horizontal tail unit
 i Induced
 K Vortex center, breakpoint, depending on context
 M Moment
 max Maximum
 min Minimum
 mod Modified
 OPT Optimum
 P Potential flow
 R Rectangular wing
 RB Wing tip edge
 S Thrust
 V Torsion
 W Turning point
 25 Quarter point of wing depth

THE AERODYNAMIC OPTIMIZATION OF WINGS AT SUBSONIC SPEEDS AND THE INFLUENCE OF WINGTIP DESIGN

H. Zimmer

Institute for Aerodynamics and Gas Dynamics
University of Stuttgart

1. INTRODUCTION

/13*

Modern aircraft development has recently had to be more attentive to matters of economy and environmental stresses, which means, among other things, attaining the lowest possible fuel consumption and noise levels. One might assume that there already was an awareness of all of these essential considerations in the field of aerodynamics and that they had been applied to aircraft development. But the latest research in this field shows that, in contrast to this assumption, there is still great potential for improvements, optimizations and the application of individual effects.

Within the context of total aircraft development, aerodynamics must be seen in connection with other criteria, e.g., the structure's stability and weight. In general, for example, an aircraft for any given purpose should have the lowest possible drag and thus the lowest possible weight. The purely aerodynamic aspects will predominate in the present work, however.

Seen aerodynamically, there are numerous potentials for improving an aircraft design. Attempts have been made, for example, to lower surface friction by laminar condition of edge surfaces, or to reduce interference drag through an appropriate design. From a flight mechanics perspective, consideration should be given to lowering trim drag by special measures, as, for example, so-called active controls (see, e.g., R.T. WHITCOMB [1] and W. PFENNINGER [2]). In addition, there are other notable possibilities for improving the power system. Thus, in recent years there has been an intensified effort to develop a propeller drive with a view toward improving its efficiency (see, e.g., I.U. BORCHERS, F.X. WORTMANN, H. ZIMMER et al. [3]) and expanding its range of application to high subsonic velocities (see, e.g., R.J. JERACKI, D.C. MIKKELSON, B.J. BLAHA [4]).

The main concern of the present work is a critical discussion of the possibilities for reducing induced drag. A significant part is played here by new - presented here - studies in the design of wings, and particularly of outer wing tips.

*Numbers in the margin indicate pagination in the foreign text.

Since induced drag accounts for about one-third of total aircraft drag in cruising flight and as much as one half in climbing, it is valuable to look more closely at this drag element to highlight the possibilities and limitations for its reduction. Although the essential pertinent principles were provided in early aviation research, specifically by L. PRANDTL, A. BETZ and C. WIESELSBERGER [5] as well as by M. MUNK [6] /14 (also see the outline in R.T. JONES [7]), the current work presents a reconsideration and critical appraisal of various model designs so that their most useful points might be applied to wing design. These questions are particularly important to understanding the background of civilian aircraft projects because an aircraft is made most economical only by those wings that produce the least drag at likewise the lowest weight and finishing costs. The amounts of finishing costs and weight shall be given consideration here, however, only secondary to establishing the most important aerodynamically relevant parameters. For that reason, the flexing moment of the wing root will be looked at first together with the flooded surface, and then attention will be given to the very simplest designs with broadly developable surfaces.

A two dimensional flow profile appears inside a wing stream. In the peak area, however, where the strongest drop in circulation and thus the most intense wake vortex occurs, the flow is changed most strongly into a three-dimensional rotation. For this reason, the present work particularly stresses the effect of wing tip designs on the circulation around the wing as regards induced drag.

In the following material there are short introductory remarks regarding the most important classes of fixed-wing aircraft designs as regards the aspect ratio, and a few remarks about rotary-wing aircraft designs. Then an overview is presented of previously studied wing designs, and particularly wing tip designs. In connection with the conclusions derived from these observations, various planar wings with systematically varied wing tip designs are given theoretical consideration. A few selected planar and nonplanar wings are then examined both from a theoretical and an experimental viewpoint. From observations on the energy in the wing wake there follows the important determination of the limits of a possible reduction of induced drag. This leads to conclusions generally applicable to wing design.

In wing development, essentially three classes of wings can be differentiated: wings of wide span, wings of moderate span and wings of short span. In terms of aircraft types, consideration is first given to fixed-wing designs (see Table 1).

ORIGINAL PAGE IS
OF POOR QUALITY

/15

① FLUGZEUG	b [m]	Λ	$\frac{A}{b}$ [$\frac{kg}{m}$]	Klasse ④	Antrieb ⑧
② Segelflugzeug	15 - 25	15 - 25	~ 30	große Streckung	} Propeller
③ Sportflugzeug	6 - 10	6 - 8	~ 120	} ⑤	
DO 228	16,97	9,0	330		
DO 24 TT	30,0	9,0	470	} mittlere Streckung	} ⑥
TRANSALL	40,0	10,0	1280		
ELECTRA	30,2	7,5	1740		
DC-9 S80	32,87	9,62	1930		
A 310	43,9	8,8	3000		
A 300	44,84	7,73	3510	} kleine Streckung	} ⑦
B 707	44,42	7,06	3400		
B 727	32,92	7,07	2880		
B 757	37,95	7,77	2740		
B 767	47,24	7,9	2880		
DC 10	47,4 - 50,4	6,8-7,5	5500		
B 747	59,64	6,96	6230		
C-5A	67,88	7,75	5200		
CONCORDE	25,56	1,7	7250		⑨ } Strahl-antrieb

Table 1 Wingspan b, Extension Λ , and span loading A/b of various aircraft (A = lift)

Key: 1) Aircraft; 2) Glider craft; 3) Sport plane; 4) Class; 5) Large extension; 6) Moderate extension; 7) Small extension; 8) Propulsion; 9) Jet propelled.

a) Wings with large extension ($\Lambda = 15 - 25$ and more)

Primary in the large extension group are glider aircraft, although special long-distance or high elevation reconnaissance aircraft, for example, occasionally have such a wing design. The span loading of these wings is very low, i.e., lift per meter of wing span, and therefore the induced drag is also very low (see Table 1). The wing flow is primarily determined here by the two dimensional flow profile. It is therefore essentially the profile that determines the efficiency of this type of aircraft. Helpful studies and developments in this field were done by F.X. WORTMANN [8], [9], and J.W. SLOOF, and F.X. WORTMANN and J.M. DUHON [10]. Several profiles have been developed that have been successfully applied internationally. A compilation of such profile types can be found, e.g., in D. ALTHAUS and F.X. WORTMANN [11]. R. EPPLER [12], [13] has also worked in this area, among others.

This aircraft class can be regarded today as being essentially almost fully optimized since the knowledge of aerodynamics has been applied to it. Optimal gliding values (i.e., ratios of lift to drag) of 40 to 50 have been attained. No other class of aircraft can even approximate these values. And yet attempts are still being made toward improvements, particularly through wing tip design (tip plates, winglets).

/16

P.F. SELINGER [14] reports, e.g., on a test with 0.65 m high wing tip plates, which, however, produced no measurable advantage; in another instance 1 m high winglets produced a slight improvement at lower velocities but a drop in performance at high speeds. Careful individual studies must be made to determine whether such "winglets" are practical on glider aircraft. Theoretical studies have generally shown, according to P.F. SELINGER [15] in particular, that a winglet must be about 1.5 m high to achieve the same improvement that can be gained by horizontally lengthening the wing 1.5 m. The problematic connected with tip plates will be dealt with further below. We expect that the effects of these modifications are relatively small here because a wing of greater extension has a relatively small wing tip area and therefore is only minimally important. Nevertheless, there can be cases in which even minimal improvements are valuable.

b) Wings of moderate extension ($\Lambda = 6 - 12$)

Nearly all of the aircraft used in general aviation fall into this category (see Table 1 above). The aircraft in this category should offer the greatest possible usage over the longest possible period at a given weight or given installed efficiency. Since these aircraft are propelled with a span loading that, in the case of propeller aircraft, is 4 to 50 times larger than that of gliding aircraft, and in the case of jet propelled planes as much as 60 to 240 times larger, they require these mid-size extensions in cantilevered construction for reasons of structure and weight. Wings with large extension are only possible up to a very limited aircraft weight because as aircraft size increases, mass increases at roughly the third power of the linear measurements. In contrast, wings of middle extension can be used economically at relatively low to very high aircraft weights.

Contouring is very important with wings of moderate extension, as it is with wings of large extension. New contour families have been developed recently, particularly the so-called "super critical profiles" (see, e.g., R. WHITCOMB [16], D. OSWATITSCH, D. RUES [17] and E. STANEWSKI, H. ZIMMER [18]), /17 which have made possible improved performance at high subsonic speeds. Several design characteristics of these profiles have provided clear advantages at moderate and low velocities as compared with the profiles previously used on wings in this class. A successful contour design of this type is presented, e.g., by D. WELTE [19].

Flow in the high range has a clear effect on wings of moderate extension. The contour design of the wing must therefore be given just as careful consideration as the profiling to achieve the most aerodynamically advantageous wing. The wings of this group are of central concern in the present study.

c) Wings with small extension (Λ below 2 - 5)

The area in which two dimensional profile flow occurs scarcely exists in wings with small extension, i.e., the entire flow around the wing is a complex three dimensional process. Such wings are primarily used when supersonic flight capability is required (typical example: the "Concorde" aircraft, see Table 1 for relevant data) and when extreme structural loads must be tolerated (e.g., in maneuvering flights of military aircraft). Because of their fully different purpose, these wings shall not be considered here.

Rotary wings make up a special wing group. These will be considered here only extraneously, yet their importance demands that they not be fully forgotten. These wings can be divided into various groups similar to fixed wings. See Table 2.

①	DREHFLOGEL	D [m]	$\frac{P}{F} \left[\frac{\text{kW}}{\text{m}^2} \right]$
②	WINDKRAFTANLAGE	6 - 100	0,1 - 0,35
③	HUBSCHRAUBER		
	BO 105	9,84	8,2
	MIL 10	35	8,5
	SIK. CH 53 E	24,08	18,0
④	NIEDERGESCHWINDIG- KEITS-PROPELLER		
	DO 27	2,13	54
	DO 228	2,73	91
⑤	HOCHGESCHWINDIG- KEITS-PROPELLER		
	DO 335	3,3	150
	TRANSALL	5,486	190
	ELECTRA	4,11	276
	PROPFAN	~ 3,0	~ 380

/18

Table 2 Diameter D and power load P/F of various rotary wings (P = output, F = rotation plane)

Key: 1) Rotary wing; 2) Wind driven arrangement; 3) Helicopter; 4) Low velocity propeller; 5) High velocity propeller.

The characteristic parameter here is the power load (P/F = ratio of rotor output i.e., power efficiency, to the rotation plane). In accordance with this, four essential groups can be identified, i.e., the rotors of wind driven crafts with a horizontal axis, most closely comparable to gliding craft wings; then the helicopter rotors with 20 - 50 times the power load; low speed propellers; and finally high speed propellers with 150 to 300 times, or even over 1000 times the power load.

Analogous to fixed wings, the fineness ratio of the blades must be lowered in rotary wings as loading increases, and therefore the flow around the blade tips and thus blade tip design becomes more important. While blade tip design becomes less important on a wind driven craft, for example, (not assuming that even the smallest improvement can become interesting over the long term) there is a clear effect on helicopter rotors and especially on propellers (see H. ZIMMER [20] and [3] above in this regard). In contrast to fixed wings, the influence of /19 wake layers on rotary wings is intensified because they run relatively close below the on-coming blades, particularly during hover and limited forward motion.

2. OVERVIEW OF PREVIOUSLY STUDIED WING DESIGNS AND PARTICULARLY WING TIP DESIGNS /20

2.1 In general

The following primarily phenomenological section sketches and discusses the most important previously studied designs of wings and particularly wing tips. The final comparative remarks will then lead to a few important conclusions.

Numerous different wings with very different tip designs have been developed and built during the now more than 80 year history of aviation. A good overview is presented, e.g., by S.F. HOERNER [21] and S.F. HOERNER, H.V. BORST [22]; T.E. DeWITT, E.E. BULLARD [23] have compiled the most important developments. The following section discusses typical wing tip designs in the context of a certain classification. This is then expanded to or compared with the basic elliptical wing and special wing designs.

2.2 Planar designs

The simplest wing tip design, namely that running in the direction of the main current, is still used relatively often today (a typical example is the "B 747" aircraft). This basic design, essentially kept intact but more rounded, is represented by the so-called "Goettinger wing tip" which B. REGENSCHNEIT [24] studied closely. This wing tip design is still the most widely used even today.

Recently a turned-under tip design has appeared, on which the outer wing edge runs essentially in the direction of the current and has a sharp edge. Fig. 1 shows this design from "JANE'S" [25], P. 311-313; in addition, the course of the retreating edge vortex is also shown.

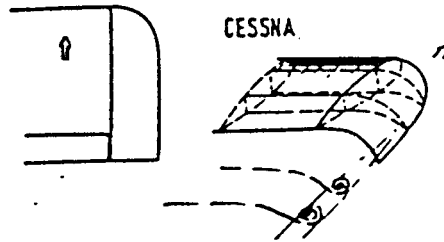


Fig. 1 Turned under, sharply edged wing edge also showing the course of the edge vortex.

Some water tunnel tests (see H. ZIMMER [26]) have led ^{/21} researchers to the conclusion that this design keeps the edge vortex directly behind the wing out far, i.e., in the area of the wing tip. A notable effect on wing drag, however, is not known.

In the beginnings of aviation, wings with backswept wing tips appeared occasionally. A similar design used today is shown in Fig. 2 (compare [25], P.245).

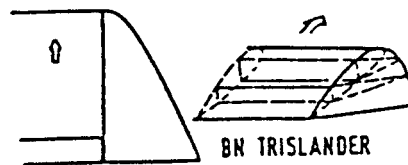


Fig. 2 Backswept, sharp edged wing tip having a soft V and raised local incidence, from [25] P. 245.

Here the nose of the wing tip is constructed with a relatively sharp edge and inclined more sharply than the rest of the wing. Its effect on wing drag is not known, but a clear effect on wing performance does exist (e.g., on the side roll moment) because the sharper incline and V of the wing tip raises the advancing wing during side slipping.

With the appearance of aircraft able to cross the sound barrier, the wing tip of D. KÖCHEMANN [27] gained importance; it is used frequently today. As Fig. 3 shows, this wing tip represents a hyperbola-like rounding of the base.

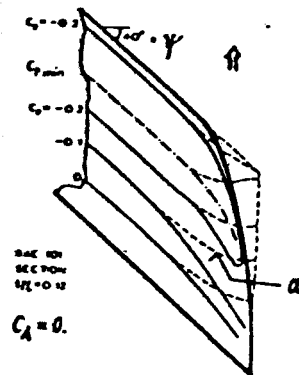


Fig. 3 Isobars in the peak area of a delta wing. Broken lines: Isobars in trimmed wing tip with constant profile. Unbroken lines: Isobars on a "KÖCHEMANN-wing tip". (From [27])

This design makes it possible for the isobars to maintain the sweep angle even in the peak area of the wing. The otherwise common elimination of the sweep in the isobars (example a in Fig. 3) actually causes the premature occurrence of what is called tip shock, which might arise at high subsonic speeds when a localized supersonic field occurs on the wing approximately from the front edge to isobars a and is occluded by a shock wave. Since isobar a has practically no sweep on the exterior, a perpendicular shock occurs at that point, while an angled shock occurs from further in toward the rear. However, since a perpendicular shock intensifies throttling more than an angled one, circulation detachment would occur first at the trimmed wing tip, with all of the detrimental results.

2.3 Nonplanar designs, simple

Even during the very early stages of aviation research, it was understood that end plates could significantly reduce induced drag. As far back as 1898, F.W. LANCHESTER was awarded a patent for installing wing end plates. But it took to the present for this idea to be fully developed in application.

The effect of an end plate can be described somewhat as /23 follows: At the outermost wing tip, the current is affected by a strong rotation at the height of the trailing edge as a result of the receding vortex; this is manifested in the current outside the wing tips being directed obliquely upward, and above the wing tips being directed obliquely inward. This kind of end plate arrangement is meant to exploit the rotating current to produce propulsion, i.e., reduce drag. The rotation of the wing wake is slightly reduced.

R.H. WHITCOMB [28] created the design shown in Fig. 4. It is used serially on four smaller business jet aircraft in the designs shown or in slightly modified designs (see the descriptions in [25], p. 114, 342-343, 354), or its application is foreseen (see K.J. MINDNER [29]).

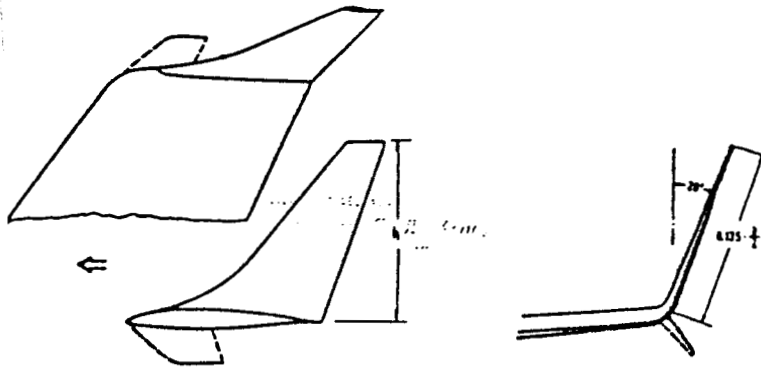


Fig. 4 Basic end plate design by R.T. WHITCOMB [28] ("Winglet"). Relative end plate height h/b (h = end plate height, b = wing span).

This basic design was tried on two large transport jets in a test phase (see K.K. JSHIMITSU [30] and McDONNELL-DOUGLAS [31]). An important goal for developing this end plate design is creating the potential for subsequently re-equipping transport aircraft already in use in order to improve their commercial ^{/24} value vis-a-vis rising fuel costs. The "KC 135" (mod. "B 707") and "DC 10" aircrafts were selected for this trial re-equipping. G.W. HANKS [32] had previously conducted extensive preliminary studies on the "B 747". A comparison of the aircraft mentioned earlier in Table 1 makes it obvious that these aircraft belong to that group of wings with very high span loading at relatively low extension, and thus with relatively high induced drag. Based on the above discussions, the outlook for a successful application of appropriate end plates appears good on . As H. ZIMMER [33] has shown, a 5 to 6% improvement in the gliding ratio can be expected in the case of the "KC 135". In any case, the outer wing must be strengthened so that the aerodynamic gain is partially compensated by the added weight. In the case of the "DC 10", a very slight modification of the wing structure might suffice instead of larger end plates -- the name "winglets" has been introduced for the more modern types ($h/b = 0.0835$ as opposed to 0.062 , see Fig. 4 above). One can deduce from Table 1 above that the span loading of the "DC 10" is notably higher than that of the "CK 135", which could explain the choice of taller end plates. In spite of that, "McDONNELL-DOUGLAS" [34] calculated an improvement in the gliding ratio, i.e., fuel savings, of only $2.5 \div 3$ %. (However, no advantage was determined in the first flight test phase.)

In general, therefore, it can be said that although the winglet design discussed above certainly offers a definite improvement, it cannot yet be declared optimal. J.E. HACKET [35] presents the configuration shown in Fig. 5 as the optimal design.

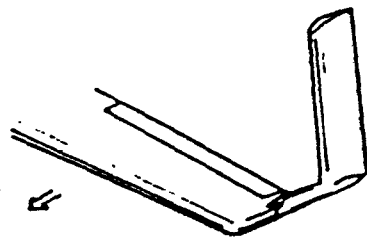


Fig. 5 End plate turned inward ("vortex diffuser"). Optimal design by J.E. HACKET [35].

In contrast to R.T. WHITCOMB's design (see Fig. 4. ^{/25} above), the end plate, which also here has the form and size of an additional wing, sits further back on top of a post and is intentionally turned inward. The aerodynamic cross-wind force (lift) of the added wing thus acts inwardly and has a downward component which serves to free the root flex moment of the wing. (In any case, it means a reduction in total lift which must be balanced out, for example, by a change in the wing's angle of incidence.)

A disadvantage of both of the configurations shown is that the added mass of the end plate rests relatively far behind the flexible spar of the wing. This adversely affects this spar's aero-flexible behavior.

Relative to this issue, it is interesting to note that, as indicated by Table 1 above, both aircraft manufacturers took a new and, as will be shown further below, a more effective approach in their later models ("DC 9 - S 80" or "B 757", "B 767"), namely that of enlarging the expansion while simultaneously drastically reducing the span loading. According to B. SWETTMAN [36], a "more traditional" flat wing of large extension with nearly 30% greater span is foreseen as the successor to the "B 747", which according to Table 1 above has the highest span loading of all commercial aircraft (except the "Concorde"). In addition, the successor to an existing smaller business jet with end plates (see [25], p. 114) also has a flat wing of large span and extension (see "ISRAEL AIRCRAFT INDUSTRIES" [37]).

2.4 Nonplanar designs, multiple sectioned

In addition to the large surface winglet types discussed above, a number of end designs have also been studied which are made from several individual wings, a design which is familiar to us from the large land soaring birds. We are reminded, for example, of the work of C.D. CONE [38], J.J. SPILLMAN [39], [40], D. HUMMEL [41] and G. LÖBERT [42] and on the previously mentioned work of W. PFENNINGER ([2]) and H. ZIMMER [33].

In his groundbreaking work, C.D. CONE ([38]) indicates that within his mathematical model the natural fanned wing design has only about 75% of the induced drag of an elliptical wing. CONE also presents structures similar to end plates that attain even lower percentages.

W. PFENNINGER ([12]) came to comparable conclusions and /26 suggests the wing tip design shown in Fig. 6 as a technological solution.

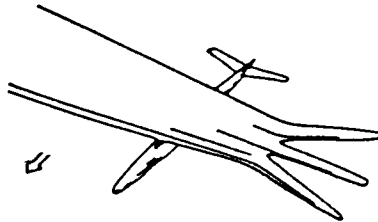


Fig. 6 Suggested technological solution for a wing with fanned ends per W. PFENNINGER [2]. The frontal partial wing is anhedral, the rear one dihedral.

D. HUMMEL ([41]) reports on exhaustive theoretical and experimental studies on wings with two or three individual wings at the ends, similar to the configuration shown in Fig. 6. The work contains extensive load dispersal measurements and detailed optimization studies, and presents a theoretically derived reduction of the induced drag to 86% as compared to an elliptical wing for one of the configurations studied.

G. LÖBERT ([42]) offers the forked points shown in Fig. 7 as an optimal wing end design based on theoretical studies.

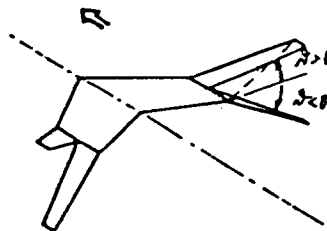


Fig. 7 The wing with forked points per G. LÖBERT [42]. The frontal partial wing is dihedral, the rear one is anhedral.

Depending on the position of the point of the Y and the angle of incidence of the partial wing to the wing surface (V-angle), LÖBERT reports a reduction of the theoretical induced drag to 60% of the value of the planar elliptical wing.

I. RECHENBERG [43] likewise reports on theoretical and 27 experimental studies on wings with fanned edges. In accordance with his deliberations, RECHENBERG concludes that the induced drag continues to drop as the tip vortex is divided into more sections. Accordingly, the wing with forked points per Fig. 7 has about 61% of the induced drag of a planar elliptical wing; a wing with three individual wings, approximately that design shown in Fig. 6, has only 45%, and an analogous design with six individual wings (or sweep feathers) has only 26%.

In general, therefore, it can be concluded that multiple sectioned, nonplanar wing end designs, at least from an aerodynamic perspective, can offer notable possibilities for reducing drag.

Only relatively few data, however, are available on measurements of wings with nonplanar, multiple sectioned edges. See, for example, the previously quoted works by SPILLMAN ([39]), HUMMEL ([41]) and ZIMMER ([33]). The initially very surprising conclusion is that an induced drag clearly below that of an elliptical wing of the same effective extension, has practically never been measured. Far more commonly, only those designs prove optimal -- as shown by their technical realization and measurement in wind or water tunnels -- which take natural principles into consideration. If these principles are insufficiently satisfied, than the results are more likely to be significantly worse than those obtained with conventional flat wings. H. ZIMMER ([33]) presents a few examples of this. It therefore seems reasonable and worthwhile to consider basic natural principles in the technological development of wings and at least to assess their value critically.

Previously, only J.J. SPILLMAN ([39]) had developed and successfully flight tested a few specialized, multiple sectioned tip designs which approximate the principal relative to natural forms. The design shown in Fig. 8, for example, had only 84% of the induced drag of a flat elliptical wing but had the same span as the original, unmodified wing. However, if drag is related to the actual greater span or extension of the modified wing, then a "subelliptical" induced drag is not attained. This situation is explored below in more depth.

28

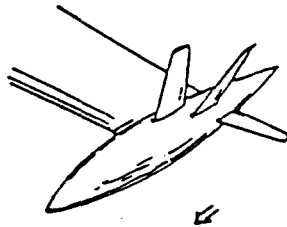


Fig. 8 A multiple sectioned wing tip design successfully flight tested by J.J. SPILLMAN [39].

The nonplanar tip designs mentioned so far have the common characteristic that the zero drag of these wings is larger than that of the original wing and that the desired reduction in drag begins only when a lift correction value of approximately $C_A = 0.04$ is exceeded. Only H. ZIMMER ([33]) reports, among other matters, on a two wing design which does not create additional drag even at a relatively low REYNOLDS-value in wind tunnel measurement.

2.5 The elliptical wing

Since the early days of aviation research the elliptical wing has been actually and scientifically considered the aerodynamic optimum against which all other wings are measured. Using a variation principle, B.M. MUNK (see [6]), for example, has proven that a wing of a given lift and a given span will manifest the minimal induced drag when the totality of all free vortices at the wing, represented by a straight-line primary vortex, induces a constant downward current. That is true in the case of the dispersion of elliptical lift. (An "elliptical wing" is to be understood primarily as one with elliptical lift dispersion. The elliptical wing structure that also results where torsion is absent from the basic theory is only of secondary importance. In his mathematical model, however, MUNK had to assume a constant downward current throughout the entire wake, i.e., a rigid vortex layer, because to determine drag, the flow around the wing is restored to the level circulation of the cross section by the wake in the so-called TREFFTZ plane. It is known, however, that as it is more precisely and ever more ^{/29} closely described, dispersion of the circulation in the wake vortex trail features a vortex strength that formally exceeds all limits, because it corresponds to the curve of the elliptical circulation dispersion at observed points on the wing. A vortex layer within this circulation dispersion does not retain its original level form, of course, but immediately rolls inward from the edges, which A. BETZ [44] had mathematically formulated (this will be referred to again later). While BETZ observed this rolled edge vortex far behind the wing, B.V.J. ROSSOW [45], for example, recently described the roll process itself using numerical methods, as Fig. 9 clearly shows.

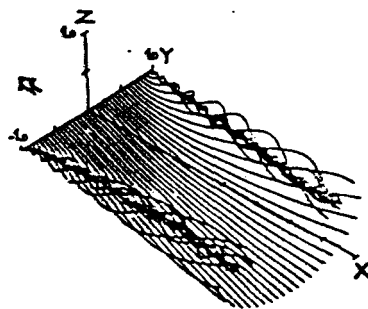


Fig. 9 The rolling of a vortex layer behind an elliptical wing, from V.J. ROSSOW [45].

In practice, the rolling of a tip vortex has a relatively small effect on drag in the case of ordinary wings of large extension (in accordance with Table 1 above), and a computational model with rigid wake will generally suffice. Nevertheless, inherent to this model is its incongruity or approximative character as shown. But this model is too simple for the interdependent relationships of the actual flow with nonplanar wake, and it is particularly inappropriate for the current study to consider it alone; the above-mentioned differences between theoretical design expectations and experimental results, in particular, must also be explained.

2.6 Natural wing designs

/30

When attempting to reduce drag in primary wings, it is useful to devote particular attention to wing designs in nature, as indicated earlier. Experience has generally shown that so-called "optimal designs" are the rule in nature, where the elliptical wing does not exist. The wings of large soaring birds, for example, have ends that either are relatively pointed, sweep backwards, or are fanned, as G. RUPPEL [46] has shown. Likewise, the fins of fast swimming fish also run in backward sweeping points, as B.H. HERTEL [47], for example, has shown.

Wind tunnel tests by C.D. CONE [48] and the previously mentioned water tunnel tests by the author [see [26]] have shown that typical bird wings do not have definite edge vortices like those familiar in fixed wings. Rather a relatively large wake is set into slow rotation behind the bird's wings. The circulation of the wake is almost fully dissipated after only a few chord lengths, while fixed wings, in my opinion, have very long lived wake vortices. Only when a single flight feather is removed intentionally from its natural position in a bird wing with a fanned edge, does the familiar edge vortex occur, as CONE [see [48]] has proven.

This situation -- to a certain extent the "paradox of the bird wing" -- has never been mathematically-physically described before. However, in the present context it is considered essential for understanding the mechanism of induced drag. This work shall therefore also examine the extent to which it can be applied to the design of a primary wing.

2.7 Deductions from the present studies

It is notable that for all the above mentioned known studies on wing tip designs, nearly all of the authors arrived at different optimal designs although they used essentially the same mathematical model, i.e., the unchanging rigid vortex wake. Disregarding the essentially pure planar designs, R.T. WHITCOMB concluded that the end plate that leans slightly outward is optimum (see Fig. 4 above), while J.E. HACKETT recommends the version that leans slightly inward, per Fig. 5. G. LUBERT considers the widely spread forked points per Fig. 7 as the best

design, while the author's opinion is that the only slightly /31 spread-out slotted design is the superior one, as will be shown further below. In contrast, W. PFENNINGS, D. HUMMEL and J.J. SPILLMAN indicate that the best configurations are those that are comparable to the tips of the feathered wings of land-based soaring birds, with three or, per I. RECHNEBERG, even more winglets. And finally, K.-H. HORSTMANN [49] concluded that an end very similar to the one developed in the current work (e.g., that of aircraft "DO 228"), and the wing tip designs comparable to those of ocean-based soaring birds are more effective on a commercial aircraft wing than lengthening the wing or even the winglet arrangement per Fig. 4 above. This conclusion will be considered again later.

The very different conclusions described as well as the strongly divergent data on possible reductions of induced drag recommend a closer look at the total issue. The conclusions that have been sketched cannot be translated as they stand into an overall wing design. To date there has been insufficient attention given to the fact mentioned above that induced drag has practically never been measured on a fanned wing edge, as opposed to end plate configurations. Particularly deserving of attention and discussion is the fact that A. RASPET [50] has not detected "subelliptical" induced drag even in land-based soaring birds in flight. For this wing represents a high grade nonplanar system, and according to common calculations with fixed vortex wake planes (e.g., per C.D. CONE [38] above), it would have to have a significantly smaller induced drag than the planar elliptical wing of equal span and equal lift.

Placing too much emphasis exclusively on MUNK's model has given rise to great hopes for nonplanar, multiple sectioned wing designs, but has provided no explanation as to why the anticipated positive results have not been achieved. This model cannot even be used to explain the deviation of natural wing designs from "optimal" elliptical wings.

To shed some light on this issue, therefore, other mathematical models should be compared to the MUNK model. Reinterpreting and recombining two familiar models, can help explain the described "paradox of natural wing designs." In /32 addition, the extent to which induced drag can be reduced under realistic physical conditions will be discussed using the results gained.

3. THEORETICAL STUDIES OF VARIOUS PLANAR WINGS WITH /33 SYSTEMATICALLY VARYING WING TIP DESIGNS

3.1 Fundamentals

Various typical wing designs will be examined from a theoretical perspective in this section. First is a calculation by C.W. LUCCHI [51] using a vortex net procedure which the author

has slightly modified for calculation purposes to make possible a simple representation of even complex, multiply constructed, nonplanar wing systems. For this, the skeleton of the wing system is represented by a vortex network (see Ill. 1). The wing is divided into a number of surface elements. An attached cross-vortex is positioned on the 25%-line of these elements, and the control point is in the middle of the 75%-line. The attached axial vortices coincide with the lateral edges of the surface elements; only at the wing's lateral outer edge are the vortices set in about one-quarter of the element's width since the flow around this edge is comparable to that of the leading edge. As Ill. 1 shows, triangular surface elements are also possible for creating occasional changeovers into smaller subdivisions. The attached axial vortices continue as free wake vortices, the wake being nonplanar since it soon bends in the direction of the free flow (see Ill. 1). The circulation of individual vortex elements is determined in such a way that the precondition for tangential downward flow is fulfilled at every control point which contributes to the solution of a coupled, linear equation system. The fluid forces and correction values are determined by the integration by the forces of all the vortex elements. Thus, induced drag in particular does not result, as is otherwise common, from the downwind integration of the TREFFTZ planes far behind the wings (see in this context, e.g., the examples by K. BRIEDEN in A. EHRHART and H. FRANKE [52] or J.H. SCHLICHTING and E. TRUCKENBRODT [53]. [54]), but by the integration of the fluid forces at the wing itself, as happens with the force effect in the physical process.

The procedure described was selected to provide the most realistic mathematical model of the physical flow of the primary wing. Although it is a procedure that can be considered relatively complex, it has proven to be both appropriate and even necessary, for the effects that appear in connection with the optimization of wing tip designs are relatively small, and an oversimplified mathematical model can easily lead to false approximations of the actual relationships.

The earlier common approach using the so-called TREFFTZ ^{/34} planes far behind the wing did not directly address the basic design of the wing because its sole concern was the distribution of the flow. The basic design must have a clear effect, particularly in the peak region, however, for according to the BIOT-SAVART law (see, e.g., the examples of A. WEISE in J. FRANKE [55]), the downwind, which is induced by a free vortex at an attached vortex, changes with angle σ which characterizes the position of the latter (see Ill. 2). According to this simple consideration, then, the localized downwind w in the peak area would have to become smaller with a sweptback wing tip.

A few typical planar wing designs are compared with one another below using the described computational process, wherein, in accordance with the above discussion, the basic design directly influences the result. Because of the computation time

necessary, very fine changes in the wing were not computed; however, the results described below demonstrate that the discretions that were chosen were sufficient to make possible the intended comparison of the individual wing designs.

The most important results from the computations of six typical wings that the author also studied for the purpose of developing a "technologically new primary wing" (TNT) for "general aviation" aircraft (see [56] and [57]) are compiled in Ill.'s 3 and 4. Ill. 3 shows the basic results regarding lift and Ill. 4 those regarding induced drag. None of the wings are warped or vaulted, and all have the same extension $\Lambda = 7.05$. The following wing designs were involved: the elliptical wing (1) for control of the computational process, the rectangular wing (2) and three wings that consisted of a rectangular base of extension $\Lambda_b = 4$ to which nearly triangular tip pieces of various sweeps were added; (straight leading edge (3), straight trailing edge (4), sweptback trailing edge (5)). In addition, a part of the base of wing (6) was also sweptback. (Notations (1) through (6) apply to Ill.s 3 and 4, as well as to all subsequent illustrations.)

The connection between lift A (or C_A) and drag W_i in Ill. 3 and Ill. 4 is clarified by Fig. 10.

/35

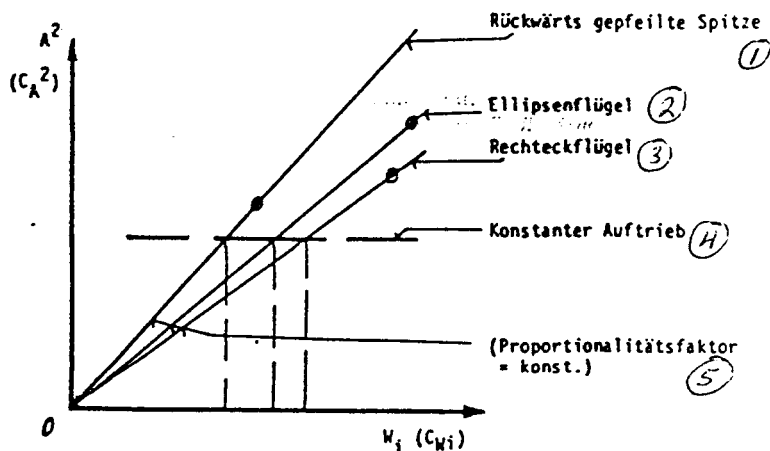


Fig. 10 Qualitative relationship between lift and drag in Ill.s 3 and 4 (Points: Observed examples)

Key: (1) Backswept ends; (2) Elliptical wings; (3) Rectangular wings; (4) Constant lift; (5) (Proportionality factor = const.)

According to the relationship in Fig. 10: W_i is qualitatively shown proportional to A^2 (i.e., C_{W_i} is proportional to C_A^2) axes with constant proportionality factor. (Also see equation (1) below.) Because the calculations to Ill. 3 and Ill. 4 were done for a constant angle of incidence,

the values of A (i.e., C_A) and W_1 (i.e., C_{W1}) vary for the individual wing designs, which the points entered in Fig. 10 clarify. In the context of the present study, then, the comparison of the proportionality factors (including x_{e11}) at constant lift A (i.e., C_A) is interesting.

The considerations that led to the design of wing type (4) are presented here in greater detail as an example. The author's observations of flows in a water tunnel showed that where the sweep of the wing's outer edge exceeds about 55° , there is the tendency for a very pronounced separation vortex to develop at the bend of the leading edge (comparable to the flow picture of a delta wing). Thus, the sweep angle must be clearly smaller than this value. From a construction perspective, however, in the sample cases dealt with here the tip was extended only the length of a wing chord in the direction of the span to make the angle of the leading edge sweep angle approximately 45° . A continuous straight trailing edge is advantageous for installing ailerons or flaps. The largest possible tapers were selected so that the largest possible extension could be gained for a given surface.

3.2 The lift of the wing types under study

/36

The vortex nets of the six wing types under study are shown under a) of Ill. 3, and under b), the load dispersion of three characteristic sections at a $= 10^\circ$ angle of incidence in the direction of the chord (x -direction); (interior section: dot-dash line (a); about two-thirds half span: broken line (b); exterior section: unbroken line (c)). In addition, localized lift correction values are entered under c), and circulation distribution under d). The total lift correction value C_A which is also presented here allows certain conclusions to be made regarding the increase in lift of each wing. Since all of the wings have the same extension and the same area where the spans are equal, the correction value presented for the root flex moment C_{MB} , and particularly its gradient above the lift correction value dC_{MB}/dC_A , is a direct measure for the wing's weight.

Load distribution in the elliptical wing (1) is equal in all sections per the rigid wake model, and the localized lift correction value is constant. With the discrepancy that appeared with the nonplanar wake per Ill. 1, a slightly raised suction point as compared to the interior section is evident in Ill. 3 under b) outside, and there appears to be a slight drop in the lift correction value in Ill. 3 under c). The deviation of the circulation distribution from the ellipse, however, is negligible (see Ill. 3, under d).

By contrast, the rectangular wing (2) features a sharp decline in load distribution and in the localized lift correction value. However, due to the large chord length outside, circulation distribution is higher there than the elliptical one; this is manifested in a raised root flex moment at a given lift.

This wing therefore has a higher weight than the elliptical wing. A comparison with the values of the remaining wing types in Ill. 3 further shows that the rectangular wing definitely has the higher weight of all the types.

The tapered designs (3) to (6) have in common the feature that the minima of load distribution and local lift correction values lie at the point where the end assembly is joined, and the maxima are at the exterior section. Load distribution is the most uniform for wing (3). The drop in circulation begins relatively early here. This wing is therefore the lightest of all the wing types.

The difference in lift behavior of the sweptback designs (4) through (6) is only slight. The maximum of the local lift correction value in the exterior section is quite high so that a burble occasionally begins here. It is noteworthy that the aerodynamic loads of the sweptback wing tips are higher than they are at the same taper as wing (3). From their lift behavior, therefore, the foreswept points of wing (3) appear to be quite advantageous. This might be the reason that such design have been the ones most studied for helicopter rotors. (See in 37 this regard, for example, J.D. BERRY and R.E. MINECK [58] and G.L. BENDER et al. [59]).

It can be deduced from the gradients of the root flex moment that the wing design with foreswept tips (3) - as mentioned earlier - have the lowest wing weight. Then follow wings (5), (6) and (4) with backswept tips that are nearly as heavy as the elliptical wings. The heaviest wing, namely - also mentioned earlier - the rectangular wing, features a weight approximately 6% higher than the elliptical wing.

3.3 The drag of the wings under study

The drag behavior of the wings under study is of primary interest within the current work. Similar in setup to that of Ill. 3, Ill. 4, in addition to the various vortex nets (under (a)), under b), shows the localized oncoming stream angle ϵ at the first attached cross vortex (compare Ill. 1). This oncoming stream angle determines induced drag, which is in fact derived in the present process through integration at the wing itself. (Because of its tendency, ϵ should also be seen as equivalent to the downwind of the primary line theory in a purely planar situation where it is known that the elliptical wing has a constant downwind.) The direction of the oncoming stream of all the other attached vortices lies by definition in the skeletal plane of the wing. Ill. 4 further shows under c) the localized drag distribution in x-direction at the three wing sections described above in Ill. 3. Just as the load distribution in Ill. 3 (under b)) represents distribution of localized lift at the section under study along the chord length (in this case a very crude approximation to the first normal distribution by BIRNBAUM), the drag distribution corresponds to the distribution

of the observed localized induced drag along the chord length (in the physical process the frictional drag element is added to this, too). Finally, Ill. 4 under d) also contains the distribution of localized induced drag along the span and the various overall correction values C_{wi} , as well as their relation to the value of the elliptical wing with rigid wake x_{e11} . (It should be noted that the x_{e11} is related to the computation of the elliptical wing with a rigid wake and does not describe the difference among the wings within the more complex computation used here.)

As the results with elliptical wing (1) indicate, a slight increase can be detected in the upwind (an increase of angle ϵ) at its tip. This manifests during drag distribution Δc_{wi} as a "leading edge suction force" that is greater at the outer section than the inner section (see Ill. 4, under c)); this is subsequently reflected in a corresponding slight drop in the induced drag at the same point (see Ill. 4, under d)).

In accordance with the rigid wake computational model, 38 the upwind and induced drag remain constant over the span of an elliptical wing. This is not the case in the present vortex net computation with surface discrepancy and a nonplanar wake. In spite of that, as ratio x_{e11} demonstrates, the drag gained from the wing integration is practically identical to the value attained from the wake integration with a rigid wake, i.e., one. In the first place, this confirms the above mentioned situation that in practice a computational model with a rigid wake is generally sufficient for calculating "conventional" straight wings of moderate to large extension, and secondly, the result leads to the conclusion that the computational process being used and the discrepancy selected are sufficiently accurate. (Otherwise an obvious unrealistic discrepancy would have to show up in the case of the elliptical wing.) As will be shown further below, this agreement exists only for "conventional" wings, however, i.e., wings that come closest to the conception of a straight primary line. Then there is the case where the foremost primary cross vortex, which features the greatest circulation analogous to load distribution (see Ill. 3), runs along a nearly straight line as in the case of wings (1), (2) and (3). By contrast, in wings (4), (5) and (6), these primary vortices are buckled toward the rear in the outer area producing special effects which will be discussed in more detail below.

Upwind distribution ϵ demonstrates characteristic progressions in wings (2) through (6) being studied in addition to the elliptical wing which are also reflected in the distributions of the induced drag. (Note that ϵ in Ill. 4 (also in Ill. 17) below is positive!) Thus, the upwind decreases toward the outside in the case of rectangular wings (2), corresponding to an increase in induced drag. Minimal upwind appears at the bend of tapered wings (3) through (6). Therefore, the upwind increases again outside the bend and substantially so at the backswept tips.

This tendency of the upwind to be minimized at the bend, however, is relatively weak for wing (3). Overall, practically no increase over the rectangular wing can be detected. Experimental confirmation of this situation can be concluded from the data of BERRY and MINECK (see [58]) who report on a study of a similar tip design on a helicopter. In addition, as BENDER et al ([59]) indicate, the flight performance of the helicopter even worsened as a result of adding these tips similar in design to (3).

It is notable that, according to Ill. 4, there is very /39 little difference among the distributions for all the wings shown under c) of the drag on the three rear facing surface elements. This can be explained as follows: The attached vortices of the rear facing elements are blown against in the plane of the skeletal surface and thereby produce drag. Only the first attached cross vortex produces propulsion corresponding to the so-called "leading edge suction force" of the physical model which, as the drawing shows, acts only upon the leading wing edge. Of course, changes in the discretion change these forces that act upon the individual vortex elements, but the localized correction values and the total correction values are only insignificantly effected, as test computations have shown.

The upwind distributions and progressions of the induced drag of the rear facing tapered tips (4) through (6) are of particular interest. The minima occurring in the upwind at the bends in the frame that produce a point in the induced drag, are directly comparable to the center effect of a tapered wing as studied by the author [60], among others. It is particularly important that the upwind in the point area is strong enough that a component appears in the direction of flight which further causes the points themselves to produce propulsion. As clarification, Ill. 5 shows a sideview of wing (4) and its wake together with the vectors of the localized oncoming flow at the three characteristic cuts a, b and c per Ill. 4. By means of their rear facing position, the tips utilize to a small extent the flow set in rotation by the primary wing to produce propulsion. Accordingly, the same effect, which nonplanar designs per Ill. 4 and Ill. 5 above should use, can also be achieved with wing types (4) through (6), even if only partially. With these planar wings, similar to those of ocean-based gliding birds, 97.6% (wing (4)) or even 95.5% (wing (6)) of the induced drag of the elliptical wing with a rigid wake is attained per drag factor x_{e11} of Ill. 4 (see under d). Such a decrease initially appears astonishing and therefore must be more closely explained below.

4.1 Wing with planar and nonplanar triangular edge

Although the wings examined in the previous section were planar, the vortex systems they represent are not flat. Ill. 6 shows a rear view of the vortex system of Ill. 1 for wings (4) through (6), parallel to the oncoming flow. It shows that the foremost attached vortex, which as previously mentioned features the greatest circulation and primarily determines the induced drag, has a thoroughly nonplanar profile which has a "subelliptical" induced drag. The first comparison, therefore, shall be with the wing having tips swept back at a specific angle and a rigid vortex wake, whose induced drag has already been determined by W. MANGLER [61]. It can be deduced from the results obtained by MANGLER per Ill. 7, that the induced drag of such a wing drops further below the value of the flat elliptical wing of equal span and extension, as the angle of the bend becomes greater. If the vortex systems of the first attached vortices of wings (4) through (6) per Ill. 6 are compared with wings like those whose tips per Ill. 7 are bent downwards so that a cross section of its rigid wing wake has the same form, then two somewhat comparable wings (4) and (6) having a rigid wake have been obtained. Per Ill. 7, these wings have 99.5% (wing (4)) and 98.5% (wing (6)) of the "elliptical" induced drag, while, as mentioned above, wings (4) and (6) themselves per Ill. 4 attain 97.6% and 95.5% of the elliptical value respectively. This result becomes plausible considering that MANGLER's ([61]) calculations did not contain the frame effects discussed in connection with Ill. 4 and 5.

The effect of nonplanarity that has been described in the behavior of wings with backswept tapered tips is relatively small, as the percentages given above show. Since no direct experimental proof of this exists because most wings in Ill. 4 have not been measured in the exact configuration presented there, an indirect proof shall be presented below.

An evaluation of the results of Ill. 3 and 4 shows that wing (4) is the most interesting example. It does not achieve the low weight of wing (3), but has a remarkably low drag and 41 despite its simple design possesses effective nonplanarity. The straight line trailing edge is of great practical importance, as mentioned above, as it greatly simplifies the mounting of ailerons or flaps, etc. For these reasons, wing design (4) was studied more closely. R. FRIEDRICHS and W. HASTREITER [62] manufactured and measured a principle model wing with several interchangeable tip designs. With a view toward developing a light transport aircraft for "general aviation" (see, e.g., B.D. WELTE et al. [63]), this model wing was given an extension of approximately $\Lambda = 9$. Ill. 8, under a), presents the vortex net for calculating this wing analogous to those of wings (1) through (6) in Ill. 4.

As indirect proof of the effective nonplanarity, two configurations are compared in calculation and in experiment, namely, those of planar wing (7) and design (8) with triangular tips turned down at $\alpha = -40^\circ$ (see Ill. 8 under a)). Since both wings are supposed to have the same span and extension, the rectangular portion of wing (8) is somewhat longer than that of wing (7). In accordance with the discussion above regarding Figs 6 and 7, the equivalent comparable wings (7)' and (8)' with a rigid wake per Fig. 7 would have an induced drag of 99.6% or 93.3% of the "elliptical value". According to the total correction values presented in Fig. 8 under a), which are derived from these calculations with the vortex net process for a nonplanar wake, correspondingly improved values result for wings (7) and (8) as a result of fundamental influences, namely 98.1% of the "elliptical" induced drag for wing (7) and 90.4% for wing (8). If this greater difference in drag values is confirmed by measurements, then the effective nonplanarity described above can be considered actually present, at least in tendency.

Fig. 8 presents the calculated and measured drag and lift measurements for wings (7) and (8), and for better resolution, the drag correction value is represented as dependent on the square of the lift correction value (called the quadratic polar). The difference between the curves of the calculated and the measured values is the friction drag. In the ideal case, this initially remains constant during increasing lift, until it finally increases progressively as a result of separation phenomena. Thus, it can be determined from Fig. 8, b), that in the present case, due to the use of a very thin profile, separation phenomena appear even above the lift correction value of approximately $C_A = 0.5$ ($C_A^2 = 0.25$), noticeable in a kink in the measured quadratic polar. Below this value, however, it runs parallel to the course of the calculated value for a while. It is noteworthy that in this area with adjacent flow, the theoretically anticipated effect, i.e., a clear difference between the values of wing (7) and wing (8), is fully confirmed by the measurements, which proves effective nonplanarity. /42

4.2 The wing with end plates

A configuration with end pieces per D.R. RILEY [64] was studied as an example of a nonplanar wing. The vortex net of the three views of this wing (9) are shown in Fig. 9 together with their adherent quadratic polars by calculation and measurement. The computation reveals that this configuration features only 70.6% of the induced drag of an elliptical wing of equal span, as the value x_{e11} given in Fig. 9, a) shows. (In comparison: a value of 71.5% is obtained by using the theory of W. MANGLER per Fig. 7, (see point (9)' in Fig. 7.) The measurement holds up to a lift correction value of approximately $C_A = 0.7$, i.e., $C_A^2 = \pm 0.5$). At greater C_A values, separation phenomena create a rising divergency (per Fig. 9, b) analogous to the previously mentioned behavior of wings (7) and (8).

The wing with end plates has a very low induced drag relative to its span, as compared to the planar wing with equal extension (represented by the broken curve in Fig. 9, b)), which has been confirmed in experiments to which reference shall be made. This advantage, however, is gained at the expense of the disadvantages of the relatively large end plates (e.g., weight). In view of the general interest prevalent in end plates at that time, as mentioned above in section 2.3, the present example should serve to point out the problematic of end plates by comparing below the results gained here with the results of section 3 above.

4.3 Comparison of "end plate" and "triangular end" wing designs /43

4.3.1 Aerodynamic properties

The greatest interest vis a vis an aircraft is not the lowest possible specific induced drag for which reference to the elliptical wing derives from the "rigid wake model", thus making the value x_{e11} determinant. Of much greater interest is the nonspecific induced drag directly. The equation at a given lift is known to apply to this drag (see, for example, B.A. WEISE [55] above, p.135)

$$W_i = \frac{K_{e11}}{qX} \left(\frac{A}{b} \right)^2 \quad (1)$$

According to the so-called "second" task of the primary wing theory for nonplanar wings, this equation directly states, among other things, that at a given lift A and a given span b , the induced drag W_i reaches its minimum when factor x_{e11} assumes the lowest possible value.

Equation (1) implies that it is generally more effective to enlarge the span, which appears quadratic, than to try to attain a lower specific induced drag x_{e11} , which appears only linearly. The determining factor of induced drag is the span loading A/b , which is therefore included in Table 1 above for the aircraft types presented.

If two different wings deliver the same lift ($A_1 = A_2$) at the same impact pressure ($q_1 = q_2$), then the following applies to their induced drags:

$$\frac{W_{i2}}{W_{i1}} = \frac{K_{e12}}{K_{e11}} \left(\frac{b_1}{b_2} \right)^2 \quad (2)$$

If two wings with different specific induced drags x_{e11} are to have the same induced drag ($W_{i2} = W_{i1}$) at the same lift, then the span ratio of these wings can be obtained per equation (2),

$$\frac{b_2}{b_1} = \sqrt{\frac{K_{cl2}}{K_{cl1}}} \quad (3)$$

Applied to the end plate configurations of Fig. 9 calculated above, equation (3) means that a rectangular wing with about 20% larger span at the same lift has the same induced drag as the above mentioned end plate configuration at a smaller span. If the end plates are then rotated into the wing's plane, as 44 they are in wing (10) of Fig. 10, then a span even 38% larger results. Thus, per equation (2) and given the values from Figs 9 and 10, the following results:

$$\frac{w_{i(10)}}{w_{i(9)}} = \frac{1.007}{0.706} \left(\frac{1}{1.38}\right)^2 = 0.749.$$

This means that with the enlargement of the span of wing (10) it is possible to achieve the same lift (as that of the basic wing (9) with end plates) with approximately a 25% lower induced drag. Even this simple consideration shows that the structural weight of an end plate is used to greater advantage for the wing plane itself. Of course, consideration must be given to the influence on the root bending moment, as will be shown below. Further, by going over to the planar wing, corner drag, which has not yet been considered, disappears.

By rotating the end plates per Fig. 10, the extension of $\Lambda = 4$ (nonplanar) increases to $\Lambda = 5.53$ (planar). This changes the theoretical quadratic polar insignificantly, as a comparison with Fig. 9 shows. The differences calculated above in the induced drags of these wings derives, therefore, from the fact that the wings have different lift correction values as a result of different effective wing surfaces, despite equal lift.

In the context of the present work, the comparison with wing design (4) from Fig. 3 and Fig. 4 is of particular interest. As the structural comparison per Fig. 10 a) shows, an extension of 7.05 is gained for wing type (4) using the same wing base at only 92.3% of the total wing surface, which, according to Fig. 10 b), results in a correspondingly improved theoretical quadratic polar. This wing (4) has been measured by the author (see [56]) with the same profile as wing (9) having end plates per Fig. 9. As Fig. 10, b) shows, a premature burble appears at the wing tips due to the very small REYNOLDS value, so that above a lift correction value of nearly $C_A = 0.5$ (i.e., $C_A^2 = 0.25$), the measurement already deviates from the calculation (diverging curve paths in Fig. 10, b). However, the measured quadratic polar of wing (4) is clearly in a better position than that of wing (9) with end plates (compare Fig. 10 b) and 9 b)). From previously available results, it can be deduced that wing design (4) uses a total given wing surface more aerodynamically than wing (9) with end plates and the rectangular wing which results when the end plates are rotated into the wing's plane.

Aerodynamic properties are not the sole criterion for evaluating a wing in the context of a practical project design, as mentioned earlier. Structural considerations, weight considerations in particular, must be considered. For a wing may be very efficient aerodynamically, but its value is reduced or even eliminated if it is more difficult to use than a comparable wing.

In the context of the present study, the weight of a wing is approximated by a "weight function" G , which is determined by the wing root flex moment M_B at a given lift and the total wing surface F_{ges} . The relative surface for lift is F_B . Thus, the following applies for the wing root flex moment,

$$M_B = C_{MB} \cdot q \cdot F_B \cdot b/2, \quad (4)$$

whereby,

$$C_{MB} = \frac{dC_{MB}}{dC_A} \cdot C_A. \quad (5)$$

The following then applies in the comparison of two wing weights per the given definition of weight function G ,

$$\frac{G_2}{G_1} = \frac{F_{ges2} \cdot M_{B2} \cdot K_2}{F_{ges1} \cdot M_{B1} \cdot K_1} = \frac{F_{ges2} \cdot M_{B2}}{F_{ges1} \cdot M_{B1}} \Big|_{K_2=K_1}. \quad (6)$$

(Note that factors K_1 and K_2 , which depend on the construction method and the material of the wing and determine the actual wing weight, are not of interest in the present study because only wings of equal construction and equal lift are being compared. It can therefore be assumed that $K_1 = K_2$ so that for the present problem, sufficient exact data regarding the relationship of the true weights of wings 2 and 1 are provided in equation (6).)

The data presented in Table 3 compare the weight functions of the three wings considered in Fig. 9 and Fig. 10.

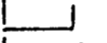
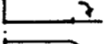
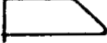
Flügelform (1)	$\frac{F_{Ges}}{F_{Ges(4)}}$	$\frac{F_B}{F_B(4)}$	$\frac{C_A}{C_A(4)}$	$\frac{dC_{mB}}{dC_A}$	$\frac{G}{G(4)}$	$\frac{W_i}{W_i(4)}$
(9) 	1.083	0.784	1.276	0.24632	0.848	1.628
(10) 	1.083	1.083	0.923	0.2177	1.035	1.215
(4) 	1.	1.	1.	0.2098	1.	1.

Table 3 Comparison of wing weight function G per equation (6) and drag W_i per equation (2) of wings (9), (10) and (4) having equal lift. The wing of reference is wing (4). (Compare Fig. 3, 4, 9 and 10.)

Key: (1) Wing design

The first column of Table 3 contains the ratios of the total wing surfaces, the second column contains those of the aerodynamic surfaces of reference, the third column contains those of the lift correction values which represent the reciprocal values of the second column. The gradients of the root flex moment in the fourth column are taken from Fig. 9 and Fig. 10. If the wings of Table 3 are assumed to have equal lift, then the result is the weight ratios per equations (4) to (6) given in the fifth column. Accordingly, rectangular wing (1) is about 4% heavier, while the wing with end plates (9) is nearly 15% lighter than the wing with the triangular tip. The following sample values apply to this last case,

$$\frac{G(9)}{G(4)} = \frac{0.24632}{0.2098} \cdot \frac{1.276}{1} \cdot \frac{0.784}{1} \cdot \frac{1}{1.5} \cdot \frac{1.083}{1} = 0.848.$$

From the standpoint of weight ratios alone, the wing with end plates initially appears to be the most advantageous in the present comparison if a given lift is to be produced. However, a comprehensive comparison of the properties of the primary wings under study must include careful consideration of the induced drag.

Per the discussion in the previous section, especially equations (2) and (3), the results obtained for W_i are included in Table 3. As can be seen from the last column of Table 3, the induced drag of the rectangular wing is about 21.5%, and that of the wing with end plates even 63% greater than that of the wing with a triangular tip. The following example per equation (2) for wing (9) may clarify this:

$$\frac{W_i(9)}{W_i(4)} = \frac{0.706}{0.976} \cdot 1.5^2 = 1.628.$$

According to this, the wing with end plates is too /47
 disadvantageous in its current form. To have the same induced
 drag as wing (4) with triangular tips having the same end plate
 size and the same lift, its span must be increased from 66.7% to
 approximately 89% of the value of the last mentioned wing, as the
 following sample calculation does: $x_{e11} = 0.77$ per Fig. 7 (see
 point (9)'_{mod}) for this new configuration (9)'_{mod}, for which
 the size of the end plate is $h/b = 0.14$ or $d_e/d_b = 0.28$.
 Thus equation (3) produces

$$\frac{b_{(9)'_{mod.}}}{b_{(4)}} = \sqrt{\frac{0.77}{0.976}} = 0.888.$$

By enlarging the span, however, the total surface of this
 wing with end plates increases about 24% and thus exceeds the
 value of reference wing (4) about 34%. As a consequence, outside
 of weight ratio considerations, the comparison is unfavorable to
 the wing with end plates.

The example, having been closely considered, shows that it
 is not possible either with end plates or by rotating end plates,
 to surpass the properties of the wing with a tapered triangular
 tip in view of the total project design.

4.4 Selecting a wing for practical application

4.4.1 General considerations

The wing that should be selected for a practical application
 in accordance with the preceding discussion is the wing that is
 the most favorable at a given lift vis a vis the induced drag,
 friction drag and wing weight.

Based on these results, the choice of recommended wing
 designs for practical use is narrowed to the basic wing having a
 planar triangular tip and an extension of $\Lambda = 9$ (See Fig. 8, wing
 (7)) and the rectangular wing of differing extension.

A comparison of this basic wing with rectangular wings of
 different extension but equal lift is given in Fig. 11. Fig. 11
 is thus an extension of the comparison in Fig. 10 and Table 3 in
 section 4.3.2. In the comparison, while dimensions of the basic
 wing ($\Lambda_b = 6$) are maintained, the extension of the rectangular
 wing is varied, keeping the chord length, i.e., that of the basic
 wing, unchanged between $\Lambda_R = 6$ and $\Lambda_R = 8$, (in Fig. 11, b)
 shown as a broken line in the base). In addition, the
 rectangular wing is also considered with an extension equal to
 that of the basic wing $\Lambda = \Lambda_R = 9$, which features a shorter
 chord length (shown by a dotted line in Fig. 11, b)). Fig. /48
 11, a) also presents the ratios obtained in Section 4.3.
 regarding surfaces F_R/F_D , root flex moments M_{BR}/M_{BD} . It
 can be deduced from this representation, for example, that the
 rectangular wing of equal surface (extension $\Lambda_R = 7.05$) has

only 92% of the weight of the basic wing, but that the basic wing has only three quarters of the induced drag of this rectangular wing. When the rectangular wing has an extension of $\Lambda_R = 7.4$, i.e., extends to the relative span length $n_R = 0.7$ (see Fig. 11, b)), then both wings have equal weight, but the induced drag of the basic wing is only 82.5% of that of the rectangular wing. The rectangular wing of equal surface and equal extension ($\Lambda = \Lambda_R = 9$) in the end has a greater weight and also a greater induced drag than the basic wing, as proven by the data for $\Lambda_R = 9$ in Fig. 11, b).

Overall, the results obtained in the previous section show on balance that every rectangular wing can be aerodynamically improved relative to the "total performance" of the primary wing design by modifying the end to tapered triangular tips. And further, either this wing can be constructed lighter with an extension of n_R above 0.7 at lower drag, or drag can be substantially further reduced when n_R is below 0.7 at a slightly higher weight.

(In addition, the previously introduced elliptical wing of aircrafts "He 111" and "Spitfire" can be slightly improved in accordance with the data presented in section 3 above by tapering the wing tips, since doing so causes an effective nonplanarity. Further, wing designs (4) and (7) are more advantageous than design (1) not only from an aerodynamic perspective (see Fig. 3 and 4), but the cost of their construction is also significantly lower since their surface is very developable.)

It should also be noted that the wing designs that at first glance appear related to Fig. 2 and D. KÖCHEMANN according to Fig. 3 above, at closer observation are actually very different from the designs described here. Thus, the wing tip per Fig. 2 is markedly more sharply tapered and not optimized in regard to induced drag but rather in regard to the flight behavior of the aircraft where a very early separation of the flow at the outer edge must be accepted in the case of a large incidence. Neither was wing design (3) primarily designed to optimize induced drag, but was designed mainly with a view toward lift and avoiding ⁴⁹ wing tip-shock wave at supersonic speeds which also led to a more hyperbolic tip design.

4.4.2 Wing tip designs developed for practical use

The case of a new layout for the design of a wing tip has been studied within the context of developing a so-called "primary wing of the new technology" (TNT). As D. WELTE, R. BIRRENBACH and W. HABERLAND (see [63] above) have described, design considerations led to the development of a rectangular trapezoidal wing which was initially given a conventional rounded tip (see Fig. 12, b) wing tip C). A backswept tapered triangular tip (wing tip A) was newly developed for this wing wherein several additional requirements, or ancillary perspectives, were considered. Further details of the process of practical development are sketched below.

Based on discoveries made during the course of "TNT" development on the primary wing (7) (see Fig. 8), its point was slightly rounded to reduce the point of the localized lift correction value at the outside (compare the shape of the curve of wing (7) in Fig. 17 c)). Then, a profile was foreseen in which the vault rose correspondingly to the rise of the localized lift correction value from the start of the wing tip outward, as shown in Fig. 12, c) (f_w indicates the corresponding vault height). In doing this, undesirable flight-mechanical effects were encountered such as the premature separation of the flow at the wing tip, which has been confirmed by flow observations. Additionally, attention has been given to the fact that when possible direction, or the zero-lift direction, of the flow does not change over the tip extension, so as not to damage the optimal condition per MUNK. Finally, the overall aim has been to keep the construction of the geometric design simple and highly adaptable to the design of the basic wing.

The tip that was finally arrived at is constructed as follows (see Fig. 12, b)): The conical surfaces of the upper and lower side of the trapezoidal outer wing are lengthened along a straight line outward to a specific line behind the wing's leading edge, which runs nearly parallel to it (line a in Fig. 12, b)). The spar case (HK) and the aileron (QR) can be continued outwards "unhindered" by the method indicated (see Fig. 12, b)). In order to fulfill the indicated aerodynamic requirements for the "triangular tip", only the leading section of the wing comes close to line a (see Fig. 12 b)). A good balance is thereby struck between aerodynamic, flight mechanics and structural requirements. (To clarify the final design ¹⁵⁰ of the wing tip, Fig. 12 a) presents three more profile cross sections together with their skeleton lines and their zero-lift directions which lie in a single plane. (Additional details are indicated in Section 6.5 below.)

The considerations regarding the relatively similar wing tips of K.-H. HORSTMANN ([49]) mentioned above in Section 2.7 are also based on a calculation process done with a planar wake in the wing's plane and attendant limitations which, among other things, are evident in less favorable values ("superelliptical" by nature) for the induced drag. Further, the study is primarily restricted to a special sample aircraft and does not delve into the questions which are very important in the present context regarding an appropriate favorable profile.

Fig. 13 shows experimental evidence for the applicability of the wing tip types described in Fig. 12. Shown there under a) is the base of the "primary wing of the new technology" with the two wing tip designs described (C = original design, A = new design) together with the distribution of torsion a_v under b). Anticipating a harmless stalling of the aircraft, the outer wings - not the wing tip area! - are rolled about 3° . That means that a slight deviation from the optimal distribution of circulation demonstrated by studies in this work have been

accepted to the advantage of the flight properties. As the circulation distributions in Fig. 13 c) show (compare [33] above), the circulation is modified despite the not very large quantitative differences between the structures with tip designs C and A over the total span, and overall the drop in circulation at the triangular tip is actually flatter. In addition, the modification also creates an increase in the extension of about 13% when the wing weight is increased only about 3%. The induced drag, finally, - which is the primary interest here - decreases about 10%. Thus overall, rather insignificant changes in the wing design show considerable success toward improving the "efficiency" of the total wing, which is the goal here.

A comparison of the measured (wind tunnel measurements) and calculated quadratic polars can be found in Fig. 13. While only the wing is considered in the calculation, the measurement applies to the total configuration. Since, however, the main concern here is a comparison of tip designs C and A, one sees in this representation that the absolute measured drag difference of the tip designs is somewhat greater than that predicted by the calculations. This is because the conventional design has proven to be slightly less favorable in practical application than was expected.

In conclusion, it should be reemphasized that a relatively small modification of the wing tip designs alone reduced the total aircraft drag at startup and in ascent ($C_A - 1.2$ to 1.3) by about 10%. /51

4.5 The wing with slotted tip and the forked tip

In section 2.4 above, an overview was given of the numerous existing studies on the problematic of wings with slotted tips, or forked tips. The theoretical considerations of multiply divided wing tips led to the expectation that they would bring about a clear reduction in drag. Further study should thus be given to the extent to which these results could be applied to wing development and to what extent the conclusion of the preceding section can also be improved even further.

In view of the difficulties that are to be anticipated for reasons of construction in the technological realization, only the simply slotted wing tip and the forked tip, which has also been proposed by G. LÖBERT (see [42] above), will initially be studied below.

In designing the slotted wing tip, the author (see [33]) assumed that the two partial wings are arranged in such a way that they favorably effect one another, i.e., they must come as close as possible to a "double decker configuration". As shown in Fig. 14, there are, per measurements by M. NENADOVITCH [65] and by E.C. OLSON [66], configurations of two partial wings that feature a lower drag in the total lift range than the equivalent single wing. In these "optimal double decker configurations" the

partial wings should not be directly over one another, but should lie at a distance of about one third of the wing chord to a full wing chord from one another. In such an arrangement, the effects of the mutual aerodynamic induction on the boundary plane and thus on drag are favorable. The described principle has already been successfully applied by the author [67] to the design of a wing system of short extension.

Fig. 15 shows the wing tip design developed from the perspectives discussed. In the basic design, the partial wings make up a nearly "optimal double decker arrangement", a wing chord distant at the point (wing (11)). When straddled, the partial wings represent a forked point (wing (12)). This tip design has also been realized in the above mentioned "DFVLR model wing" (see [62]) and measured per R. FRIEDRICHS et al. [68]. Fig. 16 reflects the measured lift correction value C_A and the pitch moment correction value C_{M25} . Together with the current divided wing tip designs, Fig. 15 and 16 compare the planar ⁵² triangular tip per Fig. 8 (wing (7)) and the flat rectangular wing per Fig. 3 and 4 (wing (1), extension $\Lambda = 7.05$).

A comparison of the pitch moment correction value C_{M25} shows the interesting result that the rectangular wing (2) features an anticipated slightly unstable behavior, but that all configurations with a tapered point - and in fact the planar as well as the nonplanar - demonstrate stable moment behavior. This is important for practical application. The same conclusion was also reached by D. HUMMEL (see [41] above) for the multiply divided wing tips that he studied.

For a comparison of the lift and, in particular, the drag of the configurations set forth in Fig. 15 and Fig. 16, calculations were done using the vortex net procedure more closely described above, the most important results of which are compiled in Figs. 17 to 19. Fig. 17 a), analogous to Figs. 3 and 4, shows first the vortex net of each wing (slotted tip (11) and forked tip (12)) used in the calculation and the attendant divisions of the local angle of the oncoming flow (see Fig. 14, b)), as well as the curves of the local lift correction value (see Fig. 17, c)) and the correction value of the induced drag (see Fig. 17, d)). In addition, the results for wing (7) with planar triangular tip per Fig. 8 is also given (dotted line).

The comparison, e.g., of the lift correction values per Fig. 17, c), shows that the interference of the partial wings among one another is very strong the case of a slotted wing tip (11), which then has the effect of aerodynamically loading the forward partial wing more strongly than the rear one. The greater lift at the larger angle of oncoming flow effects the forward partial wing by creating thrust. The rear partial wing, by contrast, delivers less lift. Since this partial wing is inclined toward the rear, it acts as a component of drag.

Where the tip is forked in Fig. 17, c), the interference of the partial wings against each other as a result of their greater distance is significantly weaker so that both partial wings are equally aerodynamically loaded. Both have nearly the same lift, and both create a thrust component so that the induced drag is reduced to only 89% of the "elliptical" value.

The planar triangular tip (7), per Fig. 17, c), features a relatively high aerodynamic load at the point. In flow observations, separation onset has actually been determined there. And for this reason, the design of this area of the tips has been revised.

A comparison of these theoretical conclusions with the 53 results of measurements follows in Figs. 18 and 19. All pertinent data have been recalculated at an extension of $\Lambda = 9$ to improve the comparison in regard to practical primary wing design. Fig. 18 also contains data for wing (7) with planar triangular tip per Fig. 8 and for rectangular wing (2) of an equal area per Figs. 15 and 16. Although wing (11) with a slotted tip theoretically features only a slightly improved quadratic polar as compared to the triangular tip-wing (7); a definite improvement is to be seen in the measurements; in fact, the induced drag is essentially unchanged while the profile friction component is reduced. This result means that the tendency of the two-dimensional measurement per Fig. 14 is also confirmed here and that a positive interference effect is present. The rectangular wing of equal area that corresponds to wing type (2) per Fig. 3 and Fig. 4, features by contrast a significantly higher drag as a result of the shorter extension.

The results corresponding to Fig. 18 for the forked points are derived from Fig. 19. The calculated improvement produced by spreading the partial wings agrees with the conclusions of G. LÖBERT (see [42] above). By contrast, the experiment shows practically no difference with a lift correction value up to $C_A = 0.5$ ($C_A^2 = 0.25$), i.e., in the area of the oncoming flow, and at higher C_A^2 values there is even a reduction of the forked tips (12) as compared with the slotted wing tip (11). The decline can be explained in that the flow prematurely separates here in the absence of positive interference. The fact, however, that even with an oncoming flow - as mentioned above - the tendency theoretically expected does not appear in the experiment, leads to the conclusion that fundamental difficulties or insufficiencies exist in the earlier calculation of such wing designs; this conclusion agrees in particular with the tendency described in sections 2.4 and 2.7 above that an induced drag significantly below that of the planar elliptical wing of equal extension (strictly speaking $\Lambda = b^2/F$) has never been previously measured for fanned wing tips, even for a soaring bird in flight.

It appears worthwhile on the basis of the results presented here to pursue the question further of whether it is practically feasible to reduce the induced drag even below the values from

Fig. 18. The previously calculated results point in the previous context to the fact that the previously applied mathematical model (see Fig. 1) delivers good results for simple planar and nonplanar wings and also for slotted wing tips whose individual wings strongly interfere with one another. By contrast, like the results discussed in Section 2.4, the predictions for reductions in drag are far too optimistic for spread, multiply divided wing tips. Although they raise great hopes for wing design, 754 since they cannot be confirmed experimentally, a fundamental explanation is required. Apparently, the previously used calculation model no longer suffices here. Therefore, a mathematical-physical model concept is sketched below which will make a more thorough examination of these questions possible.

5. DETERMINING THE LIMITS OF A REDUCTION OF INDUCED DRAG 755 FROM OBSERVATIONS OF THE ENERGY IN THE WING WAKE

5.1 Introductory remarks

In contrast to the otherwise generally applied methods for determining induced drag from downwind integration in the so-called TREFFTZ plane far behind the wing, the induced drag has been determined thus far in this work from the integration of air forces at the wing itself (see the discussions above). In doing so, a nonplanar wake from discrete elementary vortices has been used, which, however, is also "rigid and unchanging" behind the wing. As has been shown, wings having fanned tips still cannot be accurately described even with this complex and direct computational model. Therefore, the following material will present a few observations regarding the momentum and energy in the wing wake with the intention of coming closer to a solution of the problem described.

It is known that output must be continuously exercised on a primary wing moving through air, which can be calculated - ignoring friction - from the product of the induced drag with the flight speed. This output corresponds to an energy that is continuously transferred from the wing to the surrounding air and which is then present in the wing wake as kinetic energy. Since this transfer occurs "loss-free", the energy in the wake is a direct measure of induced drag.

5.2 Discussion of various wing wake models

5.2.1 The momentum model

The simplest model construct based on the observation of wing wake is the so-called momentum model. The lift A created by a wing per the momentum theory can be expressed as follows:

$$A = \dot{m} \cdot 2w, \quad \dot{m} = \rho \cdot U_w \cdot Q. \quad (7)$$

In this equation, m is the air mass picked up per unit of time by the wing, and $2w$ is the speed with which it moves downward far behind the wing (see, e.g., H. SCHLICHTING and E. TRUCKENBRODT [53], [54] above). Lift is therefore in principle the reaction of the momentum of the downward moving air mass on the wing. The following equation pertains to the energy transferred by the wing to the wake per unit of time, i.e., therefore to the output in the wake:

$$\dot{E} = \frac{1}{2} \dot{m} (2w)^2 = W_i \cdot U_w, \quad (8)$$

The following equation for induced drag derives from 56 equation (7),

$$W_i = \frac{A^2}{2 U_w \dot{m}}. \quad (9)$$

Using the common dimensionless notation,

$$C_A = \frac{A}{q \cdot F}, \quad C_{W_i} = \frac{W_i}{q \cdot F}, \quad \Lambda = \frac{b^2}{F} \quad (10)$$

the following derives from equation (9),

$$C_{W_i} = \frac{F}{4Q} C_A^2 \quad (11)$$

But since the ratio $C_{W_i} = (1/\pi\Lambda) C_A^2$ is familiar from the elliptical wing, the following derives from equation (11) for the cross section of the air mass from the elliptical wing,

$$Q_{ell} = \frac{\pi}{4} b^2. \quad (12)$$

Of concern here is the familiar result that the cross section of the air mass picked up by a smooth elliptical wing corresponds to a circular tube whose diameter equals the wing span (see, e.g., J.S. LETCHER [69]).

However, the following applies in the case of a common wing with a nonplanar wake according to equation (1) above,

$$C_{W_i} = \frac{K_{ell}}{\pi\Lambda} C_A^2. \quad (13)$$

Following from that and equation (11),

$$Q = \frac{1}{x_{ell}} \cdot \frac{\pi}{4} b \quad (14)$$

This means that in the case of a "common" wing, the drag factor x_{ell} can be conceived as the inverse of the ratio of the air mass picked up by this wing to that of the smooth elliptical wing of equal span and extension.

To clarify this matter, Fig. 20 presents the drag ratio x_{ell} for a few "classic" nonplanar wing systems per L. PRANDTL, A. BETZ and C. WIESELBERGER (see [5] above). Also shown are the flow tubes of the various air masses picked up by the three examples represented, which are a double decker, an ideal box wing, and wing (9) having end plates per Fig. 9. In accordance with the current model, the flow tubes are circular, which corresponds to the diameter obtained per equation (3) above /57 which is greater than the span of the elliptical reference wing.

According to this, the ideal box wing is the most advantageous. For example, at a height ratio of $h/b = 0.5$ per Fig. 20, a), its induced drag is only one half of the value of the smooth reference wing ($x_{ell} = 0.5$). That means per Fig. 20, b) that this wing picks up twice the air mass of the smooth reference wing of equal span and extension, i.e., that the smooth wing equivalent to this box wing must have a 41% greater span b (see, e.g., L. PRANDTL [70], p. 193 ff., dealing in general with the double decker effect, and J. DeJOUNG [71]).

The current model concept corresponds to the acceptance of the rigid wing wake and is merely another interpretation of the conclusions reached with this theory. Limits of possible drag reduction can indeed also be presented with this model, but these are practically meaningless. For example, the assertions that a wing with "infinitely" high end plates features zero drag, or that a double decker with "infinite" wing distance has half the induced drag of the single wing, are proper theoretically defined limits, but they are of no use for practical primary wing design. Additionally, a wing circulation is not simply the equal deviation of a flow tube. This model is therefore too simple for the study undertaken here and is not suitable to the "circulatory character" of the wing circulation. Therefore, the current model, as well as a few familiar fundamentals in the context of the following explanations, are only presented first as an aid to understanding and second as a limit to simple, all inclusive concepts regarding the refined models discussed below.

5.2.2 The wake vortex model of SPREITER and SACKS

According to the theory of KUTTA-JOUKOWSKI, a wing can produce lift in a flowing medium only when circulation is present. But, according to a vortex theory of HELMHOLTZ, circulation can be lost so that the attached wing circulation must also reoccur in the wake, and in fact far behind the wing in

the two wake vortices that are rotating in opposing directions (see as a basis, e.g., the explanations of A. WEISE in H. FRANKE ([55]) above). Since, in addition, according to another theory of HELMHOLTZ, a vortex filament always consists of the same particles of matter, a direct correlation exists between the circulation and the mass of the wing wake. This exists, among other things, in the fact that the "center of the circulation" of the vortex plane emanating from each wing half, is simultaneously the same point around which the rolled wake vortex later, /58 i.e., further downwind, turns. The distance of the rolled tip vortex equals $b' = \pi b/4$ far behind a wing with elliptical lift dispersal (see, e.g., [54] above).

J.R. SPREITER and A.H. SACKS [72] place two counter revolving "RANKINE vortices" in the so-called TREFFTZ plane whose centers have a radius of r_K , as shown in Fig. 21. The medium in the center rotates like a rigid body. Outside of that, there is a potential flow to which the following velocity potential applies:

$$\psi = \frac{\Gamma}{2\pi} \left(\arctan \frac{z}{y - \frac{b'}{2}} - \arctan \frac{z}{y + \frac{b'}{2}} \right). \quad (15)$$

The streamline of this potential flow from initially two vortex lines with counter circulation at $y = \pm b'/2$ describes circles with radius r , whose centers lie at $y = \pm \sqrt{(b'/2)^2 + r^2}$ (see Fig. 21). If it is determined that the flow within the circle of radius r_K (vortex center) is to rotate like a rigid body, then it is further assumed that this does not alter the flow pattern outside of the centers. Fig. 21 makes it clear in the given case where $r = r_K$ that involved in this assumption is an approximation for $r_K^2 \ll (b'/2)^2$, expressed in the different lengths $y = b'/2$ and $y = \sqrt{(b'/2)^2 + r_K^2}$, which exactly coincide only when $r_K \rightarrow 0$. (This also means in the case of Fig. 22, that for $2 r_K / b \lesssim 0.25$, i.e., for the right area of the figure unnecessary in the current context, the depiction of a quantitative statement increasingly changes into an indication of a trend.)

The kinetic energy in the vortex centers of length l (i.e., the energy per unit of length) equals

$$E_K^* = 2 \cdot \frac{\rho}{2} \int_0^{r_K} \int_0^{2\pi} v(r)^2 dF = \frac{\rho \Gamma^2}{8\pi} \quad (16)$$

with

$$v(r) = \frac{\Gamma}{2\pi r_K} \left(\frac{r}{r_K} \right). \quad (17)$$

The following approximately holds true for the energy (per unit of length) outside the center, per [72]

$$E_p^* = \frac{\rho \Gamma^2}{2\pi} \ln\left(\frac{b' - r_K}{r_K}\right) . \quad (18)$$

Thus, the following results for the energy content (per unit of length) of the wake /59

$$E^* = E_K^* + E_p^* = \frac{\rho \Gamma^2}{8\pi} [1 + 4 \ln\left(\frac{b' - r_K}{r_K}\right)] . \quad (19)$$

If the wing moves along a path s , then the energy content of the wake must correspond to the work of the induced drag along this path, i.e., the following applies

$$W_i \cdot s = E^* \cdot s . \quad (20)$$

The energy content of the wake of length l , i.e., the energy content of the two dimensional flow (of wing chord l) in a cross section of wing wake E^* is, therefore, the induced drag itself:

$$W_i = C_{w_i} \cdot q \cdot F = \frac{\rho \Gamma^2}{8\pi} [1 + 4 \ln\left(\frac{b' - r_K}{r_K}\right)] . \quad (21)$$

The following relationship can be deduced for the size of the vortex center r_K :

$$\frac{r_K}{b/2} = \frac{2}{1 + e^{\left[\frac{C_{w_i} \cdot \rho \cdot U_\infty^2 \cdot b^2}{\Gamma^2 \cdot \lambda} - \frac{1}{4} \right]}} . \quad (22)$$

The exponent requires further simplification here, however. Thus, using KUTTA's lift equation $A = \rho U_\infty \times \Gamma \times b'$ (see, e.g., [54] above) and equation (10) above, the following statement can be written,

$$\frac{\Gamma}{U_\infty b} = \frac{C_L}{2\lambda} \cdot \left(\frac{b}{b'}\right) . \quad (23)$$

Since equation (13) applies without modification for a "general wing", that is $C_{w_i} = x_{ell} q C_A^2 / (\pi \lambda)$, the following equation results from inserting equations (13) and (23) into equation (22):

$$\frac{r_K}{b/2} = \frac{b'}{b} \cdot \frac{2}{1 + e^{\left[\frac{1}{4} \cdot x_{ell} \left(\frac{b'}{b}\right)^2 - \frac{1}{4} \right]}} . \quad (24)$$

This relationship provides the size of the vortex center (r_K) in the context of the current model construct for planar or nonplanar wing systems (x_{e11}) which feature exactly or approximately a "RANKINE vortex" velocity dispersal in their center, in relation to the half span of this wing system ($b/2$). Equation (24) was reduced in the context of the current study, and the results are presented in Fig. 22. From this the relative induced drag x_{e11} and the size of the vortex center $2 r_K/b$ can be calculated for a given wing whose circulation dispersal and thus whose vortex distance b'/b is known. Thus, e.g., the radius of the vortex center in the case of an elliptical wing (Point E in Fig. 22) equals 15.4% of the half span ($2 r_K/b = 0.154$ per equation (24)).

For the application below, and analogously to earlier discussions, the relevant contexts are provided for those wing systems that have exactly or approximately a constant tangential velocity ($v = \text{const.}$) in the center. By adding to this the factor $(r/r_K) = 1$ in equation (17), the result is a design which corresponds to equation (24), fully analogous to the computational results connected with equation (17), and which merely replaces the term $1/4$ in the exponent of the denominator with the term $1/2$. An evaluation of this new equation for vortex centers with constant tangential velocity is presented in Fig. 23. The comparison with Fig. 22 for the "RANKINE vortex" velocity dispersion in the center, shows that the curves of constant related vortex distance b'/b are shifted in Fig. 23 to larger related center radii $2 r_K/b$.

The vortex model of SPREITER and SACKS which has been discussed is essentially a better description of the actual wing wake than the momentum model. Fig. 22, e.g., shows, among other things, that the diameter of the center $2 r_K/b$ enlarges as the relative induced drag x_{e11} grows smaller and the vortex distance b'/b decreases. In addition, this behavior must not be seen as an increase of the effect of friction -- the rolling process resulting from vortex induction is free of friction, of course, in the context of the current theory -- , it results rather from observations of energy per the vortex model described.

The following explanations for plausability are presented in connection with the relationship between lift and induced drag: Based on the earlier discussions on the double decker and the box wing, it is first clear that at a given lift, i.e., essentially at a given integral value of the circulation of the primary vortex, various - and particularly "subelliptical" - induced drags can occur. Now, observation of vortex behavior at a primary wing advancing horizontally, for example, makes it clear that the position of the primary vortex as it is shifted 61 forward must set air in motion which earlier was practically still. Circulation at the primary vortex's former position, however, has disappeared. The energy loss and gain from this process occurs on both sides, in other words: to gain lift, i.e.,

to gain the attached vortex, no additional energy is needed during forward motion. Because of HELMHOLTZ's theory of vortex gain, however, the receding wake vortex lengthens. As the earlier discussions of the wake model of SPREITER and SACKS, for example, now show, this needed energy doubtlessly depends - at a given, steady lift - both on the distance of the receding vortex (b'/b) and on the diameter of the center ($2 r_K/b$) of this vortex, apparently therefore on the "structure" of the wake, i.e., on the local circulation dispersal at the wing. This again makes it plausible from a "wake energy" perspective that at a given lift different induced drags can occur, depending on the circulation dispersal, and in particular, as Ill.s 22 and 23 show, even "subelliptical" ones. Thus, for a given vortex center diameter, for example, the vortex interval should be as large as possible, i.e., at a given vortex interval the vortex centers should be as large as possible to obtain a low wake energy and thus the lowest possible induced drag.

A statement about the limits of possible drag reduction, however, is not possible by means of the current model construct alone, since the relationship between wing circulation, tangential velocity dispersal of the wake vortex and diameter of the center has not yet been given. This means that from the amounts presented in Ill. 22 or Ill. 23, one must know, e.g., b'/b and x_{e11} to be able to offer $2 r_K/b$. The wake model of A. BETZ is presented below therefore to help clarify this situation.

5.2.3 The BETZ wake model

In his groundbreaking work on the behavior of the vortex system, A. BETZ (see [44]) proceeded from the assumption that, in the rolling process of the vortex layer of a primary wing to the two wake vortices, a definite correlation must exist between the circulation dispersal of a wing half and the dispersal of the circulation over the radius of a wake vortex. Therefore, in agreement with the above cited vortex theories, it is assumed that the circulation emanating from the wing reoccurs in vortices of definite diameter, i.e., that the vortex layer of a wing half develops into a spiral which forms a circular tube of a specific diameter. It is therefore also assumed that the circulation of these wake vortices is only a function of their radius, /62 i.e., their mutual induction is negligible.

As mentioned previously, the total circulation must remain constant during the rolling process, i.e., the following holds:

$$-\int_0^{1/2} \frac{d\Gamma(y)}{dy} dy = \int_0^R \frac{d\Gamma'(r)}{dr} dr = \Gamma_0 \quad (25)$$

Here $d\Gamma(y)/dy$ is the circulation emanating from the wing, i.e., the circulation dispersal of the vortex layer of the wing wake; Γ_0 is the value of the circulation in the wing's midsection;

and R is the radius of the circular tube which contains the circulation of a wing half. Since the circulation is attached to the mass in the wake, a range can be inserted here which corresponds to the so-called "polar moment of inertia" and which cannot change during the rolling process. In this sense, the "moment of inertia" of the wake vortex layer (of a wing half) created with the circulation around its center equals the moment of inertia of the vortex layer around its center which is actually identical with the first. Thus, the following correlation,

$$-\int_0^{L/2} \frac{d\Gamma(y)}{dy} (y - \frac{b'}{2})^2 dy = \int_0^R \frac{d\Gamma'(r)}{dr} r^2 dr . \quad (26)$$

Here, $b'/2$ is the position of the center of the wake circulation of a half wing, arrived at as follows (see in this connection Ill. 24, under a)):

$$\frac{b'}{2} \Gamma_0 = -\int_0^{L/2} \frac{d\Gamma(y)}{dy} y dy . \quad (27)$$

A. BETZ used these relationships to arrive at the characteristics of the rolled wake vortex behind a wing with elliptical lift dispersal. Applying this principle to the primary wing with general circulation dispersal per C. du P. DONALDSON et al. [73], then equations (25) to (27) can be generalized in the following manner:

$$-\int_y^{L/2} \frac{d\Gamma(\eta^*)}{d\eta^*} d\eta^* = \int_0^r \frac{d\Gamma'(\rho^*)}{d\rho^*} d\rho^* = \Gamma(y) , \quad (28)$$

$$-\int_y^{L/2} \frac{d\Gamma(\eta^*)}{d\eta^*} (\eta^* - \bar{y}(y))^2 d\eta^* = \int_0^r \frac{d\Gamma'(\rho^*)}{d\rho^*} \rho^{*2} d\rho^* \quad (29)$$

and

/63

$$\bar{y}(y) \int_y^{L/2} \frac{d\Gamma(\eta^*)}{d\eta^*} d\eta^* = -\int_y^{L/2} \frac{d\Gamma(\eta^*)}{d\eta^*} \eta^* d\eta^* . \quad (30)$$

These correlations are clarified in Ill. 24. The generalization exists in the fact that the above discussed considerations are not applied to the entire half wing (Γ_0), but to that portion of the wing that lies outside position y which has just been examined ($\Gamma(y)$). The integration is done for every position y, whereby the integration variable at the wing is termed η^* , and the variable at the wake vortex is termed ρ^* . Thus, equation (28) means that the circulation outside of station y has "developed" inside the circle with the radius r.

The position of the midpoint of this circle, however, is not determined by equation (27) (see Ill. 24, a)). $\bar{y}(y)$, per equation (30) is the position of the center of the portion of the wake circulation outside of station y , and equation (29) describes the moment of inertia of this portion of circulation around this very point \bar{y} .

For further analysis, equations (28) to (30) are differentiated according to r . Per [73], equation (28) becomes,

$$-\frac{d\Gamma(y)}{dy} \cdot \frac{dy}{dr} = \frac{d\Gamma'(r)}{dr} , \quad (31)$$

and equation (29) results in,

$$-\frac{d\Gamma(y)}{dy} \cdot \frac{dy}{dr} (y - \bar{y}(y))^2 = \frac{d\Gamma'(r)}{dr} r^2 , \quad (32)$$

since the statement containing $d\bar{y}/dr$ yields zero because of equation (30). Equation (31) inserted into equation (32) leads to,

$$r = \bar{y}(y) - y . \quad (33)$$

By performing the integrations from y to the wing tips $b/2$ on the wing, i.e., from $r = 0$ to radius r in the wake vortex, equation (28) leads to,

$$\Gamma(y) = \Gamma'(r) . \quad (34)$$

Equations (33) and (34) describe the rolling process of the vortex layer of the wing to the two wake vortices, whereby the midpoint of this vortex - as mentioned above - is determined by equation (27). As Ill. 24 shows, circulation $r(y)$ which /64 dominates at position y of the wing, reappears in the wake vortex at radius r , whereby this radius at the wing corresponds to the distance between the observed position (y) and the center of the wake circulation outside of position (\bar{y}).

In accordance with the theory of potentials, the tangential velocity in the wake vortices results in the following:

$$v(r) = \frac{\Gamma'(r)}{2\pi r} . \quad (35)$$

The velocity in the vortex center itself, i.e., where $r = 0$, is of particular interest. If to obtain this value one constructs the boundary transition $y \rightarrow b/2$, i.e., apparently: as the

position y approaches wing tip $b/2$, then the radius simultaneously becomes zero because $\bar{y} \geq y$ in accordance with equation (33); and the position of the center \bar{y} formally moves into the central position between y and $b/2$ (see Ill. 24). That means $d\bar{y}/dy = 1/2$, and

$$\frac{dy}{dr} = 2, \quad (r \rightarrow 0). \quad (36)$$

Thus, equation (31) becomes

$$-2 \cdot \frac{d\Gamma}{dy} \Big|_{y=b/2} = \frac{d\Gamma'}{dr} \Big|_{r=0}. \quad (37)$$

By making the boundary transition $r \rightarrow 0$, equation (35) leads to

$$v(r=0) = \frac{1}{\pi} \frac{d\Gamma}{dy} \Big|_{y=b/2}. \quad (38)$$

Equation (38) is to be interpreted as follows: If the circulation at the tip of the wing drops off with a perpendicular tangent, as, e.g., as is true with the ellipse, then the tangential velocity in the center of the wake vortex formally exceeds all boundaries. If, however, the circulation slows down with a finite gradient, then the tangential velocity in the center of the vortex remains finite.

In conclusion, it can be said that the preceding vortex model is capable of providing the correlation between circulation and tangential velocity dispersal not available in the earlier studies.

Conclusions shall now be drawn from the tangential velocity dispersal to the vortex center diameter as it applies to a "RANKINE vortex". This procedure, however, is only applicable when the wake of a wing half unrolls into only a single vortex, which is the case when the circulation dispersal features no - or only a single - inflection (but those are the basic standard cases). Lift dispersals with two or more inflections can appear, however, where a partial span flap is deflected. Where there is sufficient distance between these inflections, the wake circulation of a half wing can unroll into two or more wake vortices. Such special cases shall not be considered here, however.

As can be deduced from equation (33), the radius of the fully unrolled tip vortex corresponds to $b'/2$ (for a single half wing, the integration begins at $y = 0$, i.e., it then becomes $r = \bar{y} = b'/2$, see also Fig. 24). Since the vortices rotate essentially symmetrically, they touch the central axis according to this model. However, as indicated by Ill. 21, in which the

stream lines are raised with the radius $r = b'/2$, according to the more detailed vortex model of SPREITER and SACKS, in reality there is a clear interval in the stream as a result of the mutual influence and resulting nonsymmetry of the vortices.

Since the wake vortex of the BETZ model features a defined radius, and since both vortices of the left and right sides of the wing are assumed to be independent of each other, this model does not correspond to the complete physical reality that is naturally a part of a mutual influence of the two vortices. Thus, in and of itself, the current model construct is not appropriate for determining the induced drag, but is very appropriate for determining the tangential velocity dispersal and the diameter of the center of the wake vortex, discussed in more detail below.

5.2.4 Observations on the combined application of the wake models

The preceding section pointed out that the BETZ wake model has value in its general form only for specific wake types. But it was also indicated that certain limitations of the wake model of SPREITER and SACKS can be eliminated with the help of the BETZ concepts. Therefore, it is worthwhile to look for types of circulation dispersals that in and of themselves most completely fulfill the concepts of both theories in practice.

Ill. 25 presents a compilation of results, especially /66 the tangential velocity dispersal, representing the wake for three characteristic circulation dispersals with equal total lift.

To simplify the numeric computation, a partially straight dispersal was presumed in the elliptical lift dispersal (see Ill. 24, a)), so that the receding circulation represents a step function. As a result, the tangential velocity dispersal features a finite value in the vortex center. Because of this approximation, the center itself also lies at $n = 0.7692$ instead of the exact value of $n = b'/b = \pi/4 \approx 0.7854$. In the case of circulation dispersals with outside perpendicular tangents - as with an exact ellipse - a "viscous vortex center" that rotates like a rigid body develops in an actual stream as a result of the effect of friction, so that the current approximation is thoroughly meaningful for the elliptical wing (see Fig. 22, point E). The size of this viscous vortex center, however, can be determined only per SPREITER and SACKS - as explained in section 5.2.2 above - if the vortex interval and the relative induced drag x_{e11} is already known. This is determined in accordance with the indications resulting from the (numeric) integration of the tangential velocity dispersal per the BETZ model, i.e., per Ill. 25, a), or from equations (16) and (20). According to these, the induced drag for the elliptical wing is only 88.3% of the exact value. A result of this type is to be expected, however, due to the demonstrated imperfection of the BETZ model in general.

There also exist types of circulation dispersals, however, which feature a definite vortex center which are "frictionless" by nature. If one observes a circulation dispersal of the type shown in Ill. 25, c), that has a constant inner section and a parabolic, degressive drop outside, and that features a kink with the characteristics of an inflection (W), then one can determine that the attendant vortex strength of the wake drops off linearly outward (see $d\Gamma/dn$ in Ill. 25, c)). This type has the particular feature that its tangential velocity v corresponds exactly to the dispersal of a "RANKINE vortex", i.e., the vortex features a center that rotates like a rigid body although the unrolling proceeds theoretically completely without friction (see the v -course in Ill. 25, c)).

This third circulation type from Ill. 25, i.e., shown under c), corresponds directly to the vortex wake theory shown in section 5.2.2 above, i.e., in Ill.s 21 and 22. Thus, in this circulation type, or a corresponding attendant wing type, the previously lacking correlation between wing circulation, vortex center diameter and vortex interval is given directly, and the relative induced drag x_{e11} can be determined directly /67 from equation (24), i.e., per Ill. 22. Herein lies a way to determine reliably the possible reduction of the induced drag at least for this characteristic circulation dispersal type. Wings of the last named type, however, are relatively uncommon and therefore have not been considered in the literature. Such wing types, however, have real importance especially for the theoretical determination of wings with fanned tips, an overview of which was presented earlier (see section 2.4). In particular, there is a relationship to the wings of soaring land birds.

Another highly interesting type of circulation dispersal with a definite vortex center is the circulation dispersal shown in Ill. 25, b) that has a constant center ($d\Gamma/dn = 0$) and a linear outside drop ($d\Gamma/dn = \text{const.} < 0$). In this instance, circulation leaves the wing only from the outer 40% of the span, and with the characteristic that the vortex strength is constant there. Wake vortices develop there that have a "center" with constant tangential velocity v (see $d\Gamma/dn$ and the v course in Ill. 25, b)). Such a circulation dispersal proves itself closely related to the wings of soaring ocean birds.

Two wing types are worth consideration: one with a "RANKINE vortex" wake, and one with a wake having centers of constant tangential velocity. These types are of special interest to the current concern toward optimizing drag because - as demonstrated above - the natural forms of their actual favorable drag behavior is very important. The following section, therefore, shall more thoroughly discuss observations of the induced drag of soaring birds, which shall lead to generally applicable statements regarding drag optimization.

5.3 The induced drag of soaring birds and the limits of possible drag optimization

5.3.1 General comments

As described earlier in sections 2.6 and 2.7, several studies are known which indicate a substantial margin of possible drag reduction for wings with fanned tips. As mentioned previously, practical wing designs with these characteristics have actually been proposed (see Ill.s 6, 7 and 8 above). However, since the theoretically predicted improvements have not yet been confirmed in experiments, considerations will be presented in the following material to discover an explanation which permits closer determination of the limits to possible drag reduction that can actually be realized. /68

Since the large soaring birds feature two typical different wing types, they must be considered separately, so the fanned wings of the soaring land birds will be studied first and following that will be a discussion of the pointed, backwards tapered wings of the soaring ocean birds.

5.3.2 The induced drag of soaring land birds

As previously mentioned in section 2.6 above, observations of fanned wing types similar to those of soaring land birds have led the author to determine that relatively large, slowly rotating vortex centers develop behind the wing tips rather than the concentrated and relatively thin tip vortices known from common wings (see [26] and [56] above). While the last are relatively long lived, the first mentioned large wake vortices in nature have a relatively short lifespan. The diameter of their vortex centers which rotate like rigid bodies correspond in the first approximately to the span extension of the cascade created by the pinion feathers. That essentially means that the vortex model stressed in section 5.2.4 with the special "RANKINE vortex" wake form per Ill. 25, c), very closely approximates the aerodynamic conditions on these bird wings. In this case, the inflection (W)-like kink is situated in the circulation dispersal at the beginning of the cascade (see sketch in Ill. 26). As a result of the multiple divisions of the wing surface, the vortex strength of the receding circulation $d\Gamma/dn$ per Ill. 25, c), is the greatest here. Even the degressive drop in circulation has a real physical background: the "ideal" pinion feathers, as a result of their design and material constituency, aerodynamically and aeroelastically deform under the air's pressure in such a way that the circulation at their tips slows with a zero gradient.

In the context of the current study, the position of the inflection n_w , i.e., the beginning of the cascade, varies systematically and the diameter and positions of the vortex centers as well as each attendant induced drag has been determined for all wing types per the theory described in section 5.2.4. The result is presented in Ill. 26. Thus, for example,

the results obtained for the case in Ill. 25, c) where $n_w = 0.6$ are an interval of the wake vortices equalling 73.33% of the span (per equation (27)) and a radius of the vortex center equalling 13.33% of the span, per equation (33). With this, the relative induced drag can be determined per equation (24) (or per Ill. 22) at $x_{e11} = 1.1866$. This result is entered in Ill. 22 and Ill. 26 as point L. The surprising overall outcome of this systematic variation of n_w is shown in Ill. 26, i.e., the course of the relative induced drag x_{e11} features a distinctive minimum /69 where the onset of the cascade lies at 75% of the half span. There is also the fact that practically all wings of soaring land birds have this optimal condition as the examples in Ill. 26 show. The data from the individual soaring land birds have been obtained through measurements of flight images from various sources. The flight measurements done by A. RASPET (see [50] above) on an urubu (*Coragyps atratus*) also confirmed these facts. In total it can be concluded that the limit of drag reduction for this wing type has thus been found.

The second surprising result drawn from the current study lies in the fact that the induced drag of this optimal fanned wing is 15% above that of the planar elliptical wing (see Ill. 26), which contradicts all previous expectations. In the current context, it then follows that the often very optimistic conclusions from other mathematical model constructs are totally unrealistic and unattainable in practice.

At least one reason proposed under the current theory for the relatively poor showing by the wing types under observation can be seen formally in the fact that the vortex centers lie relatively far in. As is evident from Ill. 22, vortex interval b'/b has a significant influence. That becomes clear when the wing with end plates is compared. Thus, wing (9) per Ill. 9 with end plate height of 19.1%, when calculated in terms of the current theory, features a vortex interval that corresponds to the span. A vortex center radius of 13% of the span (per equation (33)), which closely corresponds to the initial example, yields a relative induced drag per equation (24) of only $x_{e11} = 0.7223$ (point 5 in Ill. 22), which is very close to that value computed by the vortex net process, i.e., $x_{e11} = 0.706$ per Ill. 9, and also very close to the value per W. MANGLER's theory which yields $x_{e11} = .715$ per Ill. 7. This advantage of the wing with end plates, however, contrasts with the disadvantage per section 4.3.2 of the large total surface area and the high weight. If, however, one takes into consideration the fact that the elliptical wing which is equal in lift and drag features only 93.3% of the span of the optimal fanned wing per equation (3), then one can assert that the soaring land bird attains approximately the lift and drag of the elliptical wing only by adding the points of the pinion feathers whose mass and surface are practically negligible in respect to the total wing.

The initial considerations indicated that the advantage /70 of the wing type discussed here exists in a very effectively used wing surface at a very low wing weight. This fact is

confirmed by the anatomical studies described by C.D. CONE (see [48] above). The wing measurements per [50] mentioned earlier also indicate that the "strength" of these bird types is less their favorable relative induced drag x_{e11} (although this is certainly optimal per Fig. 26), and more their very low zero drag correction value of approximately $C_{w0} = 0.006$, so that L/D ratios of 23 are achieved despite the relatively low REYNOLDS value of approximately 300000. In addition, such values can be explained only by the fact that one presupposes laminar flow over the total surface.

Finally, it can be concluded that the fanned wing types of the soaring land birds were determined to be optimal forms for this wing type by mathematical-physical methods. The bird types presented (see Ill. 26) distinguish themselves by their outstanding flight efficiency. It is interesting that the "stork" and "crane", whose extraordinary long distance flight capabilities are known, are right on the optimum. In any case, the relative induced drag of this wing type is greater than that of the elliptical wing according to the current theory.

(The reason that these wing types with - as explained - vortex centers that lie relatively far inside are preferred in the natural world over a - formally superior - type with centers farther to the outside, could lie in the fact that - likewise discussed above - other considerations of friction drag, weight and structure play a role in addition to the aerodynamically important aspect of induced drag. Birds in the category observed here feature a relatively low wing span for their given weight, i.e., for their given wing surface, often combined with strong feet and necks. In comparison to the generally stout body build of the soaring ocean birds with short feet but relatively long wings, the features mentioned represented indices for that low wing weight of the soaring land birds mentioned earlier. Therefore, one must presuppose that the actual formal optimum for technical applications in terms solely of induced drag can be slightly displaced to low values of approximately $x_{e11} \pm 1$, as will be explained in more detail below, but never to the given unrealistically low values far below one.)

As will be shown, it is generally quite possible in 71 principle, e.g., to use an end plate or rigid single wings (further data in this respect also follow) to lower the relative induced drag significantly; but taking into consideration the conclusions of section 4.3, it is evident that by doing so the wing weight and the friction drag increase unreliably strongly. This will be shown in more detail below.

5.3.3 The induced drag of soaring ocean birds

The wings of soaring ocean birds, in contrast to those of soaring land birds, generally feature a larger extension Λ and a higher surface load A/F . In their basic form with tapered, backswept tips, the corresponding wing types have already been

discussed in section 3 above, namely as wing types (4), (5) and (6) of Ill. 3 and Ill. 4. These forms, which are planar and yet, as mentioned, feature a slight effective nonplanarity, can be computed very well by the vortex net procedure. In any case, the bird wings demonstrate characteristic differences as a result of their ideal aeroelasticity when compared to the rigid wing and its attendant computation model. The computed circulation dispersal of these wings certainly shows, similarly to the elliptical wing per Ill. 3, a perpendicular tangent at the outside, but the elasticity of the feathers at the wing tips of birds lead one to the conclusion that a drop in circulation occurs with a finite gradient analogous to the middle nonelliptical dispersal in Ill. 25, b). This assumption is supported by flow observations, for concentrated tip vortices were not observed, rather only a vortex layer of weak intensity was observed which dissolved after a few wing chords (see [26] above). Diagram series in Ill. 25, b) can also verify this finding. As shown there, the strength of the wake vortex $d\Gamma/dn$ is constant which in an actual flow means that the vortex layer dissolved relatively quickly because all of the elementary vortices have equal vortex strength and rotate in the same direction, and therefore mutually disturb each other very strongly.

One can conclude from the initial considerations, that the computational model per Ill. 25, b) is adaptable to handling the wings of soaring ocean birds and related wing types. As Ill. 25, b) indicates, a tangential velocity dispersal which has a center with a constant velocity corresponds to a unique circulation dispersal with a constant wake vortex strength in the area of the wing tips. The basics for handling such wake flows were discussed in section 5.2.2 above and the results represented in Ill. 23.

In full analogy to the procedure for soaring land /72 birds, the diameter and position of the vortex center and thus of the attendant relative induced drag (x_{e11}) was determined per Ill. 23 for soaring ocean birds by systematically varying the position of the bend point n_k , i.e., the point at which the bird wing's "fan" begins. It was interesting that a curve resulted which features no definite optimum but which dropped with decreasing n_k , i.e., with longer and longer fans. Overall, clearly "subelliptical" values resulted for the induced drag which reached nearly 95% to 90% of the induced drag of the elliptical wing.

The fact that a marked optimum of induced drag cannot be determined for soaring ocean birds as it can for soaring land birds can be explained by the so-called "square-cube law", i.e., the correlation between aircraft mass and conveyable forces (see the data in section b) of the introduction above). One can determine as a result of the material characteristics of the feathers that in the case of large and heavy birds (albatross, petrel) the length of the pinion feathers is relatively small in

relation to the wing measurements, while in the case of small birds with a smaller mass, these feathers - and thus the fan - can be relatively low in comparison with the wing measurements (coastal sea swallows, gulls). Large and heavy birds therefore occupy the right side of the curve, and small and light birds the left side. In addition, since induced drag drops off as the fan becomes longer, i.e., the n_k becomes smaller, the disadvantage of increasing friction drag at decreasing REYNOLDS values is substantially balanced out in smaller birds by the drop in the induced drag. This further explains how a few smaller bird species demonstrate extraordinary efficiency in long-distance flight.

On the basis of the initial discussion, it is highly plausible that related technological wing designs for "general aviation" should without a doubt be included in the range of large n_k values, i.e., on the right side of Ill. 26, because of their size and relative weight, at the limit of the largest known soaring ocean birds or even above. In this context, see the data to wing (7) in Ill. 26, wherein the size $x_{e11} \gtrsim 0.95$ determines the limit of a possible reduction of the induced drag for technological wing designs in practice.

In conclusion, it can be determined that soaring ocean birds (and birds with similar wing types) feature a markedly lower relative induced drag than soaring land birds ($x_{e11} \approx 0.9$ to 0.95 compared to ≈ 1.15). In any case, it is interesting that this advantage is related to a higher wing weight, as was 73 already evident in the anatomical studies of soaring land birds mentioned previously [48]. Also applicable here are the previous remarks relating to fanned wings, i.e., that an even lower relative induced drag (x_{e11}) can be attained with a wing having end plates when the conclusions of section 4.3 are taken into consideration, but that these wings become significantly heavier and have a greater friction drag than the corresponding comparative wing of a soaring ocean bird. This consideration leads to the conclusion that, in total, the last wing is also considered optimal.

The studies described so far were carried out for the incompressible case, although the results basically apply for the entire subsonic speed range as long as there are not transonic interferences present. In this context, the determination is interesting that the wings of the soaring ocean birds (and of birds with similar wing types) which are recognized as optimal feature "streamlined", partially sharply tapered forms which otherwise are used only for aircraft that reach transonic velocities. "Transonic" reasons can hardly be behind the natural design, however. Rather the increased upwind in the wing tip area and the quickly dissipating vortex wake of the natural design attains a "subelliptical" induced drag, presenting a plausible justification for the applicability of these wing types to general subsonic speed ranges.

5.3.4 Summary of conclusions reached regarding soaring birds

A summary of the conclusions of the preceding sections concerning soaring land and ocean birds yields the following: The range of possible optimization of induced drag for wings with nonplanar fanned tips and for planar wing types is relatively small as compared with that of the elliptical wing. At best it can reach nearly 90%. All data previously available in the literature on somewhat spectacularly low percentages, i.e., on far more effective drag reductions, are not actual and cannot be realized in practice. Such data can be traced back to inadequacies in the various fundamental theoretical model constructs and are not supported in actual practice.

(It is also interesting from the viewpoint of natural studies, that clear relationships could be derived for the two types of soaring birds, i.e., "soaring land bird" and "soaring ocean bird", under the flow physics aspect of a lowest possible induced drag, i.e., from the flight physics aspect of good long-distance flight properties. It can be drawn from this that soaring properties play a definitive role in nature for these types of birds. The difference that exists in the favorable quantitative values of the two types (soaring land birds: optimum slightly "superelliptical", soaring ocean bird: slightly "subelliptical") might be explained by the fact that although the soaring ability as mentioned is an important feature, it is not the only one that characterizes these bird types, and other abilities such as, e.g., tight turning flight, and possibly other totally different, nonaerodynamic and nonflight related considerations also play a role.)

In the following section, two important areas of wing wake observation are explained in more detail regarding possible inadequacies.

5.4 Discussion and critique of the application of the sliding principle

MUNK's sliding principle (see [6] above), which was mentioned earlier in section 2.5, says among other things that the induced drag of a wing system that consists of several elements is independent of the position of these elements in the direction of the flow. This independence exists, however, only when the lift dispersals of these elements remain unchanged during slipping. Interesting applications of this principle in the strictest sense can be found, e.g., in E.E. LARRABEE [74] and E.V. LAITONE [75], which deal with the problem of an aircraft's trimming with rear or forward positioned stabilizers, i.e., with tandem wings. Involved is the co-called multiple decker arrangements with relatively large intervals, applying the slipping principal and the PRANDT multiple decker theory (see, e.g., [5] and [70] above). Use on wing elements in close proximity is unreliable, however, since such wing elements influence one another very strongly. As Ill. 14 shows, the

positions of the wing elements is then no longer independent from their position in the direction of the flow, but, as explained, an optimal arrangement does exist. However, the arrangement per Fig. 6 above, for example, is staggered directly opposite to the optimum, and is therefore highly unfavorable from an aerodynamic viewpoint because of its close proximities. However, the familiar slippage principle, which has been unreliable for exactly these situations, has almost without exception been applied in the earlier literature to all of these configurations that have small intervals between elements as discussed in section 2.4 above. Therefore the discrepancies between the conclusions presented there as compared to the results of the current study cannot be surprising.

In particular, an interpretation of a "sliding principle" should be considered unreliable for the observed situations when the assumption is made that rigid vortices emanate from the tips of the individual wings as, e.g., occurs in [42] and [43] above where the diameter of the vortex center is only assumed and no consideration is given to the physical mechanism of the rolling process. As explained earlier in detail, the BETZ wake model is more appropriately used in these cases because the wake circulation of the individual partial wings immediately merge to a single large wake vortex. This makes the deviations of the results quoted in section 2.4 from the assertions of the current work far more plausible. /75

5.5 Discussion and critique of the interpretation and use of the optimal condition

M. MUNK defines the so-called "optimal condition" as follows (see [6] above): "The necessary condition for the lowest drag for a primary line is an interval velocity produced equally along the entire wing by the longitudinal vortex." G. LÖBERT (see [42] above) interprets this condition to mean that in an optimal wing, "the induction of the totality of all free vortices is so structured in the TREFFTZ plane that a deformation does not occur in the vortex layer which moves downwind at a constant translational velocity." This interpretation, however, alters MUNK's condition because it adds a statement concerning the behavior of the wake farther downwind from the wing which is not contained in MUNK's original condition. In particular, this expanded interpretation does not correspond to actual physical relationships, because, as Fig. 9 in section 2.5 above and Ill. 25 show, a constant downwind lies directly at the wing, i.e., on the primary line, during elliptical circulation dispersal, but the developing vortex layer is very unstable and immediately rolls downwind from the tips to the vortices shown. Statements about reducing drag based on this expression of the optimal condition therefore undoubtedly lead to incongruities.

Applied to wing design, maintaining MUNK's original optimal condition means that the wing maintain a constant downwind direction, i.e., the demand for no wing torsion. In any case,

this condition is necessary but not sufficient; because in accordance with the above considerations, an optimal drag also requires that the energy in the wake be as low as possible at a given lift. Per section 4.3 above, the minimizing of weight at a given lift, for example, is an additional requirement in 76 practical wing design. When considered together, it becomes clear that the drag of a wing cannot be successfully optimized in practice solely on the basis of MUNK's optimal condition.

Propeller studies have likewise shown that the danger exists that MUNK's optimal condition can be wrongly interpreted when, e.g., analogous to the above comments, the requirement for constant downwind at the blade is not understood as a requirement for the downwind of the blade's trailing edge to assume the form of a helicoid (i.e., ideal torsion), but in assuming that a statement is being made about the propeller wake, requiring a constant downwind dispersal under the rotor. These requirements, i.e., constant downwind at the blade and constant downwind dispersal under the rotor, however, are only compatible where there are an "infinite" number of blades and the circular surface disturbance among them is very low. If, however, the demand for a constant downwind dispersal under the rotor is generally demanded in technological applications with higher to very high circular surface disturbance and a few blades (see, for example, the propellers per Table 2 above), then a rotor results which is clearly inferior to a rotor designed to the original optimal requirement because of the high aerodynamic load of the interior during static thrust and minimal forward motion and because of the high wake energy unnecessary for a given thrust.

6. CONCLUDING DISCUSSION OF POSSIBLE DRAG REDUCTION FOR 77 NONPLANAR AND PLANAR WING TYPES

6.1 General goals

Although the previously often encountered optimism regarding the size of an attainable optimization of induced drag through wing structure has been noticeably dampened by the preceding observations and brought into physically and mathematically proven limits, the importance of efforts at optimization should not be dismissed; in view of the desired optimization, e.g., of energy demand of an aircraft, even the smallest improvements play a significant role because they have a cumulative effect over the long term. Based on the results gained earlier, the following new look at the above studied basic wing types - with multiply divided tips, forked tips, end plates and planar end designs - is justified, the view being cast toward a proposal for the most optimal wing tip designs for practical use, their effect now set in the context of more restricted limitations for an optimization.

6.2 The wing with multiply divided tips

6.2.1 Results from the model experiment

A few configurations with multiply divided wing tips will be discussed first from which model experiment results are available. The results significant in the current context are compiled in Ill. 27 and can be compared with the natural form (Ill. 27 a), see also Ill. 26) considered optimal for this wing type. According to the results presented in section 5.3.2 above, the interval of the wake vortex centers in this optimal form is 83.3% of the span, and the center radius is 8.33% of the half span (see point OPT in Ill. 22). The relative induced drag is $x_{e11} = 1.15$ (see Ill. 26). Since the maximum L/D ratio of the above mentioned urubu per flight measurements is $(C_A/C_W)_{MAX} = 23$ (see [50]), and since this soaring land bird is not among the largest examples and also not directly at the optimal point of the drag curve per Ill. 26 (REYNOLDS value $\approx 300,000$), even higher maximum L/D ratios are expected for bird species at the optimal point. The technological applications per Ill. 27, b), c) and d) were measured at comparable REYNOLDS values, yielding a relative induced drag factor $x_{e11} \approx 1.0$. The difference from the value previously considered optimal, i.e., $x_{e11} = 1.15$, is explained by the formal possibility discussed earlier in section 5.3.2 of greater intervals between vortex centers.

This difference can be clarified by the rigidity of 78 the partial wings. This is done using the model construct of a wake with vortex centers of constant tangential velocity per Ill. 25, b), and Ill. 23, which applies to both planar and nonplanar wings! The results of the theory are presented in Ill. 27 and essentially state that the theoretically derived x_{e11} values confirm the measurement results very well and, as previously mentioned, are smaller than the optimal values of the soaring land birds. The individual sample configurations from Ill. 27 are entered in Ill.s 23 and 26 as points. The following correlations apply: Case b) in Ill. 27 corresponds to point H in Ill.s 23 and 26, and cases c) and d) correspond to point Z in Ill.s 23 and 26. In Ill. 23, these points fall logically into the range of "technological wing types". Therefore, the following correlation is proposed: The fanning and elasticity of the feathers in bird wings yields a favorable behavior as regards weight and friction drag, i.e., laminarity of the flow, in contrast to the relatively, "bad", i.e., small vortex center intervals, for the induced drag. The relationships are directly reversed for the rigid partial wing. The relatively low induced drag in the technological application is unfortunately only a "partial success" because in practice friction drag and wing weight must also be considered.

The maximal L/D ratios given in Ill. 27 show that the value of soaring bird is not attained in the experiment, although only the wing itself was measured. This means that due to the lack of ideal aeroelasticity and border layer laminarity, the friction

drag of the technological application is significantly higher than in the natural form. The comparison of the configurations per Ill. 27, c) and d) is also of interest. By combining every two partial wings into a kind of "optimal double decker configuration" per Ill. 14, the friction drag can be clearly reduced. However, as the comparison with the planar form per Ill. 27, e) (wing (4) per Ill. 10) shows, practically the same "aerodynamic efficiency" is also attained with a technologically far simpler wing design.

As regards the wing weight, only a few qualitative remarks follow: At the starting point of the partial wings of the type per Ill. 27, b) or c), only a third or a fourth of the base wing-profile height is available as structural height in the first approximation, which means $1/27$ or $1/64$ of the so-called "drag moment" of the theoretical spar curvature. Since the aerodynamic load of the partial wing corresponds approximately to that of the planar tip design per Ill. 27, e), the partial wings must be significantly heavier than the planar form. In total, the results from model studies presented here that multiply divided wing tip designs are not appropriate for practical application.

6.2.2 Results from flight tests

179

The configuration of J.J. SPILLMAN (see Fig. 8 above) shall be briefly discussed again as an example of a multiply divided wing tip form that has been studied in flight tests. From SPILLMAN's wind tunnel measurements relevant to this configuration, a relative induced drag of $x_{e11} = 0.84$ results if per Ill. 28, a) span b of the nonmodified wing is used as the basis for the reference wing. The actual span is enlarged 11% by adding the single wing to the tip structure. Recalculated on this actual larger span, a relative induced drag $x_{e11} \approx 1.0$ results, which value approaches that of the model measurements discussed in the previous section. The theory yields the point SP entered in Ill.s 23 and 26 with $x_{e11} = 1.04$. Comparing this wing with a performance of the tapered triangular tip per Ill. 28, b), which yields an equal induced drag at equal lift, one can assume a relative induced drag of $x_{e11} \approx 0.98$ for this wing per Ill. 8. Thus, in accordance with equation (3) above, an increase results in the span of this reference wing of about 8% which is shown in Ill. 28, b). This wing has a lower surface area, however, at equal "aerodynamic performance," (i.e., at equal C_A/C_w), thus a lower friction drag and a lower weight because its construction is apparently significantly less complex. (That also results in lower production costs.) Even the interference drag of the numerous corners of the multiply divided wing tip naturally ceases.

In total, this example (which initially seems favorable) also makes it clear that an aircraft equipped with the reference wing is more favorable and that a technological application of the severally divided natural forms does not appear to recommend itself.

6.3 Wings with forked tips and fanned tips

The forked tip, as an example of a simpler tip design, may initially appear to be more practically realizable because of its relative simplicity (see Fig. 7 above). In any case, the fanned tip of similar structure (see Ill. 5) is slightly superior to it, and this last provides the most favorable of all the configurations studied in terms of drag (see Ill.s 16 to 19). Reference was made previously to this difference in section 4.5 above. Using the theory per Ill. 23, one obtains the point G here and in Ill. 26, and the quadratic polars designated with "wake theory" in Ill. 19 which reflect the experimental findings very well; these satisfactorily resolve the difficulties /80 mentioned in section 4.5 regarding the theoretical description of this fanned wing design.

As the comparison of Ill. 27 (wing (12)) and Ill. 8 (wing (7)) show, the gradient of the root bending moment of the wing with the fanned tips is nearly equal to that of the simple planar form, which initially indicates comparable weights. However, since the single wings per Ill. 15 has only approximately half the absolute thickness of the simple tip form, and since therefore only about one-eighth of the spar drag moment is available at the site of its beginning, these - corresponding to the designs made to the initial examples - would have had to be made significantly heavier at approximately equal load. For this reason - and similarly because of the higher construction costs - the forked point and the fanned form are likewise not suitable for practical applications.

6.4 Wings with end plates

It can be concluded from the results of section 4.3 above that the use of an end plate can be eliminated as a result of the increased weight and addition of friction drag. (Even though the end plate has an additional stabilizing function as it does in case of the so-called canard function, for example.)

6.5 Planar wing designs

In the framework of possibilities discussed in the current work regarding drag optimization, all nonplanar wing types have proven unsuitable for practical application.

The following can generally be said in regard to planar wing types: As some studies (see S. EHEKIRCHNER, D. WELTE and H. ZIMMER [76]) have shown, all statements are true regarding the possibilities for improving primary wings by suitably designing the wing tips by and large independently from the primary wing's basic design, i.e., the design of the midsection of the primary wing, so that these statements are also relatively generally true for trapezoidal and tapered wings in particular as well as for the entire subsonic speed range. (Even in supersonic and transsonic speed ranges a few positive effects have been demonstrated in experiments according to [76].)

Among the planar wing tip types corresponding to the designs in section 4.4 above, the triangular tip design described there yields the form best suited to practical applications. (Regarding further details, also see the detailed representation of the author [77].) Thus, according to Ill. 4 (wing /81 types), Ill. 8 and Ill. 12 (as the planar wing recognized as optimal), as well as Ill. 26 (technological wing designs), the attainable limit for practical wing design lies at an induced drag of approximately 95% to 98% of the "elliptical" value.

In conclusion, two examples of realized technological applications are given: the aircraft DORNIER "TNT-experimental" with the "primary wing of new technology" (TNT) and the aircraft of the DORNIER "DO 228" series. A detailed representation of the performance of the first named aircraft can be found in H. MAX [78]. Ill. 29 shows the characteristic structure of this new wing type per DORNIER GmbH [79] which it has in common with the "general aviation" aircraft of the "DO 228" series mentioned previously (see DORNIER GmbH [80]).

REFERENCES

ORIGINAL PAGE IS
OF POOR QUALITY

- [1] R.T. MITCOMB:
Methods for Reducing Subsonic Drag due to Lift.
AGARD Report No. 654, p. 2-1 ÷ 2-17, Special Course on Concepts for
Drag Reduction, von Karman Institute, Rhode-St-Genese, 28 March -
1 April, 1977.
- [2] W. PFENNINGER:
Design Considerations of Large Global Range High Subsonic Speed LFC
Transport Airplanes.
AGARD Report No. 654, p. 3-63 ÷ 3-75, Special Course on Concepts for
Drag Reduction, von Karman Institute, Rhode-St-Genese, 28 March -
1 April, 1977.
- [3] J.U. BORCHERS, F.X. WORTMANN, H. ZIMMER, P. BARTELS, F.R. GROSCHÉ,
M. KOSTER, G. MÜHLBAUER:
Entwurf, Bau und Erprobung eines verbesserten Propellers für Flug-
zeuge der Allgemeinen Luftfahrt.
2. BMFL-Statusseminar, Luftfahrtforschung und Luftfahrttechnologie,
Vortrag Nr. 3, Teil B, S. 257 - 322, Garmisch-Partenkirchen, 8. -
9. Oktober 1980.
- [4] R.J. JERACKI, D.C. MIKKELSON, B.J. BLAHA:
Wind Tunnel Performance of Four Energy efficient Propellers designed
for Mach 0.8 cruise.
NASA TR 79124, April 1979.
- [5] L. PRANDTL, A. BETZ, C. WIESELSBERGER:
Ergebnisse der Aerodynamischen Versuchsanstalt zu Göttingen,
I. - III. Lieferung.
Druck und Verlag von R. Oldenbourg, München und Berlin 1923.
- [6] M. MUNK:
Isoperimetrische Aufgaben aus der Theorie des Fluges.
Inaugural-Dissertation, Georg-August-Universität zu Göttingen, Druck
der Dieterichschen Universitäts-Buchdruckerei (W. Fr. Kaestner),
Göttingen 1919.
- [7] R.T. JONES (Hrsg.):
Classical Aerodynamic Theory.
NASA RP-1050, Dec. 1979.

ORIGINAL PAGE IS
OF POOR QUALITY

- [8] F.X. WORTHMANN:
Design of Airfoils with High Lift at Low and Medium Subsonic Mach-
numbers.
AGARD-CP-102, p. 7-1 : 7-9, Fluid Dynamics of Aircraft Stalling,
Lisbon, 1972.
- [9] F.X. WORTHMANN:
The Quest for High Lift.
AIAA Paper No. 74-1018, 2nd International Symposium on the Technology
and Science of Low Speed and Motorless Flight.
Cambridge, Massachusetts, Sept. 11-13, 1974.
- [10] J.W. SLOOF, F.X. WORTHMANN, J.M. DUHON:
The Development of Transonic Airfoils for Helicopters.
MLR MP 75032U, 31st Annual National Forum of the American Helicopter
Society, Washington DC, May 1975.
- [11] D. ALTHAUS, F.X. WORTHMANN:
Stuttgarter Profilkatalog I.
Verlag Friedr. Vieweg & Sohn, Braunschweig/Wiesbaden 1961.
- [12] R. EPPLER:
Laminarprofile für Reynoldszahlen größer als $4 \cdot 10^6$.
Ingenieur-Archiv, 38, 232-240 (1969).
- [13] R. EPPLER:
Turbulent Airfoils for General Aviation.
Journal of Aircraft, 15, 93-99 (1978).
- [14] P.F. SELINGER:
ASVZOPP-Segelflugzeug mit Schwungfeder.
FLUGREVUE • Flugwelt, Heft 8, S. 72 (1981).
- [15] P.F. SELINGER:
Winglets für Segelflugzeuge.
FLUGREVUE • Flugwelt, Heft 4, S. 58 (1982).
- [16] R.T. WHITCOMB, L.R. CLARK:
An Airfoil shape for Efficient Flight at Supercritical Mach Numbers.
NASA TMX-1109, 1965.
- [17] K. OSWATITSCH, D. RUES (Hrsg.):
Symposium Transsonicum II, Göttingen, Sept. 8-13, 1975.
Springer-Verlag, Berlin/Heidelberg/New York 1976.

ORIGINAL PAGE IS
OF POOR QUALITY

- [18] E. STANEWSKI, K. ZIMMER:
Die Entwicklung und Windkanalerprobung von drei überkritischen Trag-
flügelprofilen für Verkehrsflugzeuge.
ZfV 23, 246 - 256 (1975).
- [19] D. MELTE:
Profilentwurf für einen Tragflügel neuer Technologie für Flugzeuge der
Allgemeinen Luftfahrt.
DGLR-Jahrestagung 1977, Vortrag Nr. 77-027, 13. - 15. Sept., Berlin,
1977.
- [20] K. ZIMMER:
The Rotor in Axial Flow.
AGARD-CP-111, Aerodynamics of Rotary Wings, 13. - 15. Sept., Marseilles,
1972.
- [21] S.F. MOERNER:
Fluid Dynamic Drag.
Moerner Fluid Dynamics, Brick Town, N.J., 1975.
- [22] S.F. MOERNER, H.V. BORST:
Fluid Dynamic Lift.
Moerner Fluid Dynamics, Brick Town, N.J., 1975.
- [23] T.E. De VITT, E.E. BULLARD (ed.):
Evolution of Aircraft Wing Design.
AIAA-Symposium, Airforce Museum, Dayton, Ohio, March 18-19, 1960.
- [24] B. REGENSCHEIT:
Untersuchungen über den Einfluß der Randkappenform auf die Tragflügel-
meßergebnisse.
Technische Berichte, Herausgegeben von der Zentrale für wissenschaft-
liches Berichtswesen der Luftfahrtforschung des Generalluftzeugmeisters,
Berlin-Adlershof, Bd. 11, 113-118, 1944.
- [25] "JANE'S":
All the World's Aircraft, 1980/81.
Jane's Publishing Co. Ltd., London 1980/81.
- [26] K. ZIMMER:
Über die Wirbelbildung an Tragflügeln großer Streckung; Strömungsbe-
obachtungen im Dornier-Wasserkanal.
Bericht Nr. 71/4B, Dornier GmbH, Friedrichshafen, Jan. 1971.

ORIGINAL PAGE IS
OF POOR QUALITY

- [27] D. KUCHEMANN:
The Aerodynamic Design of Aircraft.
Pergamon Press, Oxford, New York, Toronto, Sydney, Paris, Frankfurt.
1978.
- [28] R.T. WHITCOMB:
A Design Approach and Selected Windtunnel Results at High Subsonic
Speeds for Wing Tip mounted Winglets.
NASA TM-D-8260, July 1976.
- [29] K.J. MINDNER:
Canadair CL 600 Challenger-Portrait eines Herausforderers.
Aerokurier 3, 278-291 (1982).
- [30] K.K. ISHIIKITSU:
Aerodynamic Design and Analysis of Winglets (for B-707).
AIAA Paper No. 76-940, Sept. 1976.
- [31] "McDONNELL-DOUGLAS":
Design and Windtunnel Test of Winglets on a DC-10 Wing.
NASA CR-3119, April 1979.
- [32] G.W. HANKS:
Technology Advancements for Energy Efficient Transports.
AIAA Paper 80-0906, AIAA International Meeting & Technical Display
"Global Technology 2000", Baltimore, Md, USA, May 6-8, 1980.
- [33] H. ZIMMER:
Die Bedeutung der Flügelendformen beim Tragflügelentwurf für Flugzeuge
der zivilen Luftfahrt.
DGLR-Jahrestagung 1977, Vortrag Nr. 77-030, Berlin, 13.-15. Sept. 1977.
- [34] "McDONNELL-DOUGLAS":
Winglet-Equipped DC-10 Makes First Flight.
Aviation Week & Space Technology, Sept. 14, p. 49, 1981.
- [35] J.E. MACKET:
Vortex Drag Reduction by Aft-Mounted Diffusing Vanes.
12th JCAS Congress 1980, Paper Nr. 13.4, p. 542-553, Munich,
12-17 Oct. 1980.
- [36] B. SWEETMAN:
Boeing's 747 rides the roller-coaster.
FLIGHT International, 20 Febr., p. 436, 1982.

ORIGINAL PAGE IS
OF POOR QUALITY

- [46] G. ROPPEL:
Vorgelflug.
Rowohlt-Verlag, Reinbek bei Hamburg, September 1980.
- [47] M. MERTEL:
Struktur, Form, Bewegung.
Krausskopf-Verlag, Mainz, 1963.
- [48] C.D. CONE:
Thermal Soaring of Birds.
American Scientist, p. 180-209, March 1962.
- [49] K.-H. WORSTMANN:
Einfluß verschiedener Flügelendformen auf die Wirtschaftlichkeit von
Verkehrsflugzeugen.
Institut für Aerodynamik der DFVLR Braunschweig, Abteilung Entwurfs-
aerodynamik, Bericht Nr. 151-78/22, Braunschweig, Juni 1977.
- [50] A. RASPET:
Leistungsmessungen an einem Segelvogel.
Industrial and Engineering Research Station, Mississippi State College,
Enthalten in: THERMIK-Modellflug, Okt. 1951.
- [51] C.W. LUCCI:
Berechnung der aerodynamischen Beiwerte von Fluggeräten mit Mantel-
schrauben.
DORNIER GmbH, Friedrichshafen, Bericht Nr. 75/46B, Dez. 1975.
- [52] A. EHMART, M. FRANKE (Hrsg.):
LUEGER Lexikon der Technik, Band 1, 4. Auflage.
Deutsche Verlags-Anstalt GmbH, Stuttgart 1960.
Darin: K. BRIEDEN: Strömungsmechanik, herausgegeben von A. WEISE.
Stichworte: Aerodynamik, Tragflügelumströmung.
- [53] H. SCHLICHTING, E. TRUCKENBRODT:
Aerodynamik des Flugzeuges.
Band 1.
Springer-Verlag, Berlin/Göttingen/Heidelberg, Berichtiger Nachdruck,
1962.
- [54] H. SCHLICHTING, E. TRUCKENBRODT:
Aerodynamik des Flugzeuges.
Band 2.
Springer-Verlag, Berlin/Göttingen/Heidelberg, 1960.

ORIGINAL PAGE IS
OF POOR QUALITY

M. FRÄNKE (Hrsg.):

Lexikon der Physik.

3. Auflage.

Franckh'sche Verlagshandlung, W. Keller und Co., Stuttgart 1969.

Darin A. WEISE: Strömungslehre.

Sichthorte: BIOT-SAVARTSches Wirbelgesetz, Widerstand, Wirbel, Wirbelsätze, Wirbelströmung.

H. ZIMMER:

Widerstandsverminderung an Tragflügeln.

Teil 1: Wasserkanaluntersuchungen.

DORNIER GmbH, Friedrichshafen, Bericht Nr. 74/48, April 1974.

K. ZIMMER:

Widerstandsverminderung an Tragflügeln.

Teil 2: Theorie des induzierten Widerstandes unter Berücksichtigung dreidimensional deformierter Wirbelschichten und Anwendung auf den Tragflügelentwurf.

DORNIER GmbH, Friedrichshafen, Bericht Nr. 75/158, August 1975.

J.D. BERRY, R.E. MINECK:

Wind-tunnel test of an articulated helicopter rotor model with several tip shapes.

NASA-TM-80080, AVRADCOM-TR-79-49, 1979.

G.L. BENDER, H. ARNATZ, D. OTTOMEYER, R. WORATSCHEK, L. HIGGINS,

J.S. TULLOCH:

Preliminary airworthiness evaluation of an AH-1S helicopter with ogee tip shape rotor blades.

Army Aviation Engineering Flight Activity, Edwards AFB, Ca.

USAAEFA-77-25, April 1980.

H. ZIMMER:

Berechnung von Profilformen bei Pfeilflügeln.

Diplomarbeit, Institut für Aerodynamik und Gasdynamik der Universität Stuttgart, Stuttgart 1964.

ORIGINAL PAGE IS
OF POOR QUALITY

- [61] W. MANGLER:
Die Auftriebsverteilung am Tragflügel mit seitlichen Scheiben.
Luftfahrt-Forschung, Herausgegeben von der Zentrale für Wissenschaft-
liches Berichtswesen der Luftfahrtforschung des Generalluftzeugmei-
sters, Berlin-Adlershof, Bd. 16, 219-228, 20. Mai 1939, Verlag von
R. Oldenbourg, München/Berlin, 1939.
- [62] R. FRIEDRICHS, W. HASTREITER:
Windkanaluntersuchungen an neuartigen Flügelendformen.
DFVLR, Zentralabteilung Niedergeschwindigkeits-Windkanäle, Braunschweig,
Bericht Nr. IB 157-75A15, Sept. 1976.
- [63] D. MELTE, R. BIRRENBACH, W. HABERLAND:
Wing Design for Light Transport Aircraft with Improved Fuel Economy.
Z. Flugwiss. Weltraumf. 5, No. 5, p. 294-303, (1981).
- [64] D.R. RILEY:
Wind-Tunnel Investigation and Analysis of the Effects of Endplates on
the Aerodynamic Characteristics of an Unswept Wing.
NACA TN 2440, Aug. 1951.
- [65] M. KENADOVITCH:
Recherches sur les Cellules Biplanes d'Envergure Infinie.
Publications Scientifiques et Techniques du Ministère de l'Air,
No. 86, Institut Aérotechnique de St.-Cyr, Paris 1936.
- [66] E.C. OLSON:
Experimental Determination of Improved Aerodynamic Characteristics
Utilizing Biplane Wing Configurations.
M.S. Thesis, Mechanical and Aerospace Engineering Dept., Univ. of
Missouri-Rolla, Rolla, Mo., 1974.
- [67] M. ZIMMER:
Das Hochauftriebsverhalten beim Rautenflügelkonzept.
DGLR Jahrestagung 1978, Vortrag Nr. 78-114, Darmstadt, 19. - 23. Sep-
tember 1978.
- [68] R. FRIEDRICHS, W. HASTREITER, C. PAOLETTI:
Windkanaluntersuchungen an neuartigen Flügelendformen.
2. Meßabschnitt.
DFVLR, Zentralabteilung Niedergeschwindigkeits-Windkanäle, Braunschweig,
Bericht Nr. IB 157-77A07, Febr. 1977.

ORIGINAL PAGE IS
OF POOR QUALITY

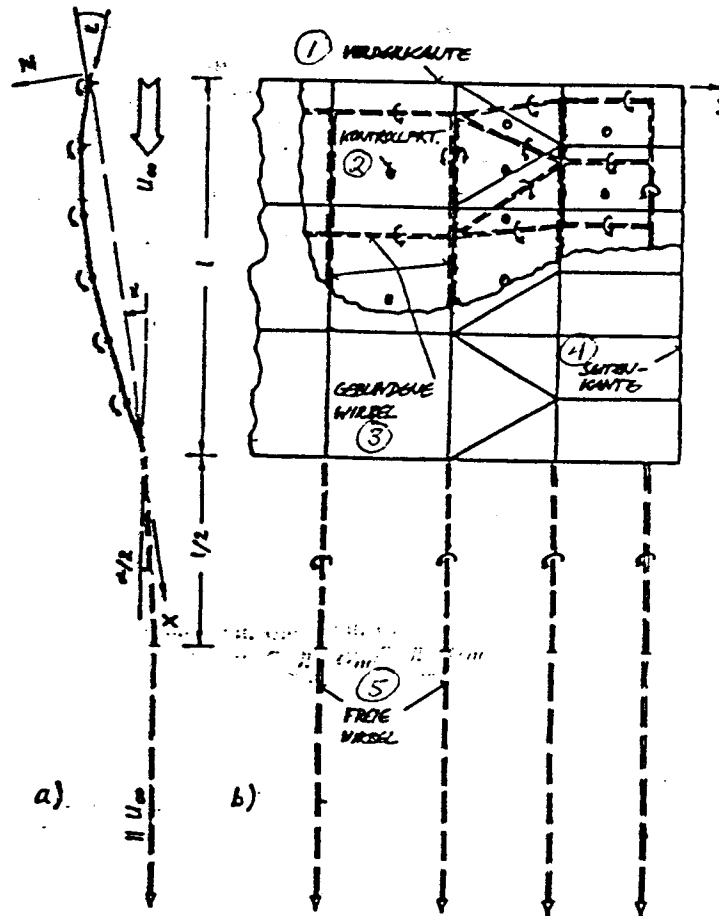
- [69] J.S. LETCHER:
Y-Wings and Diamond Ring-Wings of Minimum Induced Drag.
J. of Aircraft, 9, 605-607 (1972).
- [70] L. PRANDTL:
Führer durch die Strömungslehre.
Verlag Friedr. Vieweg & Sohn, Braunschweig, 1942.
- [71] J. DeYOUNG:
Induced Drag Ideal Efficiency Factor of Arbitrary Lateral-Vertical
Wing Forms.
NASA Contractor Report 3357, Dec. 1980.
- [72] J.R. SPREITER, A.H. SACKS:
The Rolling Up of the Trailing Vortex Sheet and its Effect on the
Downwash Behind Wings.
Journal of the Aeronautical Sciences, Volume 18, No. 1, 21-32 (1951).
- [73] C. du P. DONALDSON, R.S. SNEDEKER, R.D. SULLIVAN:
A Method of Calculating Aircraft Wake Velocity Profiles and Comparison
with Full-Scale Experimental Measurements.
AIAA 12th Aerospace Sciences Meeting, Paper No. 74-39, Washington D.C.,
Jan. 30 - Feb. 1, 1974.
- [74] E.E. LARRABEE:
Trim Drag in the Light of Munk's Stagger Theorem.
Proceedings of the NASA, Industry, University-General Aviation Drag
Reduction Workshop, University of Kansas, Lawrence Kansas, July 1975.
- [75] E.V. LAITONE:
Prandtl's Biplane Theory Applied to Canard and Tandem Wing Aircraft.
Journal of Aircraft, 17, No. 4, 233-237, (1980).
- [76] S. EHEKIRCHER, D. MELTE, H. ZIMMER:
Rollsteuerung durch drehbare Flügelspitzen.
Dornier GmbH, Friedrichshafen, Bericht Nr. 77/438, Dez. 1977.
- [77] H. ZIMMER:
Quertriebskörper, insbesondere Flugzeugtragflügel.
Deutsches Patentamt, Patentschrift DE 29 09 245 C2, 27.1.1983, München.

**ORIGINAL PAGE IS
OF POOR QUALITY**

- [78] K. MAX:
Aerodynamische Leistungen des Tragflügels neuer Technologie (INT),
ein Vergleich zwischen Auslegungserwartung und Flugversuchsergebnis.
2. BfW-Statusseminar, Luftfahrtforschung und Luftfahrttechnologie,
Garmisch-Partenkirchen, 8./9. Oktober 1980.
- [79] "DORNIER GmbH":
Tragflügel Neuer Technologie.
Information Nr. PR 80045000.
- [80] "DORNIER GmbH":
Specification DORNIER 228-100, Oct. 1980.

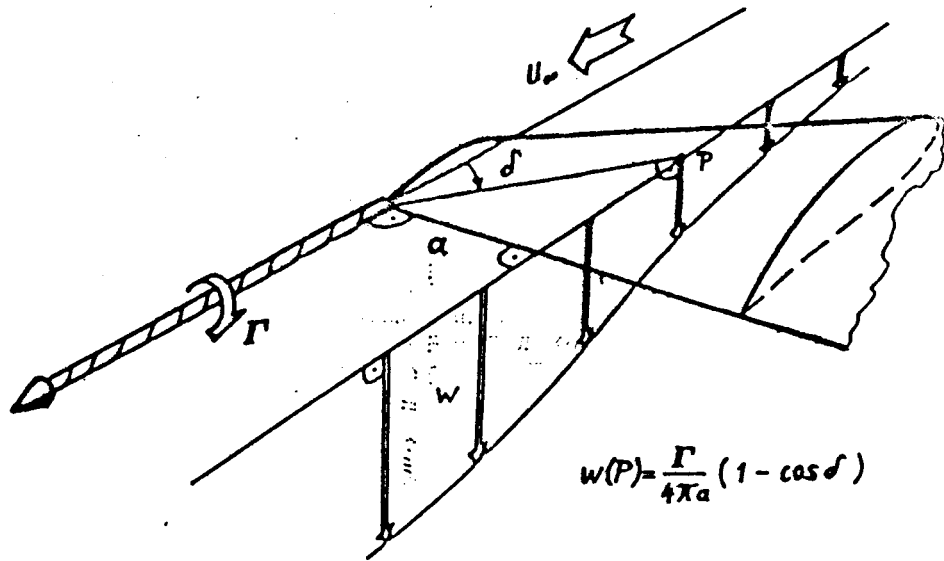
ILLUSTRATIONS

ORIGINAL PAGE IS
OF POOR QUALITY



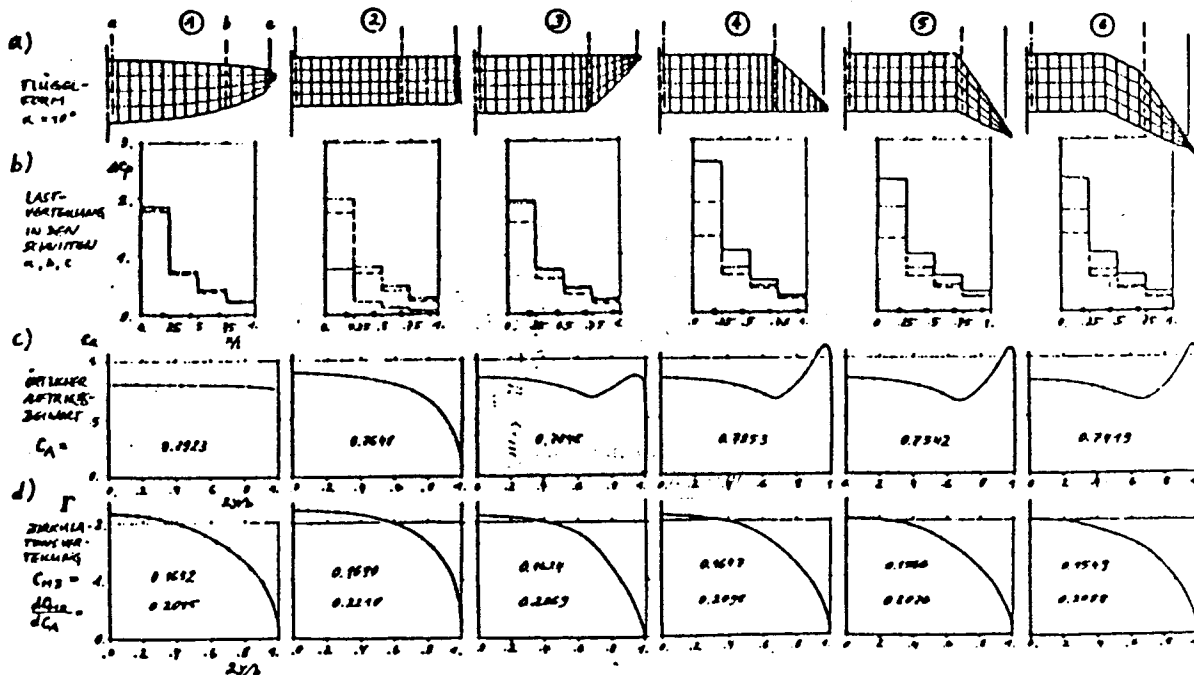
Ill. 1: A) side view and b) top view of vortex model used in computation of a primary wing by the vortex net procedure.

Key: (1) Leading edge; (2) Control point; (3) Attached vortex; (4) Side edge; (5) Free vortices.



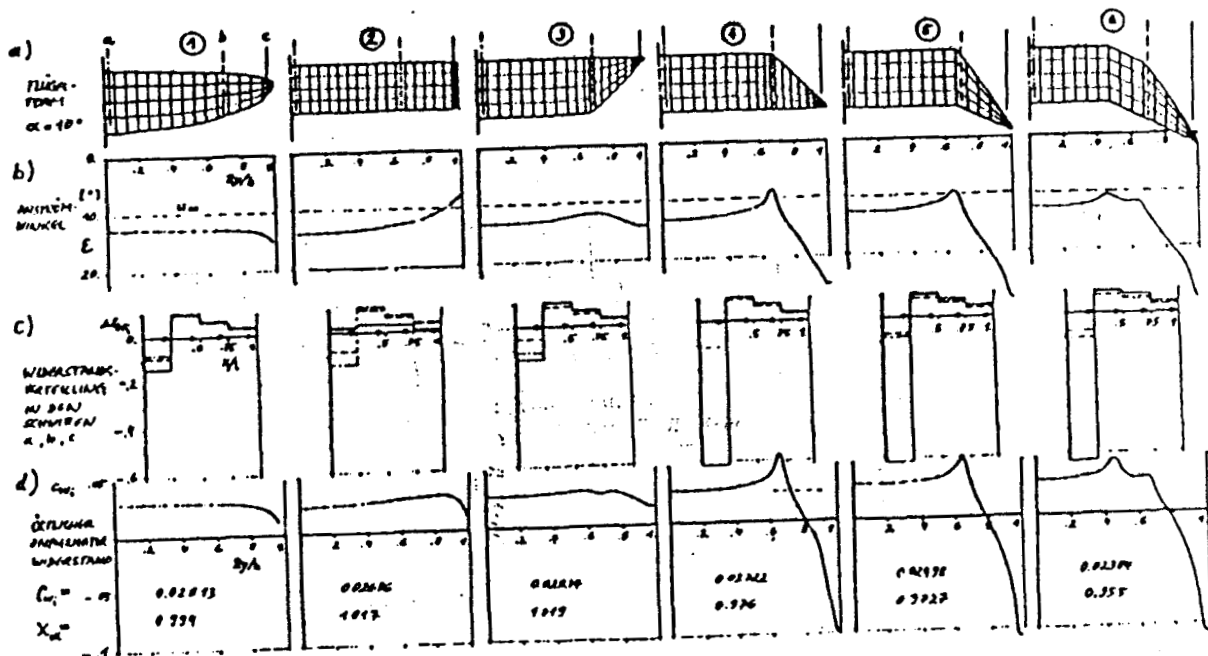
Ill. 2: Induced downwind from tip vortex at the wing tip after the BIOT-SAVART principle (schematic).

ORIGINAL PAGE IS
OF POOR QUALITY

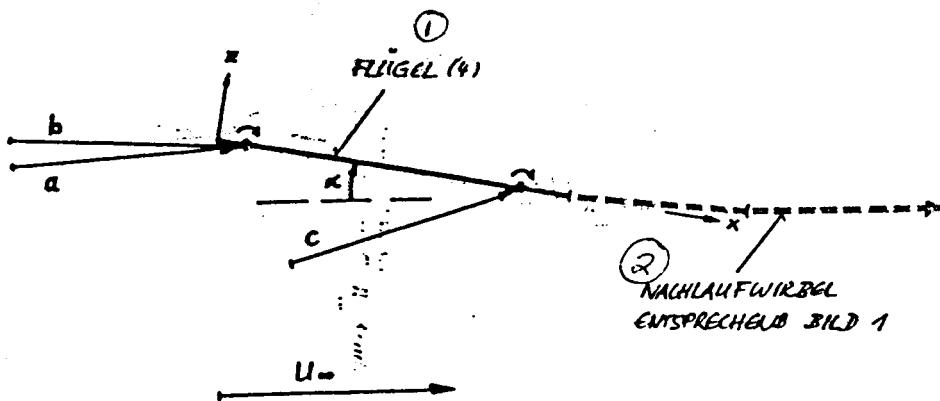


Ill. 3: The lift of various wing designs with extension $\lambda = 7.05$. a) Wing design with divisions a, b, c; b) Load dispersal Δc_p in divisions a, b, c; c) Local lift correction value c_a and total lift correction value C_A ; d) Circulation dispersal r , root bending moment correction value C_{MB}/dC_A .

ORIGINAL PAGE IS
OF POOR QUALITY

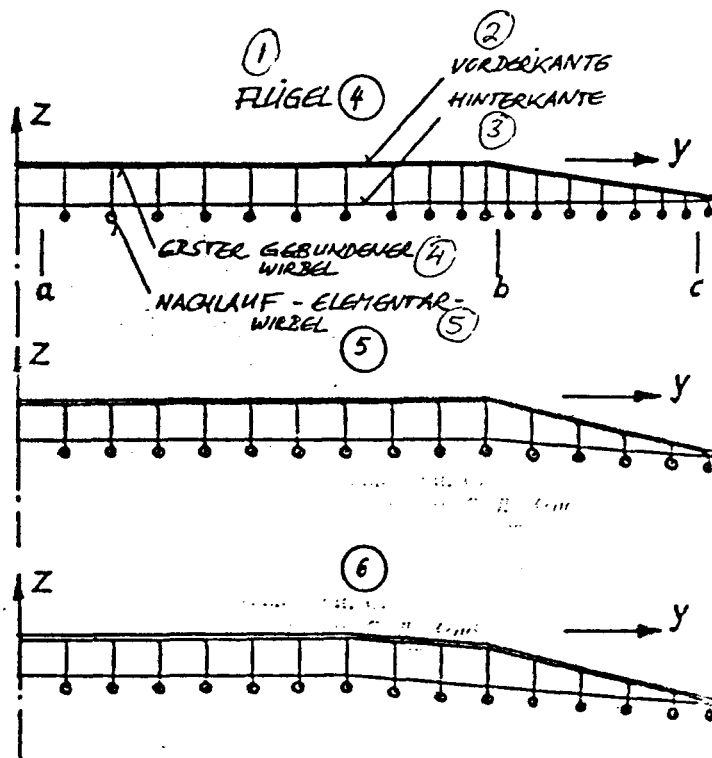


Ill. 4: The drag of various wing design with extension $\lambda = 7.05$. a) Wing designs with division a, b, c; b) Local upwing angle E on the first attached vortex; c) Drag dispersal ΔC_{wi} , total correction value of the induced drag C_{wi} , relative induced drag x_{ell} (n.b., E is entered positive below).



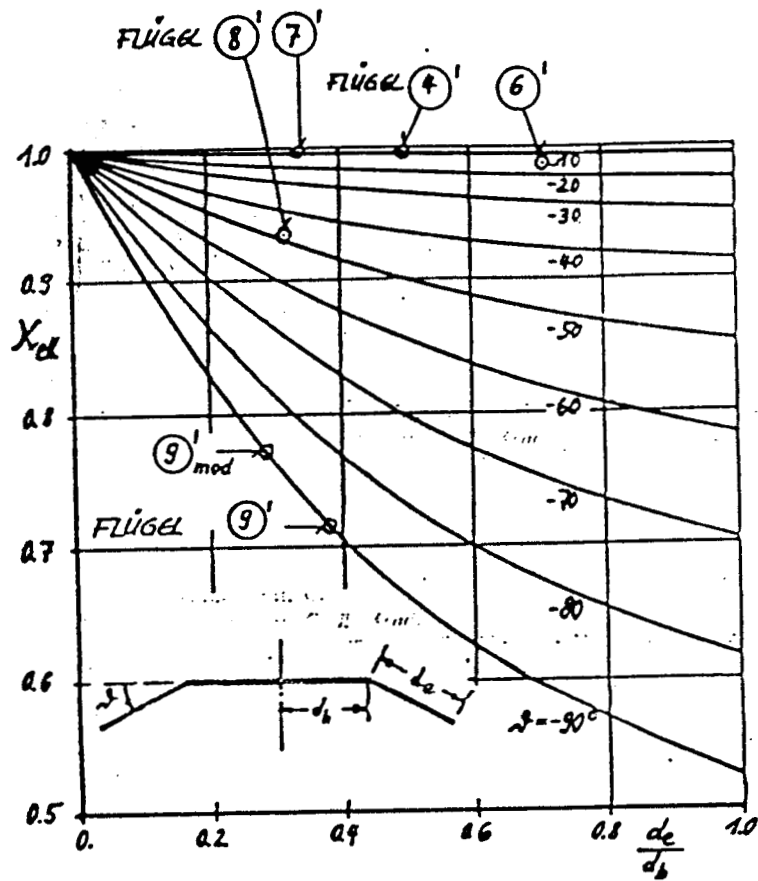
Ill. 5: Upwing velocity vectors on the first attached vortex of wing (4) in divisions a, b, c per Ill. 4, view in direction y (side view), $\alpha = 10^\circ$.

Key: (1) Wing (4); (2) Wake vortex corresponding to Ill. 1.



Ill. 6: View of vortex system of wings (4), (5), (6) in direction of flight at $\alpha = 10^\circ$ (view from behind).

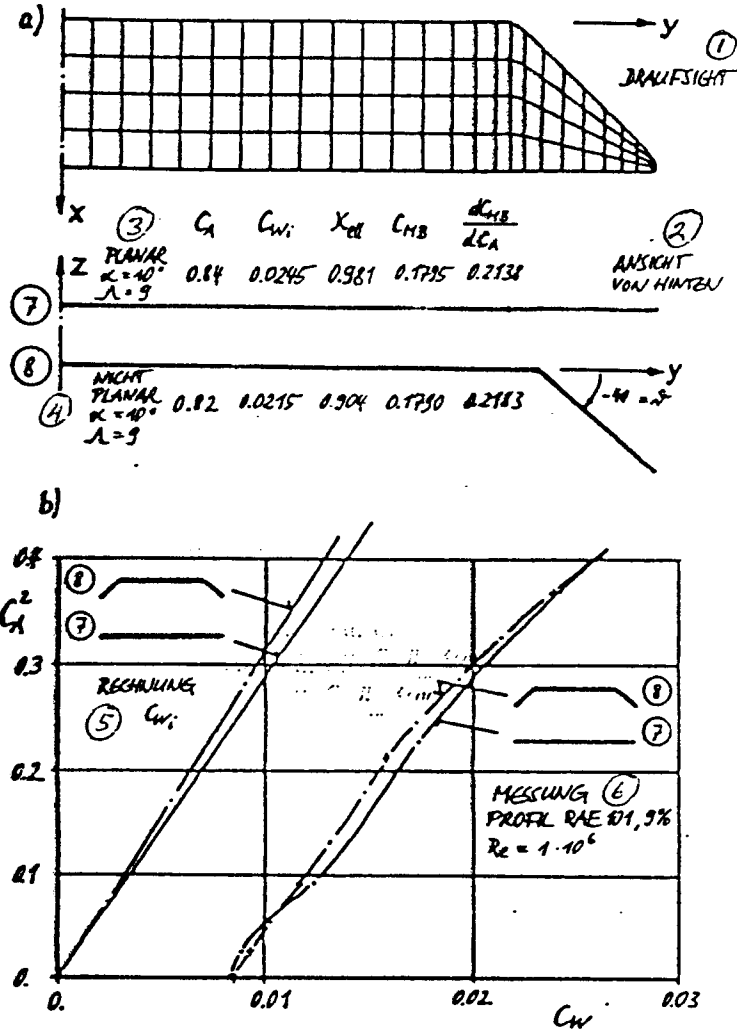
Key: (1) Wing (4); (2) Leading edge; (3) Trailing edge; (4) First attached vortex; (5) Wake - elementary - vortex



Ill. 7: The relative induced drag factor x_{el} of primary wing with turned down wing tips at angle of α ; rigid vortex wake independent of the size of the wing tip d_a/d_b per W. MANGLER [61].

Key: Flügel = Wing

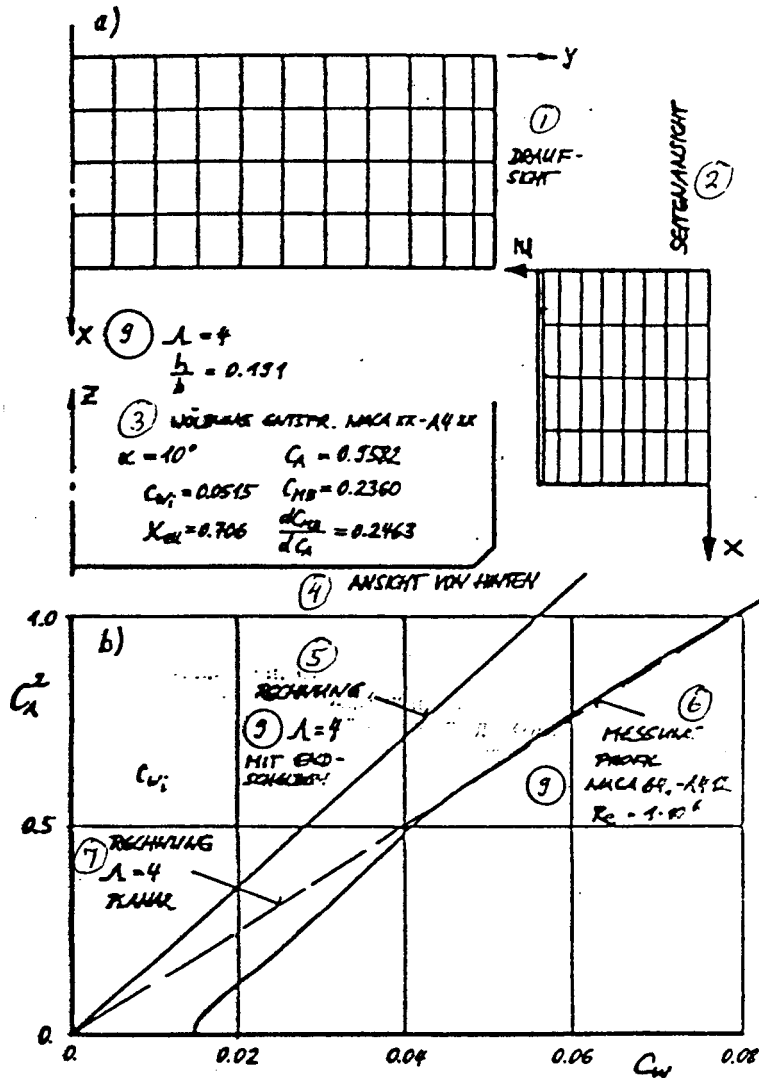
ORIGINAL PAGE IS
OF POOR QUALITY



- Ill. 8: The wing with planar (7) and nonplanar (8) triangular tip of extension $\Lambda = 9$.
a) Vortex net in top view and rear view, computed total correction values for $\alpha = 10^\circ$.
b) So-called quadratic polars per computation and measurement

Key: (1) Top view; (2) Rear view; (3) Planar; (4) Nonplanar; (5) Computation C_{wi} ; (6) Measurement profile

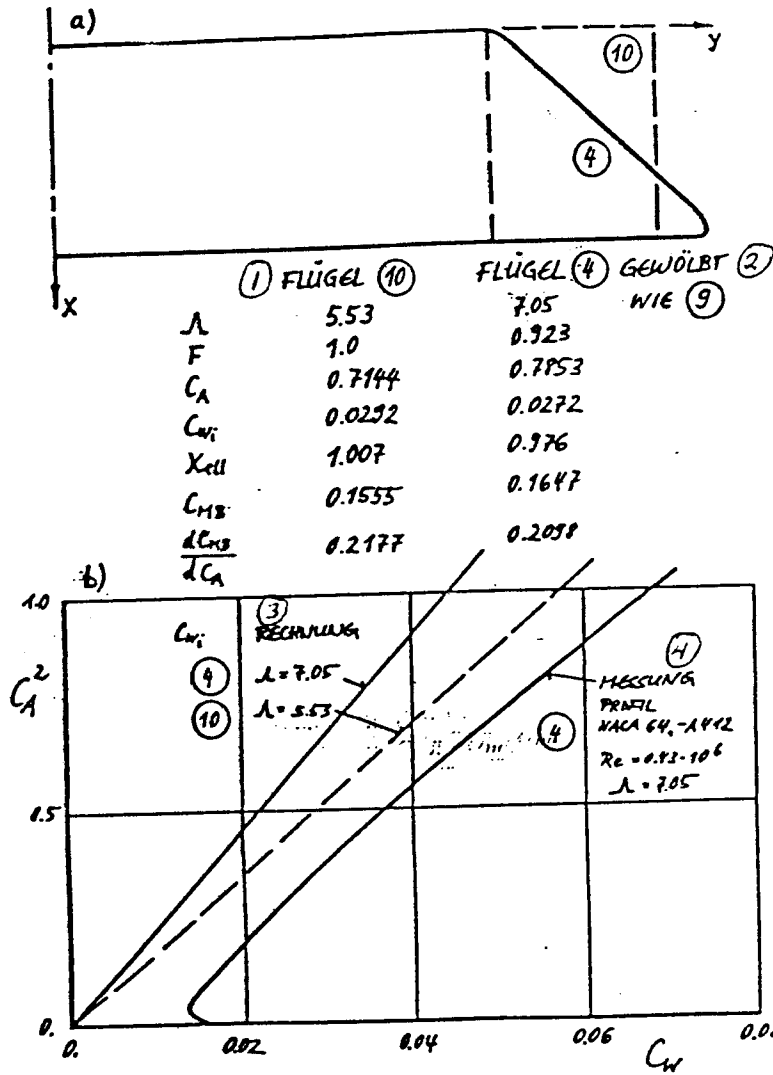
ORIGINAL PAGE IS
OF POOR QUALITY



- Ill. 9: Wing with endplates (9) of extension $\Lambda = 4$.
a) Vortex net in three views, calculated total correction value for $\alpha = 10^\circ$.
b) Quadratic plars per calculation and measurement

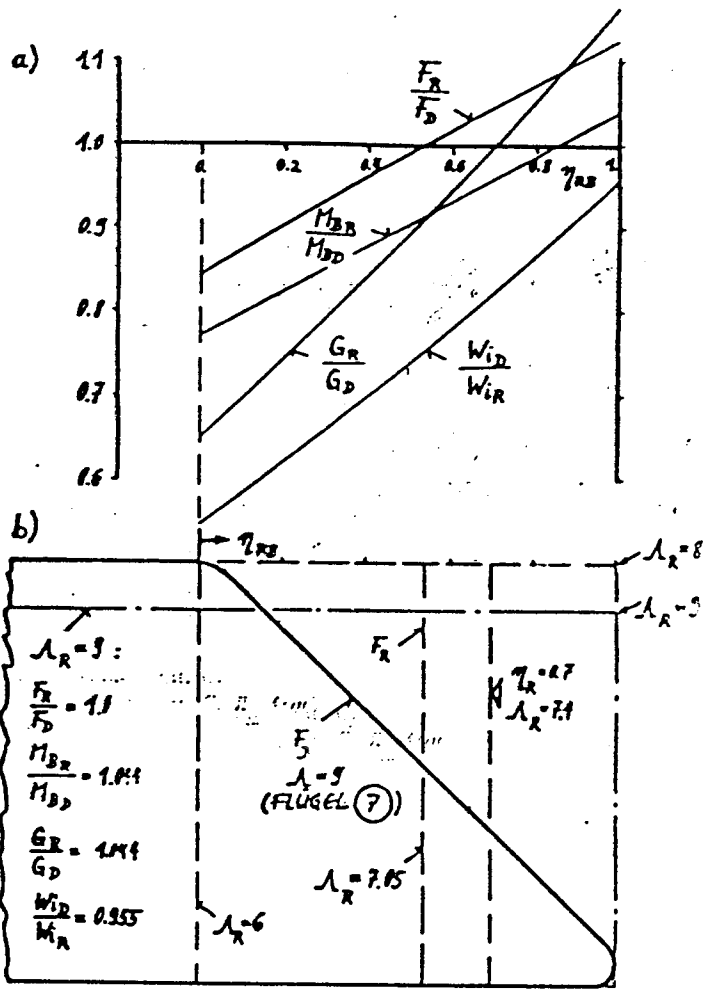
Key: (1) Top view; (2) Side view; (3) Camber per NACA xx - A4xx; (4) Rear view; (5) Calculation (9) $\Lambda = 4$ with end plates; (6) Measurement profile NACA 64.-A412; (7) Calculation $\Lambda = 4$ planar.

ORIGINAL PAGE IS
OF POOR QUALITY



- Ill. 10: The rectangular wing with level endplates (10) compared with wing (4)
a) Base comparison of wings (4) and (10), calculated total correction values for $\alpha = 10^\circ$
b) Quadratic plars per calculation and measurement

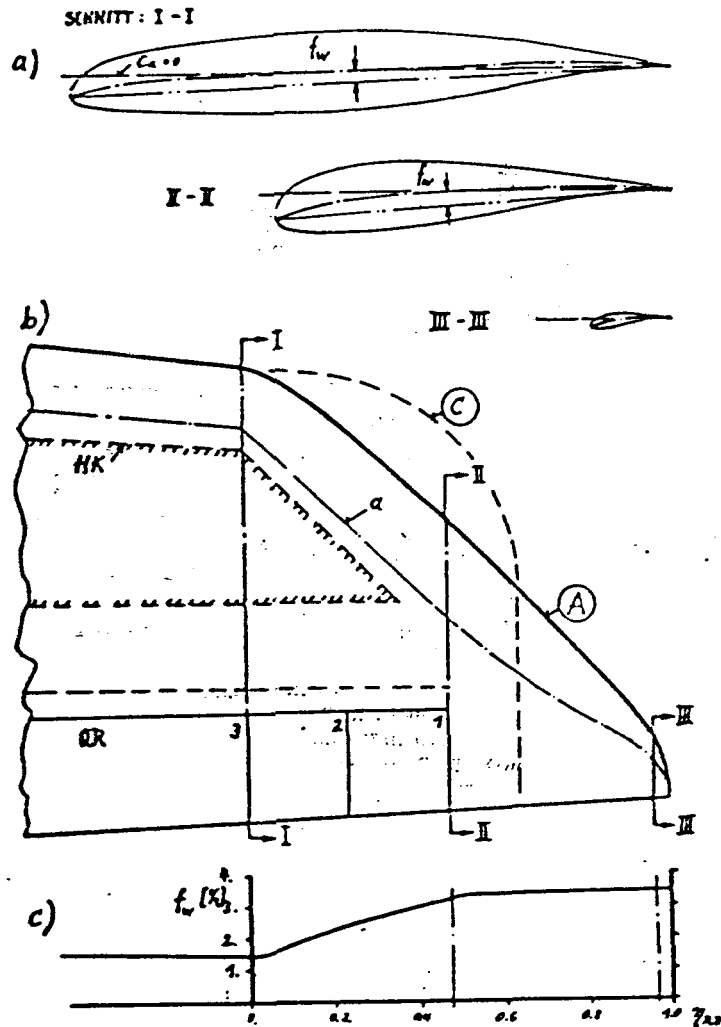
Key: (1) Flügel = Wing; (2) Cambered like (9); (3) Calculation; (4) Measurement profile.



Ill. 11: Comparison of wing (7) of extension $\lambda = 9$ with triangular tip (D) with various rectangular wings (R):
 a) Comparison of surfaces F_R/F_D , the root bending moments M_{BR}/M_{BD} , wing weights G_R/G_D , and the induced drags W_{ID}/W_{IR} ($= 1/(W_{IR}/W_{ID})$);
 b) Base comparison of wing (7) with various rectangular wing of extension 6 to 9. Total correction values for the rectangular wing of extension $\lambda = 9$ ($\gamma_{RB} = 2y_{tip}/b$)

Key: Flügel = Wing.

ORIGINAL PAGE IS
OF POOR QUALITY.

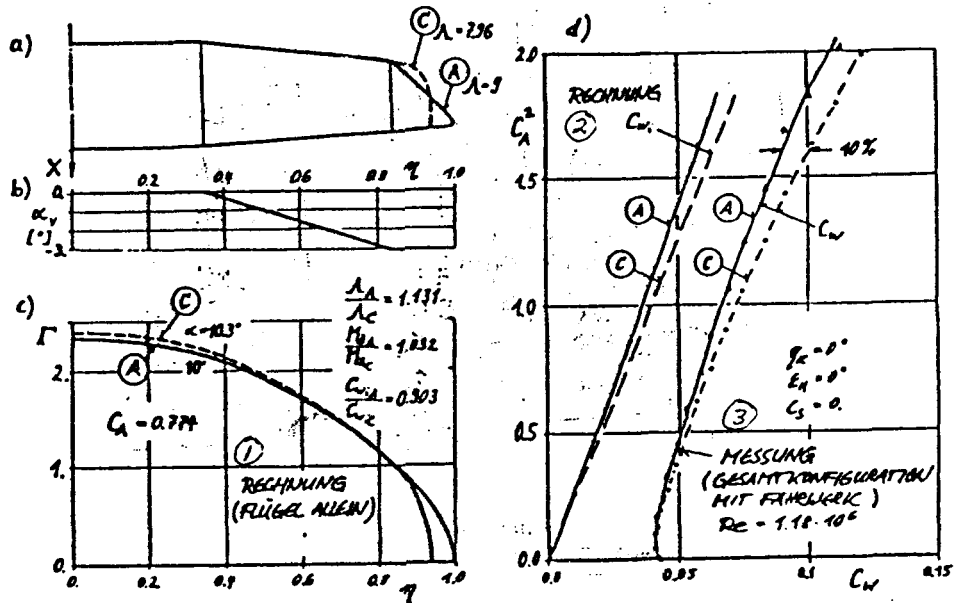


Ill. 12: Geometry of tip design for primary wing of new technology (TNT)

a) Cross section with zero lift direction ($c = 0$, broken line), skeleton line (dotted line) and camber height f_w ;

b) Base with triangular tip (A), conventional tip (C), spar box HK, border line of linear "Strak" a, various aileron extensions QR 1, 2, 3 and position of cuts I, II, III;

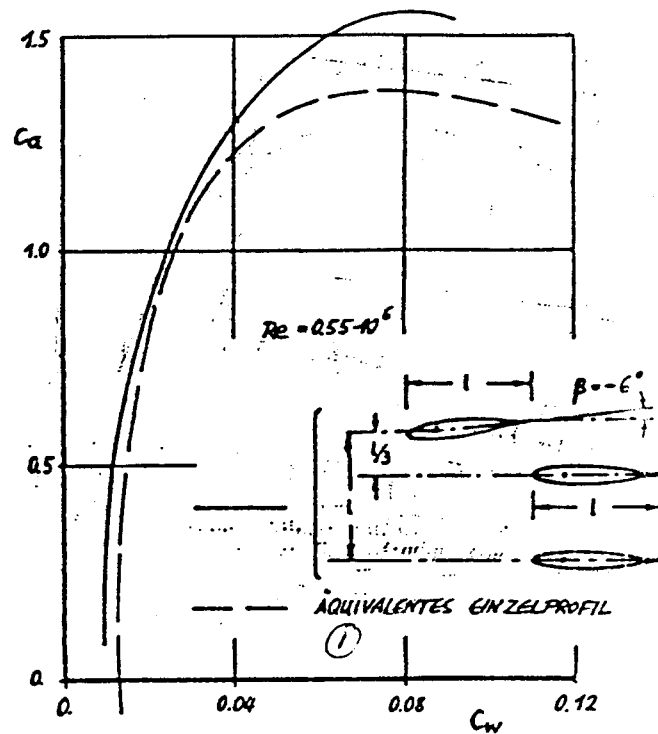
c) Dispersal of camber height in tip area;
(Expanded drawing after H. ZIMMER [77])



Ill. 13: Influence of wing tip design of the "TNT" on circulation dispersal and drag:

- a) Base with triangular tip (A) and conventional tip (C);
- b) torsion of the wing;
- c) Influence of the tip design on circulation dispersal Γ and the total correction values of wing root bending moment and of the induced drag at a total lift correction value $C_A = 0.774$;
- d) Influence of the tip design on the theoretical induced drag and on the measured total drag

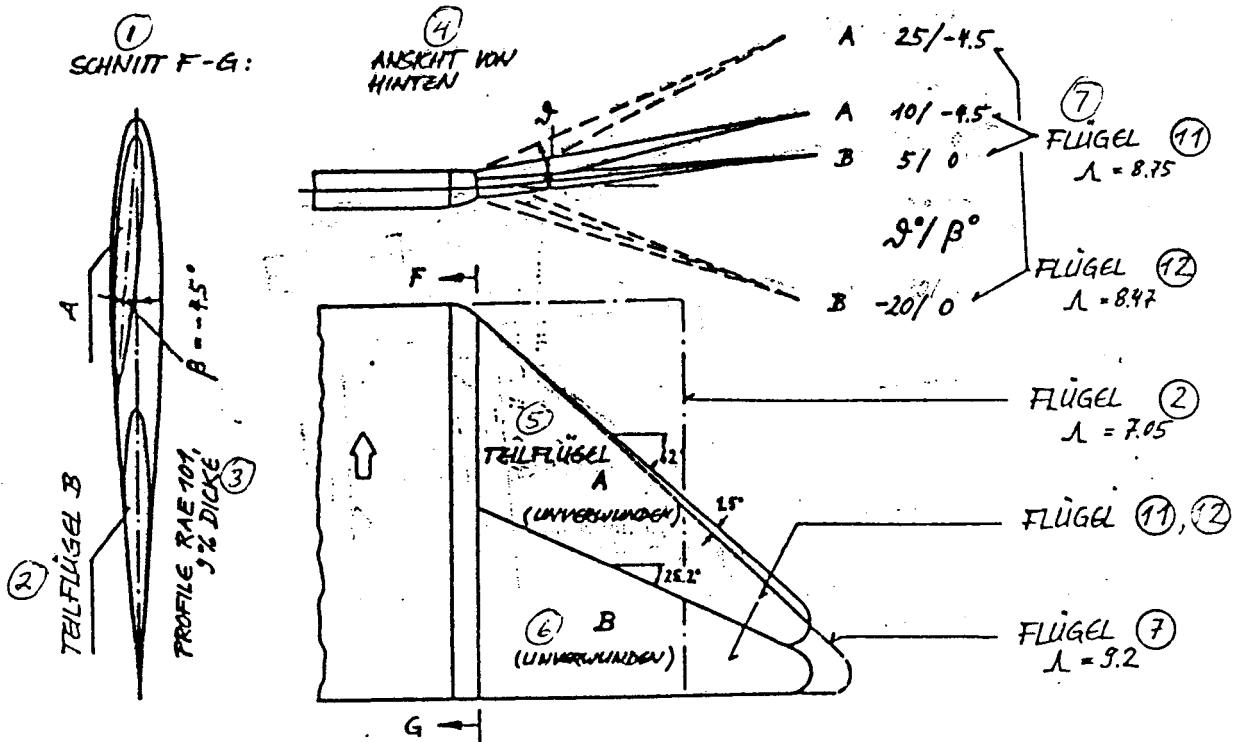
Key: (1) Calculation (wing alone); (2) Calculation C_{wi} ; (3) Measurement (total configuration with landing gear).



Ill. 14: Polars of the optimal biplane arrangement in two dimensional flow (of two mutually limited single non-overlapping profiles with an interval of a third to one wing chord) compared with the polar of the equivalent single profile [65], [66]. (JOUKOWSKI profiles, 12% thick, symmetrical)

Key: (1) Equivalent single profile.

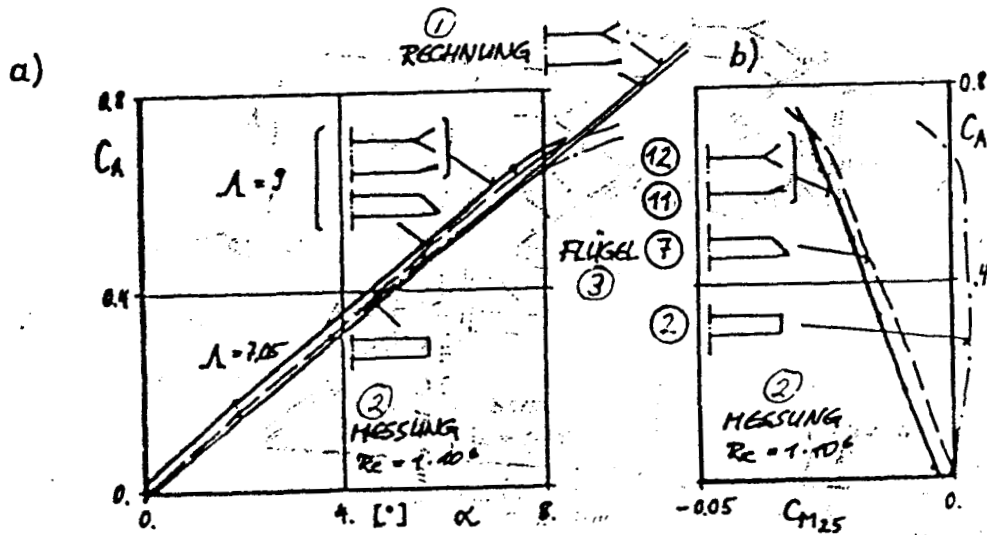
ORIGINAL PAGE IS
OF POOR QUALITY



Ill. 15: The geometry of various measured planar and nonplanar wing tip designs: the fanned tip (wing (11)), the forked tip (wing (12)), the planar wings (2) and (7) for comparison. (Expanded drawing after H. ZIMMER [33]).

Key: (1) Cut F-G; (2) Partial wing B; (3) 9% thickness; (4) Rear view; (5) Partial wing A (unwarped); (6) B (unwarped); (7) Flügel = Wing.

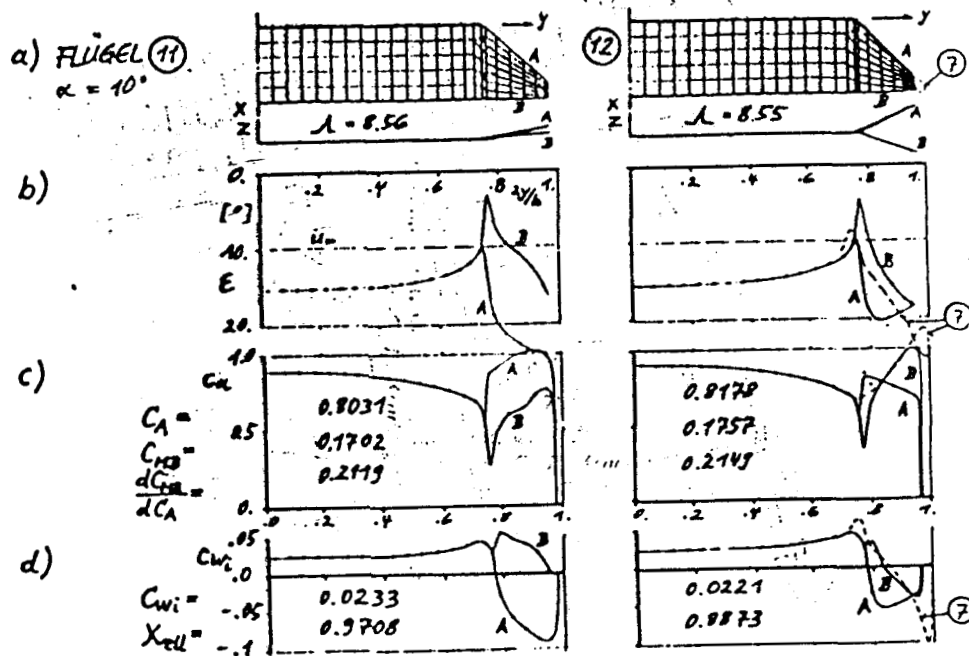
ORIGINAL PAGE IS
OF POOR QUALITY



Ill. 16: Lift and pitch moment of wings with various planar and nonplanar tip designs:
a) Calculated and measured lift correction value of wings with fanned tip (11) and with forked tip (12). Measured lift correction value of wings (2) and (7).
b) Measured pitch moment correction value of the wings.

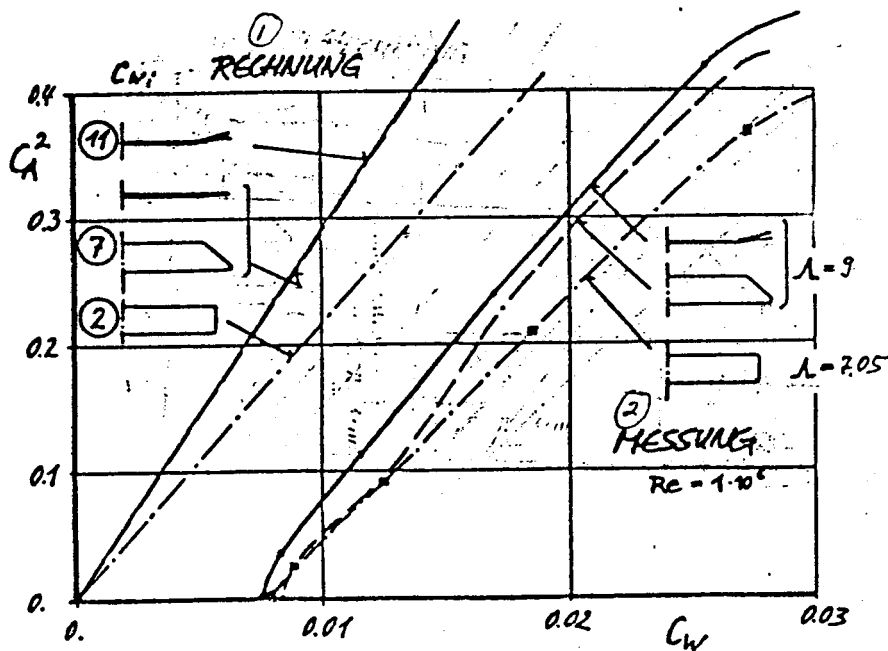
Key: (1) Calculation; (2) Measurement; (3) Wing.

ORIGINAL PAGE IS
OF POOR QUALITY



Ill. 17: Theoretical comparison of wings with fanned tip (11) from partial wings A and B, and with forked tip (12); a) the vortex net that was used; b) local upwind angle E on the first attached vortex; c) local lift correction value c_a and total correction value of lift C_A , root bending moment C_{MB} and its gradient dC_{MB}/dC_A ; d) local induced drag correction value c_{wi} , total correction value of the induced drag C_{wi} , relative induced drag X_{rel} (As comparison, wing (7) with planar triangular tip; E is entered below positive).

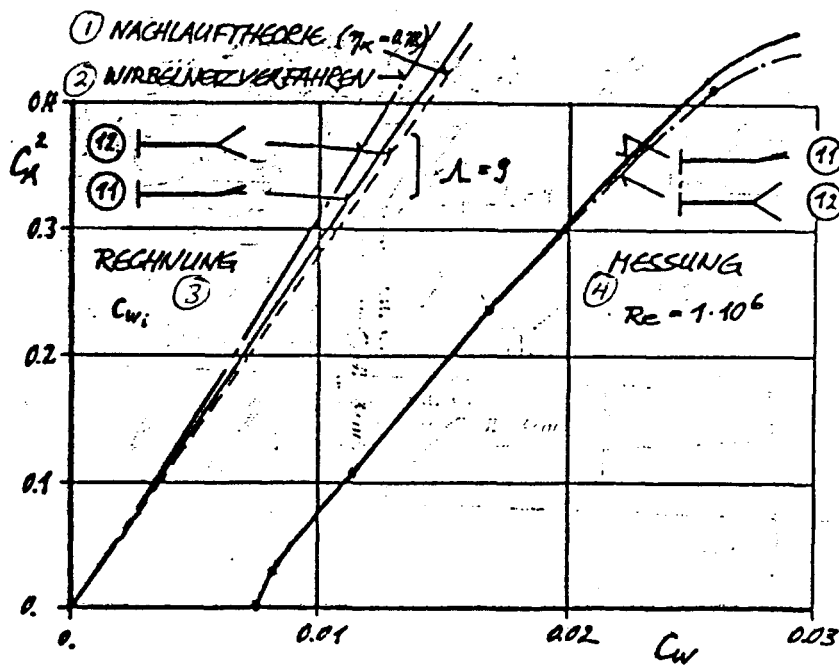
Key: Flügel = Wing



Ill. 18: Comparison of the theoretical quadratic polars with the measurements: Wings with fanned tip (11), with planar triangular tip (7) and rectangular wing (2).

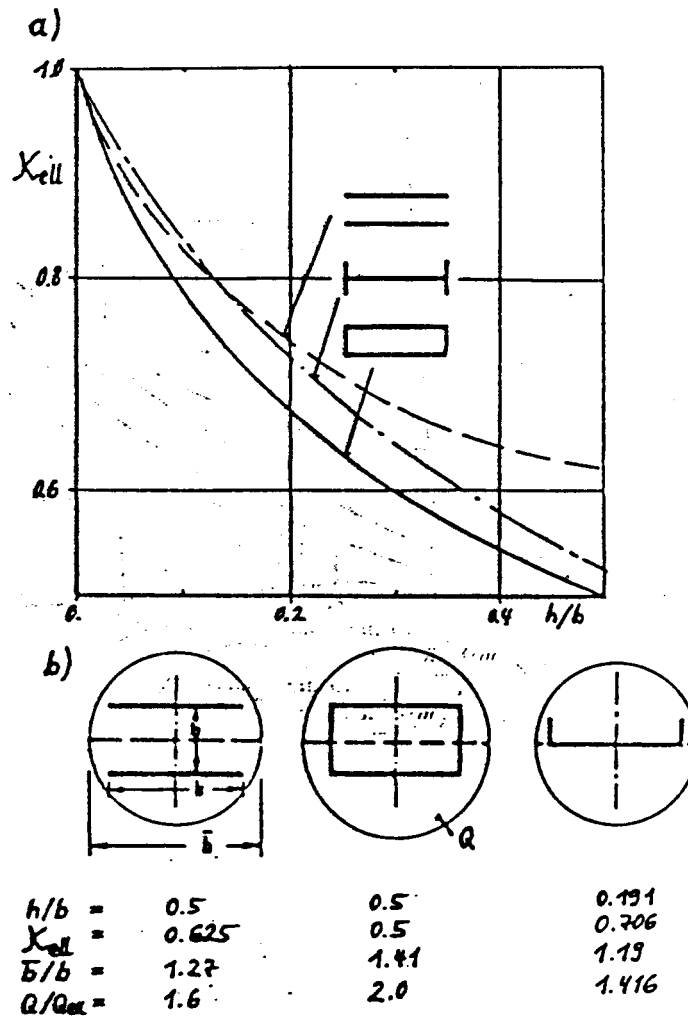
Key: (1) Calculation; (2) Measurement

ORIGINAL PAGE IS
OF POOR QUALITY



Ill. 19: Comparison of the theoretical quadratic polars with the measurements on a wing with a fanned tip (11) and with forked tips (12)

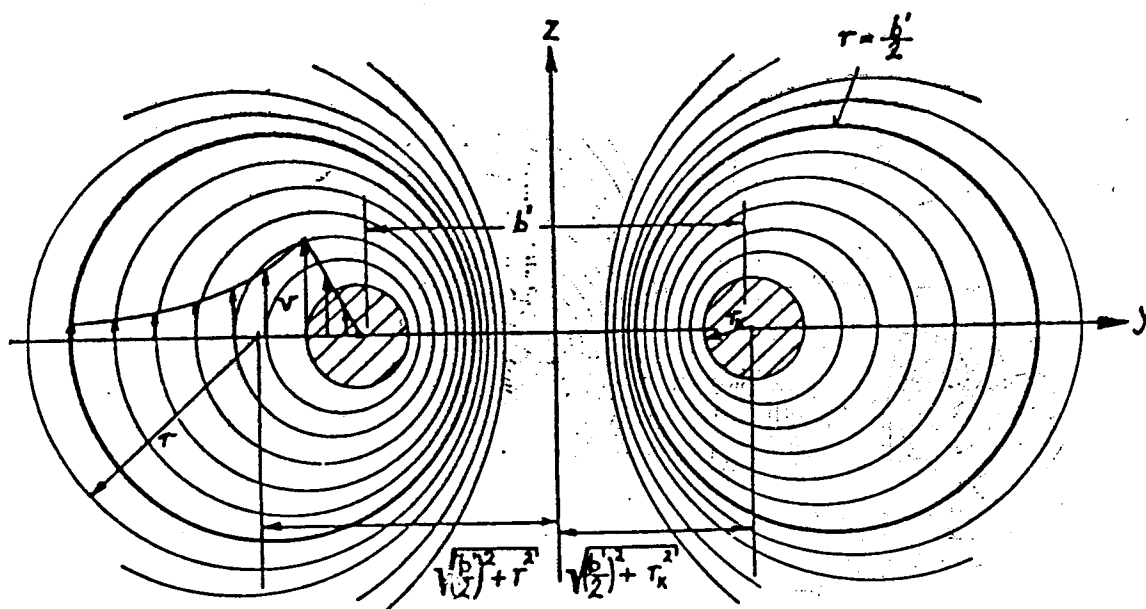
Key: (1) Wake theory; (2) Vortex net procedure; (3) Computation; (4) Measurement.



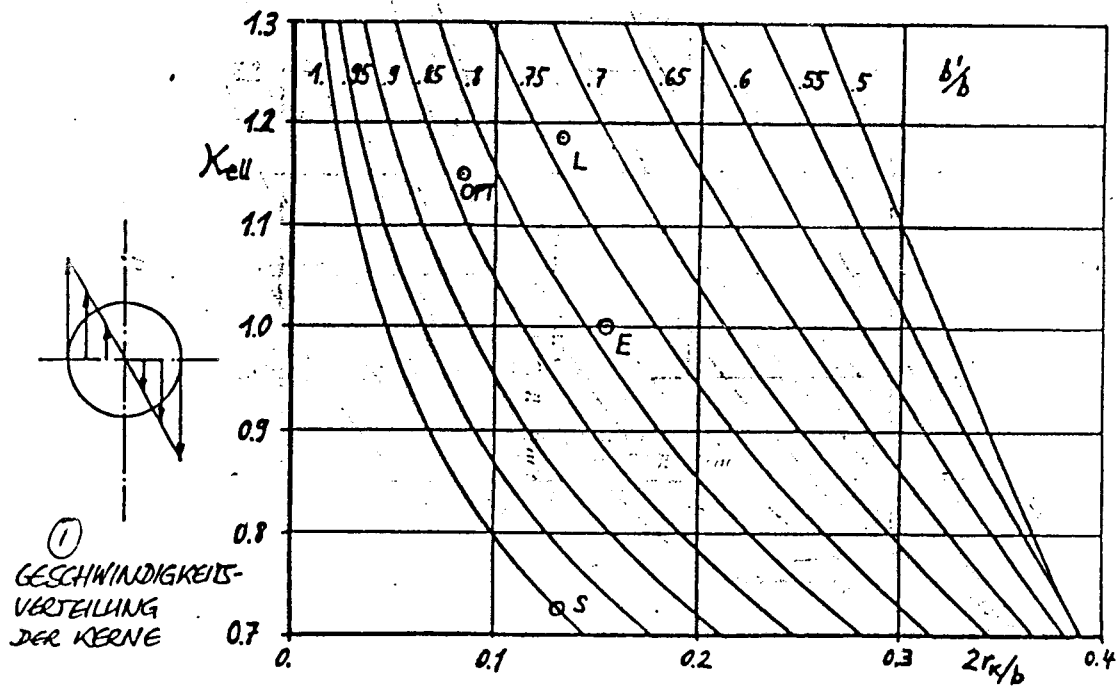
Ill. 20: Application of the impulse model to nonplanar wing systems:

a) The relative induced drag x_{ell} of three nonplanar primary wing systems independent of their height ratio h/b per PRANDTL et al. [5]; b) The picked-up air mass Q/Q_{ell} relative to the level elliptical wing of equal span b from three examples of nonplanar primary wing systems. (b is the span of the equivalent level wing)

ORIGINAL PAGE IS
OF POOR QUALITY

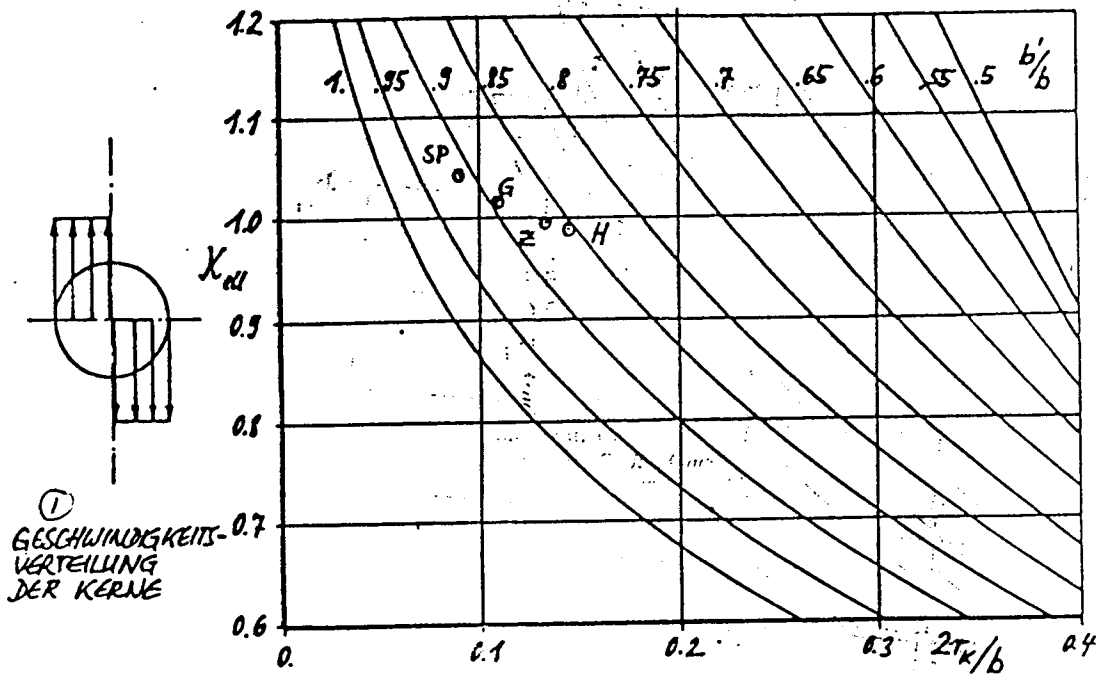


Ill. 21: Flow lines in a cut through the wake far behind the wing in accordance with the wake model per SPREITER and SACKS [72], consisting of two "RANKINE vortices" with center radius r_k and tangential velocity dispersal v .



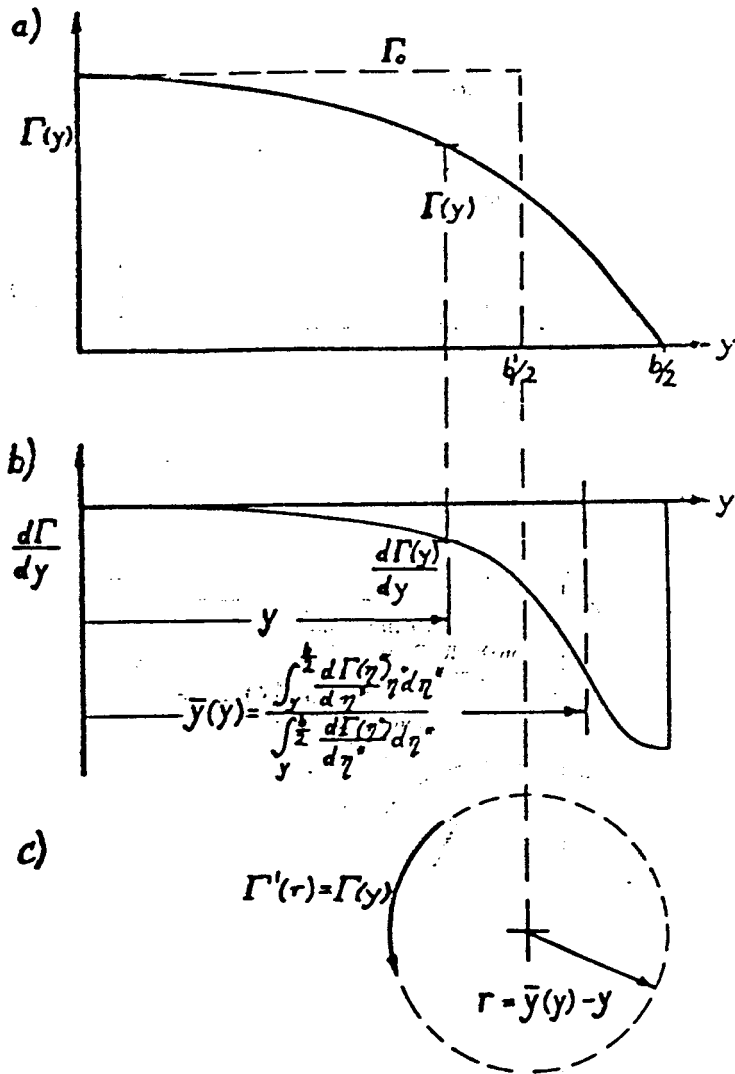
Ill. 22: The relative induced drag x_{e11} of a general wing system dependent on the size of the RANKINE wake vortex center $2r_k/b$ and its relative interval b'/b . (Points OPT, L, E, S correspond to the wing designs discussed in the text; increasingly qualitative character of results for $2r_k/b \gtrsim 0.25$).

Key: (1) Velocity dispersal of the centers

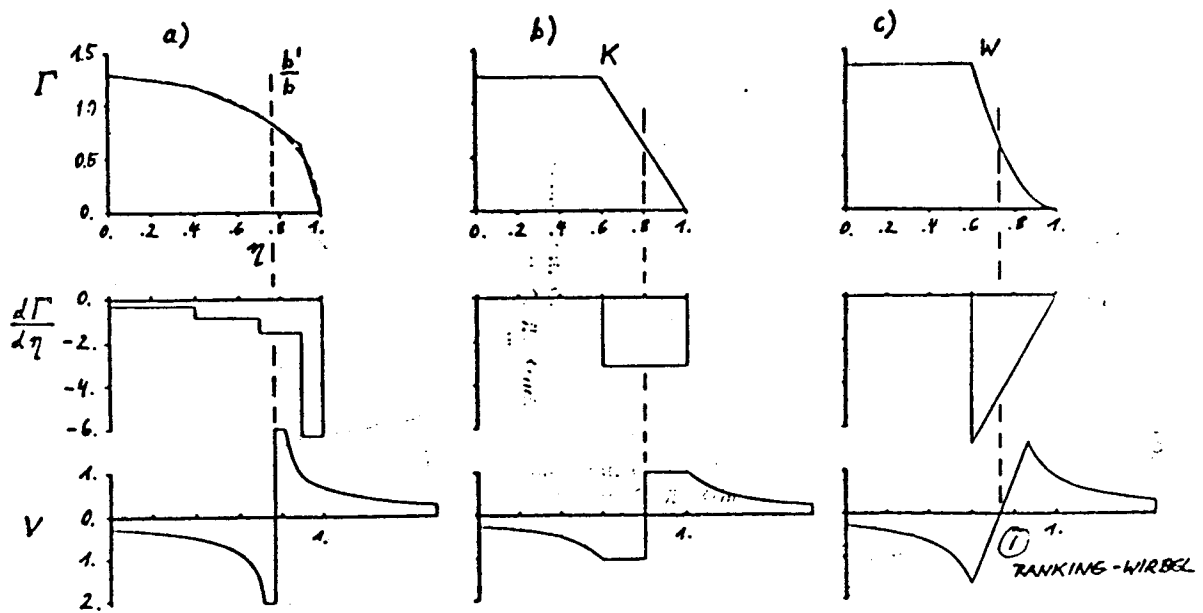


Ill. 23: The relative induced drag x_{ei} of a general wing system dependent on the size of the wake vortex centers with constant tangential velocity $2r_k/b$ and their relative interval b'/b . (Points G, H, SP, Z correspond to wing designs discussed in the text; increasingly qualitative character of results for $2r_k/b \gtrsim 0.25$).

Key: (1) Velocity dispersal of the centers.

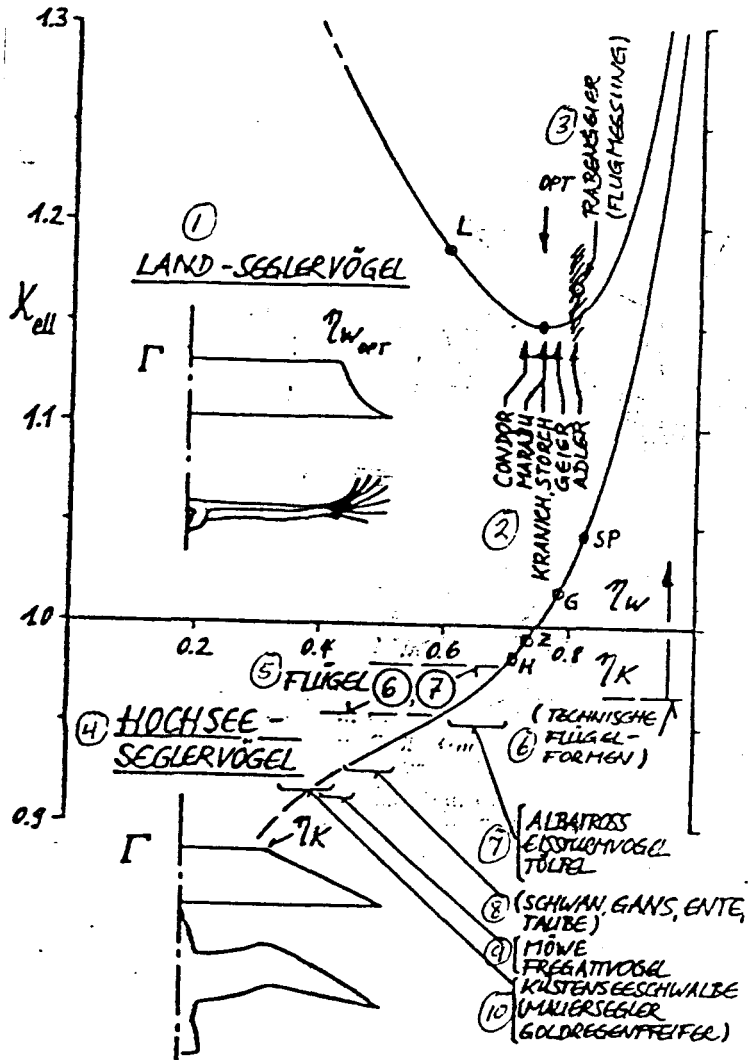


Ill. 24: The wake model per BETZ [44] and DONALDSON et al. [73]. a) Circulation dispersal at wing Γ ; b) the receding circulation or wake vortex strength $d\Gamma/dy$; c) a rolled up wake vortex.



Ill. 25: The rolling process of the wake vortex layer behind the wings with various circulation dispersals r at equal lift, receding circulation - or wake vortex strengths - $d\Gamma/dy$. Tangential velocity dispersal in the rolled up wake vortex v . a) Approximate elliptical circulation dispersal; b) Constant circulation and linear drop in interior; c) Constant circulation and parabolic, degressive drop in interior (W = bend with "inflection-like character", K = bending point)

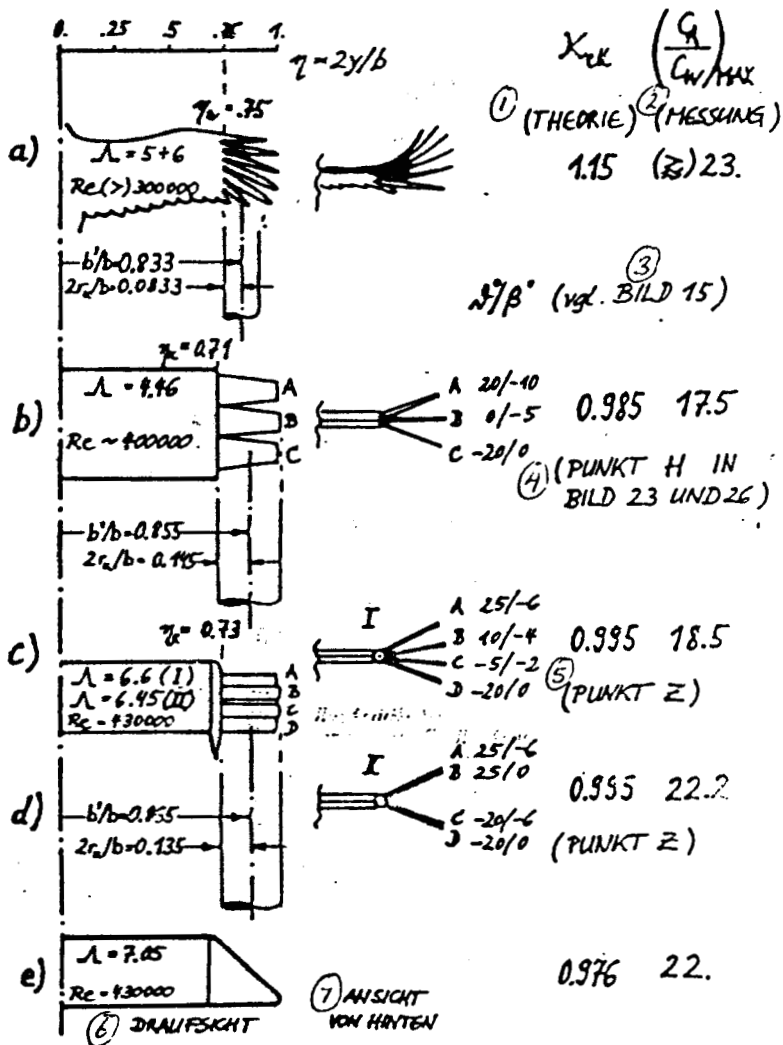
Key: (1) RANKINE vortex.



Ill. 26: The induced drag of soaring land and ocean birds (related to the planar elliptical wing with rigid wake) x_{ell} as a function of the size of the wing tip (n_w = position of the inflection point in the circulation dispersal, n_k = position of the bend in the circulation dispersal) (points G, H, SP, Z correspond to wing designs discussed in the text).

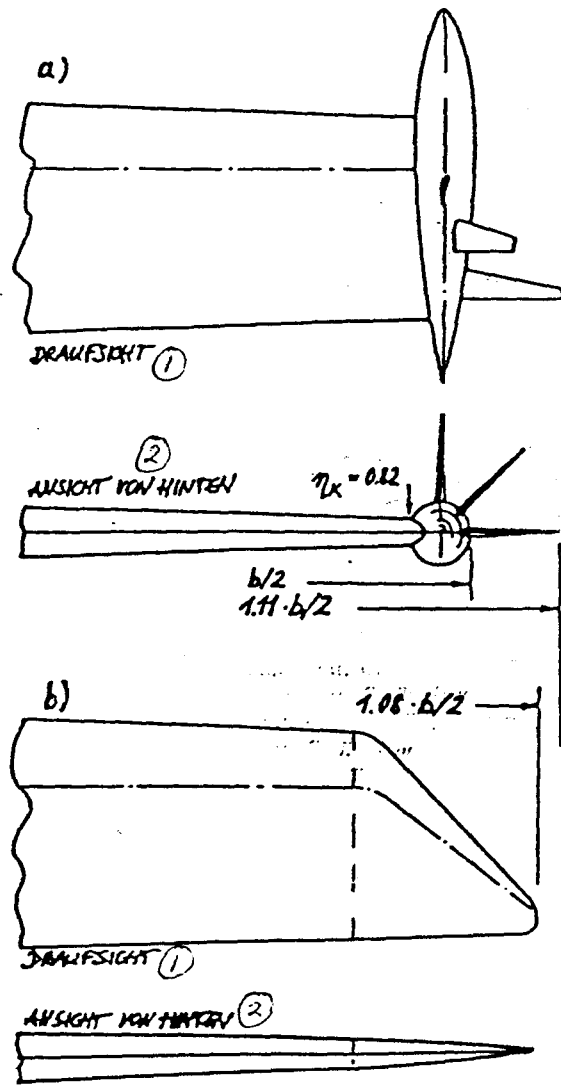
Key:

(1) Soaring land birds; (2) Condor; Marabu; Crane, Stork; Vulture; Eagle; (3) Urubu (flight measurement); (4) Soaring ocean birds; (5) Wings (6), (7); (6) (Technological wing types); (7) Albatross; kingfisher; gannet; (8) Swan, goose, duck, dove; (9) Gull; frigate; (10) Coastal sea swallow; [Mauersegler]; Golden plover



Ill. 27: Comparison of the wake vortex centers $2r_k/b$, of the relative induced drag x_{rel} and the maximal L/D ratio $(C_A/C_W)_{MAX}$ of various wings with multiply divided tips; a) Optimal soaring land bird; b) Configuration per HUMMEL [41]; c) and d) Configurations per studies by the author [56], [57]; e) Wings (4) for comparison (see Ill. 10).

Key: (1) Theory; (2) Measurement; (3) See Ill. 15; (4) Point H in Ill.s 23 and 26; (5) Punkt = Point; (6) Top view; (7) Rear view.



Ill. 28: a) Wing with fanned tip per SPILLMAN [39];
 b) Wing modified to a triangular tip of equal lift and equal induced drag.

Key: (1) Top view; (2) Rear view.

RESUME

Name: Herbert Fritz Zimmer

Birthdate: [REDACTED]

Primary education: 1947 - 1951 in Dirmingen

Secondary education: 1951 - 1959 in Lebach and Neunkirchen

Final exam: March 10, 1959 at the State Liberal Arts High School, Neunkirchen

Practical experience: Trainee at Ehrhardt & Sehmer, Saarbrucken (pumps, compressors gas machines); 1960 work-study student at Daimler-Benz AG, Stuttgart.

College: 1959 - 1965 at the University of Stuttgart; Major: aviation technology

Degree examination: August 13, 1965 graduate exam for aviation engineering (Grad.-Eng.) at the University of Stuttgart, Ph.D. work at the Institute for Aerodynamics and Gas dynamics, guidance by Prof. Dr. Eng. A. Weise.

Professional experience: Project engineer since September 11, 1965 in the "Aerodynamics" section of Dornier, GmbH, Friedrichshafen;

In charge of the "Rotor aerodynamics" area since April 1, 1972;

In charge of the "Rotor and wing aerodynamics" area since May 1, 1980, and representative for the chief of the "Aircraft-Project-Aerodynamics" section in the area of "Flight physics and experimental flight".